

การพัฒนาไปโอเซ็นเซอร์และการประยุกต์เพื่อตรวจวัดมลพิษโมเนลลาไทฟ์และคาร์ซิโนเอมบริโอนิก
แอนติเจน

นางสาววิจิตรา เตือนฉาย

วิทยานิพนธ์นี้เป็นส่วนหนึ่งของการศึกษาตามหลักสูตรปริญญาวิทยาศาสตรดุษฎีบัณฑิต

สาขาวิชาเคมี ภาควิชาเคมี

คณะวิทยาศาสตร์ จุฬาลงกรณ์มหาวิทยาลัย

ปีการศึกษา 2553

ลิขสิทธิ์ของจุฬาลงกรณ์มหาวิทยาลัย

DEVELOPMENT OF BIOSENSORS AND APPLICATIONS FOR THE
DETECTION OF *Salmonella typhi* AND CARCINOEMBRYONIC ANTIGEN

Miss Wijitar Dungchai

A Dissertation Submitted in Partial Fulfillment of the Requirements
for the Degree of Doctor of Philosophy Program in Chemistry

Department of Chemistry

Faculty of Science

Chulalongkorn University

Academic year 2010

Copyright of Chulalongkorn University

วิจิตรา เตือนฉาย : การพัฒนาไบโอเซ็นเซอร์และการประยุกต์เพื่อตรวจวัดซัลโมเนลลาไทพีและคาร์ซิโนเอมบริโอนิกแอนติเจน. (DEVELOPMENT OF BIOSENSORS AND APPLICATIONS FOR THE DETECTION OF *Salmonella typhi* AND CARCINOEMBRYONIC ANTIGEN) อ. ที่ปรึกษาวิทยานิพนธ์หลัก : รศ. ดร.อรวรรณ ชัยลภากุล 154 หน้า.

การพัฒนาไบโอเซ็นเซอร์เพื่อวินิจฉัย ณ จุดดูแลผู้ป่วยในราคาไม่แพงถูกรายงานในวิทยานิพนธ์นี้สามส่วนที่สำคัญประกอบด้วยเทคนิคทางเคมีไฟฟ้าร่วมกับอิมมูโนแอสเสย์ วัสดุตั้งต้นราคาไม่แพง และการปรับปรุงความไวถูกพัฒนาขึ้นเพื่อใช้เป็นไบโอเซ็นเซอร์ที่ราคาไม่แพง ในส่วนแรกเทคนิคทางเคมีไฟฟ้าร่วมกับอิมมูโนแอสเสย์สำหรับการหาปริมาณซัลโมเนลลาไทพีได้ถูกพัฒนาขึ้นโดยการใช้คอปเปอร์ซายาลัญญานของทองขนาดนาโนเมตรที่เป็นตัวติดฉลากด้วยเทคนิคแอนติบอดีที่จับกับโวลแทมเมตรี ความสูงของกระแสไฟฟ้าจากแอนติบอดีที่จับมีความสัมพันธ์เป็นเส้นตรงกับความเข้มข้นของซัลโมเนลลาไทพีในช่วง 1.30×10^2 ถึง 2.6×10^3 คอโลนีต่อมิลลิลิตร ในส่วนที่สองวัสดุตั้งต้นกระดาษถูกใช้สำหรับการวิเคราะห์ทางชีวภาพแทนแผ่นเยื่อเนื่องจากกระดาษเป็นวัสดุที่ราคาไม่แพง อุปกรณ์ของไหลจุลภาคบนกระดาษถูกศึกษาในส่วนนี้เพราะเป็นการรวมความง่ายของการตรวจวัดบนกระดาษเข้ากับความสามารถประยุกต์ใช้งานที่ซับซ้อนของเทคนิคของไหลจุลภาค โดยในส่วนนี้การใช้อินดิเคเตอร์หลายชนิดสำหรับสารที่สนใจหนึ่งชนิดและเทคนิคทางเคมีไฟฟ้าถูกประยุกต์กับอุปกรณ์ของไหลจุลภาคบนกระดาษเพื่อปรับปรุงการวิเคราะห์เชิงปริมาณ ช่องไหลสารจุลภาคบนกระดาษถูกเตรียมด้วยเทคนิคโฟโตลิโทกราฟีและขั้วไฟฟ้าใช้งานถูกสร้างบนอุปกรณ์ด้วยเทคนิคพิมพ์สกรีน ประสิทธิภาพพื้นฐานของการตรวจวัดด้วยเทคนิคทางเคมีไฟฟ้าถูกแสดงด้วยการใช้เทคนิคไซคลิกโวลแทมเมตรี หลังจากนั้นประโยชน์ของเรถูกแสดงด้วยการหาปริมาณกลูโคส แลกเทส และกรดยูริกในซีรัมตัวอย่างโดยอาศัยปฏิกิริยาของเอนไซม์ออกซิเดส (กลูโคสออกซิเดส แลกเทสออกซิเดส และยูริเคส ตามลำดับ) ยิ่งไปกว่านั้นเทคนิคการพิมพ์สกรีนแว็กซ์ซึ่งมีราคาไม่แพง ง่าย และรวดเร็ว สำหรับการสร้างอุปกรณ์ของไหลจุลภาคบนกระดาษได้ถูกรายงานไว้ด้วย ไบโอเซ็นเซอร์ที่ถูกพัฒนาขึ้นเหล่านี้แสดงแนวโน้มที่เหมาะสมสำหรับการวิเคราะห์ทางชีวภาพที่มีราคาไม่แพงสำหรับประเทศที่มีทรัพยากรจำกัด ในส่วนสุดท้ายเม็ดแม่เหล็กขนาดไมโครเมตรปริมาตรน้อยถูกพัฒนาเพื่อเพิ่มพื้นที่ผิวสำหรับการยึดเกาะของแอนติเจนและแอนติบอดี การใช้ประโยชน์ของเม็ดแม่เหล็กขนาดไมโครเมตรร่วมกับเทคนิคอิมมูโนแอสเสย์ถูกศึกษาด้วยการหาปริมาณของคาร์ซิโนเอมบริโอนิกแอนติเจนในซีรัมของมนุษย์ ซีดต่ำสุดที่สามารถวัดได้เป็นค่าต่ำลงไปถึง 0.69 นาโนกรัมต่อมิลลิลิตรถูกได้รับ

ภาควิชา.....เคมี.....ลายมือชื่อ.....
 สาขาวิชา.....เคมี.....ลายมือชื่อ อ. ที่ปรึกษาวิทยานิพนธ์หลัก.....
 ปีการศึกษา.....2553.....

##4873851623 : MAJOR CHEMISTRY

KEYWORDS : BIOSENSOR / *Salmonella typhi* / CARCINOEMBRYONIC ANTIGEN

WIJITAR DUNGCHAI : DEVELOPMENT OF BIOSENSORS AND APPLICATIONS FOR THE DETECTIONS *Salmonella typhi* AND CARCINOEMBRYONIC ANTIGEN. THESIS ADVISOR : ASSOC. PROF. ORAWON CHAILAPAKUL, 154 pp.

The development of biosensors for low-cost point-of-care diagnostic test is reported in this dissertation. Three important parts including electrochemical immunoassay, low-cost material substrate, and improvement of sensitivity were developed to achieve the low-cost biosensors. In the first part, electrochemical immunoassay for the *Salmonella typhi* (*S. typhi*) determination has been developed by using a copper-enhanced gold nanoparticle label coupled with anodic stripping voltammetry. The anodic stripping peak current was linearly dependent on the *S. typhi* concentration over concentration range of 1.30×10^2 to 2.6×10^3 cfu/mL in a logarithmic plot, with a detection limit as low as 98.9 cfu/mL. In the second part, paper-based substrates were used for bioassays instead of membrane due to the ultra-low cost of the paper materials. Paper-based microfluidic devices (μ PADs) were investigated in this part because they combined the simplicity of paper strip tests and the complexity of the conventional microfluidics. In this part, the use of multiple indicators for a single analyte and electrochemical detection were applied for μ PADs to improve quantitative analysis. The paper-based microfluidic channels were prepared by photolithography and the working electrode was built into devices using screen-printing technology. The basic electrochemical performance of the system was demonstrated using cyclic voltammetry. The utility of our devices was then demonstrated with the determination of glucose, lactate, and uric acid in serum samples using oxidase enzyme (glucose oxidase, lactate oxidase, and uricase, respectively) reactions. Moreover, wax screen-printing as a low-cost, simple, and rapid method for fabricating paper-based microfluidic devices (μ PADs) is reported here. These developed biosensors show significant promise for inexpensive bioassay for limited resource environments. Lastly, a small volume magnetic microbead-based immunoassay was developed to increase the surface area for immobilization of antigen or antibody. The utility of magnetic microbead-based immunoassay was investigated by the determination of carcinoembryonic antigen (CEA) in human serum. The limit of detection as low as 0.69 ng/mL was achieved.

Department : Chemistry Student's Signature

Field of Study : Chemistry Advisor's Signature

Academic Year : 2010

ACKNOWLEDGEMENTS

Firstly, I owe my deepest gratitude to my advisor, Assoc. Prof. Dr. Orawon Chailapakul, who encourage, guidance, support, and give the great opportunity throughout my dissertation. She continually and convincingly conveyed a spirit of adventure in regard to research and scholarship, and an excitement in regard to teaching. I am also grateful to thank my co-advisors, Assoc. Prof. Dr. Charles S. Henry at Colorado State University, USA., for his challenging ideas, support, advice, suggestions, and belief in my spirit over the year of conducting research. In addition, I would like to thank my committee members, Assoc. Prof. Dr. Sirirat Kokpol, Assoc. Prof. Dr. Nattaya Ngamrojanavanich, Assist. Prof. Dr. Narong Praphairaksit, and Dr. Weena Siangproh who give helpful comments and advices in this dissertation.

I would like to show my gratitude to the members of the Sensor Research Unit, Department of Chemistry, Chulalongkorn University and the members of Henry's group at Colorado State University, for being my great friend and providing their help throughout this research. I also would like to gratefully acknowledge the financial support from the Thailand Research Fund through the Royal Golden Jubilee Ph.D. Program (Grant No. PHD/0039/2548) and Center for Petroleum, Petrochemicals, and Advanced Materials.

Finally, I am affectionately thankful to my Family and Ekkachai Yingyongsakul for their sincere unlimited support, belief, encouragement, and respect throughout my education.

CONTENTS

	PAGE
ABSTRACT (in Thai)	iv
ABSTRACT (in Eng)	v
ACKNOWLEDGMENTS	vi
CONTENTS	vii
LIST OF TABLES	xiii
LIST OF FIGURES	xiv
ABBREVIATIONS	xxi
CHAPTER I INTRODUCTION	1
1.1 Introduction.....	1
1.2 Research objective.....	3
1.3 Scope of research.....	4
1.4 Research utilization.....	5
1.5 References.....	6
CHAPTER II THEORY AND LITERATURE SURVEY	9
2.1 Immunoassay.....	9
2.2 Electrochemical method.....	14
2.2.1 Voltammerty.....	16
2.2.1.1 Cyclic voltammetry.....	17
2.2.1.2 Stripping voltammetry.....	20
2.2.2 Chronomethods.....	21

	PAGE
2.3 Pathogenic bacteria.....	23
2.4 Paper-based microfluidic.....	29
2.5 References.....	31
CHAPTER III ELECTROCHEMICAL IMMUNOASSAY.....	34
Abstract.....	35
3.1 Introduction.....	36
3.2 Experimental methods.....	38
3.2.1 Instrumentation.....	38
3.2.2 Materials and methods.....	38
3.2.3 Preparation of the antibody-colloidal gold conjugate.....	39
3.2.3.1 Preparation of gold nanoparticles.....	39
3.2.3.2 Antibody-colloidal gold conjugate.....	39
3.2.4 Immunoassay Procedure.....	40
3.3 Results and discussion.....	41
3.3.1 Preparation of the antibody-colloidal gold conjugate.....	41
3.3.1.1 Preparation of the gold nanoparticles.....	41
3.3.1.2 Preparation of the antibody-colloidal gold conjugate	42
3.3.2 Determination of copper (II) ion at a glassy carbon electrode...	44
3.3.2.1 The effect of the deposition potential	44
3.3.2.2 The effect of the deposition time.....	45
3.3.2.3 Linearity.....	45
3.3.3 Optimization of the immunoassay conditions	47
3.3.3.1 The effect of the concentration and the reaction	
time of copper enhancer solution.....	47
3.3.3.2 The effect of the immunoassay incubation time.....	50
3.3.3.3 The effect of the dilution ratio and the incubation	
time of the antibody-colloidal gold conjugate.....	50

	PAGE
3.3.4 Analytical performance.....	52
3.3.5 Analytical applications.....	54
3.4 Summary.....	55
3.5 References.....	55
CHAPTER IV PAPER-BASED MICROFLUIDICS.....	59
PART A	
Electrochemical Detection for Paper-Based Microfluidics.....	60
Abstract.....	61
4.1 Introduction.....	62
4.2 Experimental methods.....	64
4.2.1 Materials and equipment	64
4.2.2 Preparation of paper-based microfluidic devices	64
4.2.3 Design and preparation of electrochemical detector for paper-based microfluidic devices	65
4.2.4 Design and preparation of paper-based microfluidic devices for multianalyte determination	66
4.2.5 Human serum sample.....	67
4.3 Results and discussion.....	67
4.3.1 Characterization of electrochemical detection for paper-based microfluidic devices	68
4.3.2 Choice of detection potential for hydrogen peroxide.....	70
4.3.3 Analytical performance.....	74
4.3.4 Analytical applications.....	77
4.4 Summary.....	78

PAGE**PART B**

Use of multiple colorimetric indicators for paper-based microfluidic devices.....	80
Abstract.....	81
4.5 Introduction	82
4.6 Experimental methods.....	83
4.6.1 Materials and equipments.....	83
4.6.2 Preparation of paper-based microfluidic devices.....	84
4.6.3 Design of multiple oxidative indicators for paper-based Microfluidic devices.....	84
4.6.4 Effect of reagent and sample volume.....	85
4.6.5 Preparation of multiple oxidative indicators for paper-based microfluidic devices.....	85
4.6.6 Human serum sample.....	86
4.6.7 Lifetime of the devices.....	86
4.7 Results and discussion	87
4.7.1 Colorimetric bioassays.....	87
4.7.2 Effect of reagent and sample volume.....	91
4.7.3 Simultaneous measurement of three analytes.....	92
4.7.4 Semi-quantitative measurement of three analytes in real samples	95
4.7.5 Lifetime of the devices.....	98
4.8 Summary.....	101

PART C

A low-cost, simple, and rapid fabrication method for paper-based microfluidics using wax screen-printing.....	103
Abstract.....	104
4.9 Introduction.....	105
4.10 Experimental.....	106

	PAGE
4.10.1 Materials and equipment.....	106
4.10.2 Wax screen-printing method.....	107
4.10.3 Study of molten wax spreading in paper.....	107
4.10.4 Wax screen-printing resolution.....	108
4.10.5 Applications.....	108
4.10.6 Human serum sample.....	109
4.11 Results and discussion.....	109
4.11.1 Wax screen-printing.....	109
4.11.2 Wax spreading.....	110
4.11.3 Wax screen-printing resolution.....	113
4.11.4 Applications.....	115
4.12 Summary.....	119
4.13 References.....	120
CHAPTER V SENSITIVITY IMPROVEMENT OF IMMUNOASSAY	129
Abstract.....	130
5.1 Introduction.....	131
5.2 Experimental methods.....	132
5.2.1 Instrumentation.....	132
5.2.2 Materials and Methods.....	133
5.2.3 Immunoassay procedure.....	133
5.2.4 Micro-plate chemiluminescence immunoassay (micro-plate CLEIA).....	134
5.2.5 Data analysis.....	134
5.2.6 Human serum sample.....	135
5.2.7 Statistical analysis.....	135
5.3 Results and discussion	135
5.3.1 Optimization of immunoassay reagents.....	135

	PAGE
5.3.2 Physicochemical parameter optimization.....	136
5.3.2.1 Effect of immunoassay incubation time.....	137
5.3.2.2 Influence of the reaction time between AMPPD CL substrate and ALP-anti CEA antibody.....	137
5.3.2.3 Effect of the shaking time to capture efficiency....	137
5.3.2.4 Effect of magnetic beads volume.....	138
5.3.2.5 Effect of the substrate volume to bead-based CLEIA	138
5.3.3 Non-specific adsorption.....	141
5.3.4 Linearity-dilution effect.....	142
5.3.5 Calibration and sensitivity.....	142
5.3.6 Precision.....	144
5.3.7 Quantitative determination of CEA in human serums: comparison with commercially available CEA CL-EIA kit	144
5.4 Summary.....	147
5.5 References.....	148
CHAPTER VI CONCLUSIONS AND FUTURE PERSPECTIVE.....	152
6.1 Conclusions.....	152
6.2 Future perspective.....	153
VITA.....	154

LIST OF TABLES

TABLE	PAGE
2.1	Detector molecules commonly used in immunoassay..... 12
2.2	The transmission, diseases, treatment, prevention and laboratory diagnosis of some pathogenic bacterium..... 26
3.1	The reproducibility of the proposed method 53
3.2	Results of <i>S. typhi</i> in human serum sample..... 55
4.1	Linear dynamic range, limit of detection and limit of quantification of the proposed method..... 77
4.2	Determination of glucose, lactate, and uric acid in control samples..... 78
4.3	Concentrations of glucose, lactate, and uric acid in each level of standard solution..... 86
4.4	Slope, intercept and R^2 of the linearity curve and the matching percentage of slope and intercept between hydrophobic barrier width at front and back of paper devices..... 112
4.5	Determination of glucose and total iron in control samples..... 119
5.1	Studied of non-specific adsorption..... 141
5.2	Precisions of the micro-magnetic CL-EIA..... 144
5.3	oncentration of CEA in spiked human serum, measured by the commercial micro-plate and magnetic microbead CL-EIA..... 145

LIST OF FIGURES

FIGURE	PAGE
2.1	Schematic diagrams of the different immunoassay concepts..... 10
2.2	Comparative representations of typical standard curves of a competitive and a sandwich assay 12
2.3	Reactions between ALP and AMPPD..... 14
2.4	Potential excitation signals used in voltammetry..... 17
2.5	Typical cyclic voltammogram for a reversible redox process..... 19
2.6	Anodic stripping voltammetry: the potential-time waveform (top), along with the resulting voltammogram (bottom)..... 21
2.7	Chronoamperometry (A) Excitation potential step; (B) Concentration profiles for various times into the experiment; (C) Chronoamperometric response..... 23
2.8	An example of a μ PAD with a central channel that wicks fluids into nine independent test zones..... 31
3.1	Schematic diagram of the proposed <i>S. typhi</i> immunoreactions 41
3.2	TEM images of the gold nanoparticles..... 42
3.3	UV-vis absorption spectra of (A) Gold(III) solution; (B) Gold nanoparticles; (C) Antibody-colloidal gold conjugate..... 43
3.4	Relationship between absorbance and antibody concentration coated on the surface of the gold nanoparticles..... 44
3.5	(A) The effect of the deposition potential of the Cu (II) ion under a 3 min deposition time with a concentration of Cu (II) 1×10^{-5} M in a 0.1 M nitric acid solution; (B) The effect of the deposition time of Cu (II) ion under a -0.5 V deposition potential with a concentration of Cu (II) 1×10^{-5} M in a 0.1 M nitric acid solution; (C) The calibration plots of the Cu (II) ion for a -0.5 V deposition potential and for a 6 min deposition

FIGURE	PAGE
time, $n = 3$	47
3.6 The effect of the copper concentration and (B) the ratio between <i>S. typhi</i> signal and the background signal. The following conditions were used: 2.6×10^3 cfu/mL of <i>S. typhi</i> , a 60 min incubation time for the <i>S. typhi</i> with the monoclonal antibody and the antibody-colloid gold conjugate, a 1:1 dilution ratio of the antibody-colloid gold conjugate, and a copper enhancement time of 10 min, $n = 3$	49
3.7 (A) The effect of the reaction time of the copper enhancer solution and (B) the ratio between <i>S. typhi</i> signal and the background signal. The following conditions were used: 2.6×10^3 cfu/mL of <i>S. typhi</i> , a 60 min incubation time for the <i>S. typhi</i> with the monoclonal antibody and the antibody-colloid gold conjugate, a 1:1 dilution ratio of the antibody-colloid gold conjugate, and the copper concentration 0.20 M, $n = 3$	52
3.8 The effect of the incubation time between the <i>S. typhi</i> and either (A) the monoclonal antibody or; (B) the antibody-colloid gold conjugate; (C) The effects of antibody-colloidal gold conjugate dilution. The same conditions were used as those in Fig. 3, $n = 3$	50
3.9 The relationship between the anodic stripping peak current and concentration of <i>S. typhi</i> (with concentrations of 0 and 1.30×10^2 to 4.30×10^3 cfu/mL). The calibration plot for the <i>S. typhi</i> determination ($1.30 \times 10^2 - 2.60 \times 10^3$ cfu/mL) is shown in the insert, $n = 3$	54
4.1 Basic design of the electrochemical detection cell for paper-based microfluidic devices. WE: working electrode, RE: reference electrode, CE: counter electrode.....	66
4.2 Picture of a three electrode paper-based microfluidic devices. The hydrophilic area at center of the device wicks sample into the three	

FIGURE	PAGE
separate test zones where independent enzyme reaction occur. The silver electrodes and contact pads are made from Ag/AgCl paste with the black electrode portions are the PB-modified carbon electrodes. The device size is 4 cm x 4 cm.....	67
4.3 Representative cyclic voltammograms of the PB-modified carbon electrodes at various scan rates (a: 2.5, b: 5, c: 10, d: 25, e: 50, f: 100 mV/s) in 0.1 M potassium phosphate buffer (pH 6).....	69
4.4 The relationship between anodic and cathodic currents and the square root of scan rate.....	70
4.5 (A) Cyclic voltammograms of the carbon mediator Prussian blue electrode in the absence (dashed line) and presence of 1 mM H ₂ O ₂ (solid line) at a 100 mV/s scan rate. (B) Hydrodynamic voltammograms of 1 mM H ₂ O ₂ (solid line), and background (dashed line) for 100 s sampling time, from 3 separate devices. (C) Hydrodynamic voltammogram of signal-to-background ratios extracted from the data shown in B.....	73
4.6 The relationship between cathodic current and hydrogen peroxide concentration in the range 0-2 mM (A) and 0-0.10 mM (B).....	74
4.7 Chronoamperograms of (A) glucose (a: 100, b: 50, c: 10, d: 2 mM, e: Bg), (B) lactate (a: 50, b: 25, c: 10, d: 2 mM, e: Bg), and (C) uric acid (a: 35, b: 20, c: 10, d: 5 mM, e: Bg) determination at 0 V versus an on-chip Ag/AgCl. The calibration plot of anodic currents at 100 s of sampling time for determination of three analytes are shown in the insert, $n = 3$	76
4.8 Design of multiple oxidative indicators for paper-based microfluidic devices which determine three analytes simultaneously with nine test zones. Back and white colors refer to hydrophobic and hydrophilic area, respectively. The device size is 2 cm x 2 cm. Position numbers 1-4: glucose test zones, 5-7: lactate test zones, 8-9: uric acid	

FIGURE	PAGE
test zones.....	90
4.9 (A) Paper-based microfluidic devices after spotting red food dyes of various volumes (0.4, 0.5, and 0.6 μL into the position numbers 1–3, 4–6, and 7–9, respectively of the detection zones). (B–E) Paper-based microfluidic devices after spotting 5 (B), 7 (C), 9 (D), and 11 μL (E) of red food dye respectively into the central of devices. (F–H) Multiple oxidative indicator for paper-based microfluidic devices after spotting level 4 of standard solution including 5 mM glucose, 10 mM lactate, and 4.5 mM uric acid with 11 μL of controlled standard volume (f) and unknown of standard volume (G and H).....	92
4.10 Multiple oxidative indicators system designed on paper-based microfluidic devices for the simultaneous semi-quantitative analysis of glucose, lactate, and uric acid. Pictures were captured after spotting varying concentration of three analytes for 10 min.....	93
4.11 Multiple oxidative indicators system designed on paper-based microfluidic devices for the simultaneous semi-quantitative analysis of glucose, lactate, and uric acid. Pictures were captured after spotting varying concentration of three analytes for 10 min.....	95
4.12 Multiple oxidative indicators system designed on paper-based microfluidic devices for the simultaneous semi-quantitative analysis of glucose, lactate, and uric acid in real biological samples.....	96
4.13 Single indicator system designed on paper-based microfluidic devices for the simultaneous semi-quantitative analysis of glucose, lactate, and numbers 1–4: glucose test zones using Y +AB indicator, 5–7: lactate test zones using Y +OD indicator, 8–9: uric acid test zones using AB indicator.....	97
4.14 Comparison of percentages of the correct answer where a corrected	

FIGURE	PAGE
answer was determined to be within ± 0.5 mM of the certified concentration between single and multiple-indicator systems ($n = 10$). U1: level I urine human, U2: level II urine human, S1: level I serum human, S2: level II serum human, error bar: standard deviation ($n = 3$).....	98
4.15 Lifetime of our devices kept at 8 °C, room temp. (~22 °C), and 40 °C. Background signals were obtained by spotting 0.1 M of phosphate buffer solution while standard test signals were obtained by spotting all levels of standard solution.....	100
4.16 Lifetime of our devices kept at 8 °C, room temperature (~22 °C), and 40 °C. Background signals were obtained by spotting 0.1 M of phosphate buffer solution while standard test signals were obtained by spotting 10 mM glucose, 20 mM lactate, and 6 mM uric acid.....	101
4.17 Schematic diagram of the fabrication step for wax screen-printing method.....	107
4.18 Picture of μ PAD for the dual electrochemical/ colorimetric method (WE: working electrode; RE: reference electrode; CE: counter electrode).....	109
4.19 Plot of the width of the resulting hydrophobic barriers after melting the wax as a function of the printed width line of wax in a) front and b) back of paper devices.....	112
4.20 Schematic representation of the spreading of wax in paper and definition of variables: W_{PC} is the printed width of the channel, W_{PB} is the printed width of the wax hydrophobic line, W_{RC} is the resulting width of hydrophilic channel after melting of wax, W_{RB} is the resulting width of hydrophobic barrier after melting of wax, L is the spreading of wax from the original edge of wax line....	113
4.21 Resolution of the wax screen-printing method showing the smallest hydrophobic barrier width.....	114

FIGURE	PAGE
4.22 Resolution of the wax screen-printing method showing the smallest hydrophilic channel width.....	114
4.23 Cross reaction test with BCA assay (A) paper devices fabricated by our method and (B) photolithography.....	116
4.24 Photographs of the result for the total iron analysis using colorimetric method.....	116
4.25 The calibration plot of total iron concentration and the red color intensity subtracting with background.....	117
4.26 Cyclic voltammograms of the carbon mediator Prussian blue electrode in the absence and presence of 0.1 mM H ₂ O ₂ , 0.5 and 5 mM of glucose at a 100 mV/s scan rate.....	118
4.27 Chronoamperograms of glucose (a: 10 mM, b: 5 mM, c: Serum level 2, d: 2.5 mM, e: Serum level 1, f: 1 mM, g: 0.5 mM, h: background) determination at -0.2 V versus an on-chip Ag/AgCl. The calibration plot of anodic currents at 20 s of sampling time for determination of three analytes are shown in the insert, $n = 3$	118
5.1 Schematic representation of bead-based chemiluminescence enzyme immunoassay for CEA detection.....	134
5.2 The relationships between concentration of FITC-labeled anti-CEA antibody and the dilution ratios of ALP-labeled anti-CEA antibody on the RLU values, using the standard CEA concentration of 162 ng/mL. The five curves were represented the different dilution ratio of ALP-labeled anti-CEA antibody at 1:500, 1:1,000, 1:2,000, 1:3,000 and 1:5,000, respectively.....	136
5.3 Physicochemical parameter optimization. (A) Influence of immunoassay incubation time on CL intensity. The antigen and antibody were incubated at different time (between 30 and 120 min) (B) Effect of the length reaction time between CL substrate and ALP-	

FIGURE	PAGE
labeled anti-CEA antibody (C) Effect of the shaking time to capture efficiency between coated micro-magnetic beads and sandwich reaction (D) Influence of the volume of magnetic beads for the CL reponse and (E) Effect of substrate volume on the bead-based chemiluminescence enzyme immunoassay response.....	141
5.4 Relationship between the dilution factor, diluted concentration and the CL intensity. (A) Linearity-dilution test curve was plotted between diluted concentration and dilution factors (B) Calibration graph of bead-based chemiluminescence enzyme immunoassay for the determination of CEA.....	143
5.5 Comparing two measurement methods, bead-based chemiluminescence enzyme immunoassay and commercial test kit, for the determination of CEA in (A) normal human serums, and (B) disease serums by spiking CEA in normal human serums.....	147

ABBREVIATIONS

A	ampere
A	electrode area
Ab	antibody
Ag	antigen
AgAb	antigen and antibody complex
ALP	alkaline phosphatase
$C_O(0,t)$	concentration of oxidized form at the electrode surface at time t
$C_R(0,t)$	concentration of reduced form at the electrode surface at time t
D	diffusion coefficient
E^0	standard potential
E_p	peak potential
$E_{p,a}$	anodic peak potential
$E_{p,c}$	cathodic peak potential
$E_{p,a}$	anodic peak potential
ELISA	enzyme-linked immunosorbent assay
F	Faraday constant (96,487 coulombs)
$i_{p,a}$	anodic peak current
$i_{p,a}$	anodic peak current
$i_{p,c}$	cathodic peak current
K	affinity constant
mol	mole
μ PAD	paper-based microfluidic device
N	number of electrons transferred in the reaction

POC	point-of-care
R	universal gas constant ($8.314 \text{ JK}^{-1}\text{mol}^{-1}$)
Re	Reynolds number
<i>S. typhi</i>	<i>Salmonella typhi</i>
T	Kelvin temperature
ν	scan rate

CHAPTER I

INTRODUCTION

1.1 Introduction

In recent years, electrochemical immunoassay has become an important analytical technique due to the combination of a highly specific immuno-interaction and highly sensitive electrochemical detection. The high specificity and affinity of an antibody for its antigen allows a selective binding of the analyte (antigen) which is present in the nano- to picomolar range in the presence of hundreds of other substances. Therefore, immunoassays can handle samples without any analyte enrichment, purification or pretreatment, which is normally necessary for standard methods such as high performance liquid chromatography (HPLC), mass spectrometry (MS) or gas chromatography (GC). Especially for clinical diagnostics, where complex samples such as whole blood, serum or urine containing different substances (i.e. proteins, amino acids, sugars, hormones etc.) have to be analyzed, immunoassays have considerable advantages over standard methods with respect to sample preparation time [1]. Electrochemical techniques are well known, inexpensive and highly sensitive analysis methods. Moreover, it can be miniaturized and does not need large energy sources [2-4]. After specific immunointeraction occurs, electrochemistry was used for measuring the amount of electroactive label conjugated to either the antibody or the antigen or the amount of electroactive substrate produced from an enzyme label.

From report of bureau of general communicable disease (department of disease control MOPH, Thailand), an estimated 135,563 illnesses and 5 deaths are attributable to food borne illness in Thailand in 2006 [5]. Furthermore, there is an increasing tendency for food borne illness from 209.04 to 226.62 illnesses per 100,000 populations during 2003-2006. *Escherichia coli*, *Listeria monocytogenes*, *Campylobacter jejuni*, and *Salmonella* have been identified as the major food borne pathogens in Thailand. Conventional methods for pathogen identification involve pre-enrichment growth,

selective enrichment culture and selective diagnostic plating followed by biochemical identification and serological confirmation of the results. The whole procedure takes typically between 7 and 10 days. There is a range of so called rapid methods available on the market, mostly based on immunological identification techniques. These methods typically detect culture densities of 10^4 - 10^6 colony-forming units (cfu)/ml which are applied after the selective enrichment step and cutting the total identification time by 3-5 days. While faster than traditional assays, a method for pathogenic bacteria detection with increased sensitivity and selectivity and a reduction in analysis time is still needed. Electrochemical immunoassays have been an attractive alternative method for pathogenic bacteria detection due to many merits [2-4]. Therefore, the development of electrochemical immunoassay for pathogenic bacteria detection in real samples with a low limit of detection, high accuracy, and fast analysis time is one aim of this research. *Salmonella typhi* (*S. typhi*) was used as the model to evaluate our developed method. The motivation and detail of method development are described in Chapter III [6].

In addition to the electrochemical immunoassay development, one of long term goals is to develop miniaturized immunoassay devices which would enable us to measure analytes at the point-of-care (POC), e.g. for doctors offices, small clinical laboratories, patient self-control and field measurements. Paper strip tests are suited to portable POC diagnostics and on-site detection because they hold great promise for improving global health, and other applications [7]. These devices are easy to handle, reliable, inexpensive and produce results within a few minutes. Paper strip tests are commercially available for pregnancy [8], diabetes [9,10], drugs of abuse [11,12], and biomarkers of pathogens test [13,14]. A well-known example is the pregnancy test strip that uses an immunochromatographic technique for separation and detection. Typically, these tests are based on a strip of paper (or membrane) modified with a capture antibody specific to an antigen of interest. When the sample is applied, the antigen binds to conjugate antibody which is conjugated to a signal indicator (e.g., colloidal gold). The antigen/conjugate antibody complex flows along the paper matrix, which is driven by the capillary force, and is subsequently captured by the capture antibody on the paper strip. A colorimetric signal can be visualized within a few minutes, indicating the presence of

the target antigen [15,16]. Although they have many advantages suited to portable POC diagnostics, they are normally not capable of doing multiplex and quantitative analysis. Recently, paper-based microfluidic devices (μ PADs), representing the next generation of paper strip test devices, have been introduced by Whitesides and coworkers [17-19]. μ PADs combines many advantages of paper strip tests with the utility of microfluidics. They have the potential to be good alternatives for point-of-care testing over traditional paper strip tests because they are capable of simultaneous multiplex analyte detection. Most μ PADs use visible color changes (known as colorimetric detection) for qualitative analyte detection. However, qualitative analysis is not sufficient when analyte levels are important for diagnosis or treatment. Much effort has therefore been directed towards the development of quantitative μ PADs. One of our approaches to overcome the limitations of colorimetric methods for μ PADs is to use multiple indicators for a single analyte. Greater visual discrimination is possible when more than one color is developed as opposed to different hues or intensities of a single color [20]. Our research also developed the first prototype of electrochemical detection for μ PADs. Moreover, the novel fabrication method for μ PADs was invented with a reduced fabrication costs, time and requiring minimal external instrumentation for implementation in developing countries. Chapter IV describes the design and fabrication method for both electrochemical detection and μ PADs [21,22].

Lastly, improvements in the sensitivity of immunoassays were studied in our research because small increases or decreases in levels of some analytes e.g. pathogenic bacteria or tumor markers can be indicative of disease progression or early recurrence of disease [23-25]. To reach our goal, a small volume magnetic microbead-based immunoassay is being developed to increase the surface area for immobilization of antigen or antibody [26,27]. Tumor marker was used as the model in this section because a sensitive and rapid method for the tumor marker analysis is still needed for making a commercial tumor marker test kits [28,29]. Therefore, magnetic microbead-based immunoassay for the determination of tumor marker in human serum was preliminary to demonstrate the sensitivity enhancing of method as described in Chapter V [30].

1.2 Research objective

There are three targets for this research.

1. To develop the electrochemical immunoassay for *S. typhi* determination in real samples with a low limit of detection, high accuracy, and fast analysis time.
2. To invent inexpensive paper devices for point of care testing.
 - 2.1. To improve the greater visual discrimination of colorimetric detection for μ PADs
 - 2.2. To develop the first prototype of electrochemical detection for μ PADs.
 - 2.3. To invent a novel fabrication method for μ PADs with a reduced fabrication cost, time and requiring minimal external instrumentation for implementation in developing countries.
3. To improve sensitivity of immunoassay using a micro-magnetic bead.

1.3 Scope of research

To achieve the research objectives, the following scope was set.

1. The critical parameters for electrochemical immunoassay based on copper-enhanced gold nanoparticle label such as concentration of copper and gold, incubation time, and deposition potential of copper were optimized by anodic stripping voltammetry on glassy carbon electrode. Electrochemical immunoassay based on copper-enhanced gold nanoparticle label was also applied for *S. typhi* determination in real sample under optimal condition.
2. The use of multiple indicators for a single analyte for μ PADs was studied in an effort to improve the ability to visually discriminate between analyte concentrations. The utility of our approach was demonstrated by using the mixture of indicators for simultaneous semi-quantitative measurement of glucose, lactate, and uric acid on a μ PAD.

3. Electrochemical detection for μ PADs was designed and constructed. The utility of our devices was then demonstrated for the determination of glucose, lactate, and uric acid in biological samples using oxidase enzyme (glucose oxidase, lactate oxidase, and uricase, respectively) reactions.
4. Wax screen-printing is developed for fabricating μ PADs. The utility of wax screen-printing was demonstrated for the simultaneous determination of glucose and total iron in control human serum samples using an electrochemical method with glucose oxidase and a colorimetric method with 1,10-phenanthroline.
5. The important parameters for a micro-magnetic bead chemiluminescence enzyme immunoassay such as bead volume, incubation time, and shaking time of bead were studied. The determination of carcinoembryonic antigen in real sample was used as the model to demonstrate the utility of a high sensitive micro-magnetic bead chemiluminescence enzyme immunoassay.

There are six chapters in this research. Chapter I is the introduction. Chapter II gives theory for this research including the electrochemical technique, immunoassay, bacterial pathogenic and paper-based microfluidics. Chapter III reports on an electrochemical stripping metalloimmunoassay based on copper-enhanced gold nanoparticle label for the *S. typhi* determination. Chapter IV presents the development of μ PADs for biomarker analysis. Chapter V is improving sensitivity of enzyme immunoassay using micro-magnetic bead. Lastly, Chapter VI is the conclusions and future perspectives.

1.4 Research utilization

1. Obtain the novel knowledge about electrochemical immunoassay, paper-based microfluidics and enhancing sensitivity of immunoassay technique for analytical and bioanalytical application.
2. Obtain high accurate, sensitivity, and low-cost technique for *S. typhi* determination in real samples.

3. Succeed in inventing the paper-based microfluidic devices coupled with electrochemical detection.
4. Succeed in improving the sensitivity of immunoassay.
5. Obtain the model test kit for biomarker analysis and bacterial pathogenic detection.

1.5 References

- [1] Warsinke, A.; Benkert, A.; Scheller, F. W. Electrochemical immunoassays. Fresenius J. Anal. Chem. 366 (2000): 622-634.
- [2] Dong, H.; Li, C. M.; Zhou, Q.; Sun, J. B.; Miao, J. M. Sensitive electrochemical enzyme immunoassay microdevice based on architecture of dual ring electrodes with a sensing cavity chamber. Biosens. Bioelectron. 22 (2006): 621-626.
- [3] Preechaworapun, A.; Ivandini, T. A.; Suzuki, A.; Fujishima, A.; Chailapakul, O.; Einaga, Y. Development of amperometric immunosensor using boron-doped diamond with poly(o-aminobenzoic acid). Anal. Chem. 80 (2008): 2077-2083.
- [4] Preechaworapun, A.; Dai, Z.; Xiang, Y.; Chailapakul, O.; Wang J. Investigation of the enzyme hydrolysis products of the substrates of alkaline phosphatase in electrochemical immunosensing. Talanta. 76 (2008): 424-431.
- [5] Bureau of general communicable disease. Annually report. Department of disease control MOPH: Thailand, 2009.
- [6] Dungchai, W.; Siangproh, W.; Chaicumpa, W.; Tongtawe, P.; Chailapakul O. *Salmonella typhi* determination using voltammetric amplification of nanoparticles: A highly sensitive strategy for metalloimmunoassay based on a copper-enhanced gold label. Talanta. 77 (2008): 727-732.
- [7] Zhao, W.; Van den Berg, A. Lab on paper. Lab on Chip. 8 (2008): 1988-1991.
- [8] One Step HCG Urine Pregnancy Test (Strip). Shandong China: AI DE Diagnostica Co. Ltd., 2009.
- [9] Hones, J.; Muller, P.; SurrIDGE, N. The technology behind glucose meters: test strips. Diabetes Technol. Ther. 10 (2008): S10-S26.

- [10] Kristensen, G. B .B.; Monsen, G.; Skeie, S.; Sandberg, S. Quality Assurance of Self-monitoring of Blood Glucose at the General Practitioner's Office. Point of Care. 5 (2006): 100-104.
- [11] Penttila, A.; Karhunen, P. J.; Pikkarainen, J. Alcohol screening with the Alcoscan test strip in forensic praxis. Forensic Sci. Int. 44 (1990): 43-48.
- [12] One Step Drugs of Abuse Test. Beijing China: Core Technology Co. Ltd., 2009.
- [13] Oberhofer, T. R.; Towle, D. W. Evaluation of the rapid penicillinase paper strip test for detection of beta-lactamase. J. Clin. Microbiol. 15 (1982): 196-199.
- [14] Mosley, L. M.; Sharp D. S. The hydrogen sulphide (H₂S) paper strip test. SOPAC Technical Report 373 (2005).
- [15] Von Lode, P. Point-of-care immunotesting: approaching the analytical performance of central laboratory methods. Clin. Biochem. 38 (2005): 591-606.
- [16] Mabey, D.; Peeling, R. W.; Ustianowski, A.; Perkins, M. D. Diagnostics for the developing world. Nat Rev Microbiol. 2 (2004): 231-240.
- [17] Martinez, A. W.; Phillips, S. T.; Butte, M. J.; Whitesides, G. M. Patterned Paper as a Platform for Inexpensive, Low-Volume, Portable Bioassays. Angew. Chem. Int. Ed. 46 (2007): 1318-1320.
- [18] Bruzewicz, D. A.; Reches, M.; Whitesides, G. M. Low-Cost Printing of Poly(dimethylsiloxane) Barriers To Define Microchannels in Paper. Anal. Chem. 80 (2008): 3387-3392.
- [19] Martinez, A. W.; Phillips, S. T.; Carrilho, E.; Thomas, S. W.; Sindi, H.; Whitesides, G. M. Simple Telemedicine for Developing Regions: Camera Phones and Paper-Based Microfluidic Devices for Real-Time, Off-Site Diagnosis. Anal. Chem. 80 (2008): 3699-3707.
- [20] Fung, K. K.; Chan, C. P. Y.; Renneberg, R. Development of enzyme-based bar code-style lateral-flow assay for hydrogen peroxide determination. Anal. Chim. Acta 634 (2009): 89-95.
- [21] Dungchai, W.; Chailapakul, O.; Henry, C. S. Electrochemical Detection for Paper-Based Microfluidics. Anal. Chem. 81 (2009): 5821-5826.

- [22] Dungchai, W.; Chailapakul, O.; Henry, C. S. Use of multiple colorimetric indicators for paper-based microfluidic devices. Anal. Chim. Acta 674 (2010): 227-233.
- [23] Mayer, R. J. Scientific American Medicine. New York: Scientific American, 1996.
- [24] Delwiche, R.; Zamcheck, N.; Marcon, N. Carcinoembryonic antigen in pancreatitis. Cancer, 31 (1973): 328-330.
- [25] Loewenstein, M. S.; Zamcheck, N. Carcinoembryonic antigen (CEA) levels in benign gastrointestinal disease states. Cancer, 42 (1978): 1412-1418.
- [26] Farrell, S.; Ronkainen-Matsuno, N. J.; Halsall, H. B.; Heineman, W. R. Bead-based immunoassays with microelectrode detection. Anal Bioanal Chem, 379 (2004): 358-367.
- [27] Biagini, R. E.; Smith, J. P.; Sammons, D. L.; MacKenzie, B. A.; Striley, C. A. F.; Robertson, S. K.; Snawder, J. E. Development of a sensitivity enhanced multiplexed fluorescence covalent microbead immunosorbent assay (FCMIA) for the measurement of glyphosate, atrazine and metolachlor mercapturate in water and urine. Anal Bioanal Chem, 379 (2004): 368-374.
- [28] Carcinoembryonic Antigen (CEA) Enzyme Immunoassay Test Kit, Catalog Number: BC-1011, California, Biocheck Inc.
- [29] CEA ELISA Kit, Catalog Number: EK-38, Budapest Hungary, Institute of Isotopes Ltd.
- [30] Dungchai, W.; Siangproh, W.; Lin, J. M.; Chailapakul, O.; Lin, S.; Ying, X. Development of a sensitive micro-magnetic chemiluminescence enzyme immunoassay for the determination of carcinoembryonic antigen Anal. Bioanal. Chem. 387 (2007): 1965-1971.

CHAPTER II

THEORY AND LITERATURE SURVEY

2.1 Immunoassay [1,2]

Immunoassay is an assay that quantifies antigen (a stimulating molecule) or antibody (an immuno-response molecule) by immunochemical means. The antigen can be a relatively simple substance such as a drug, or a complex one such as a protein, bacteria, or a virus. Immunoassay as an analytical technique was introduced by Rosalind Yalow and Solomon Berson in 1960 with their use of anti-insulin antibodies to measure the concentration of the hormone in plasma [1]. This advance, for which Rosalind Yalow was awarded the Nobel Prize, was probably the most important single advance in biological measurement of the following two decades. Examples of the use of immunoassay may now be found in almost all areas of analytical biochemistry. The antigen-antibody interaction is reversible and does not involve the formation of covalent bond. This interaction is controlled by the law mass action:



$$\text{And} \quad K = [\text{AgAb}] / [\text{Ag}] [\text{Ab}] \quad \text{mol}^{-1} \quad (2)$$

Where K is the affinity constant, Ag is antigen, Ab is antibody, and AgAb is the antigen and antibody complex. High affinity constant, resulting from strong AgAb reaction, lead to lower limits of detection (LOD) in immunoassays.

Two general systems of immunoassays can be basically differentiated. The competition assay is based on the competition between antigen labeled with a molecule which may be readily observed (for example, radioisotope, enzyme) and unlabeled antigens for a limited number of antigen binding sites. The second, also very popular, variation is the sandwich assay. Figure 2.1 clarifies the fundamental principles of the different immunoassay concepts.

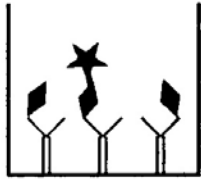
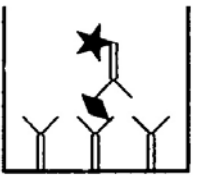
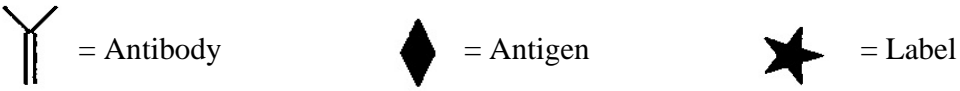
Immunoassays	Schematic diagram	
1. Competitive assay		<ul style="list-style-type: none"> - Control the labeled antigen level - Measure the antigen - Inversely relate to the concentration of antigen in the unknown
2. Sandwich assay		<ul style="list-style-type: none"> - Control the labeled antibody level - Measure the antigen - Directly relate to the concentration of antigen in the unknown
		

Figure 2.1 Schematic diagrams of the different immunoassay concepts.

The competitive assay is based on competition of two antigen populations for the same free binding sites of an antibody population in a defined volume of solution. One of the two antigen populations consists of labeled antigens; the other is made up of similar but unlabelled antigens. A competitive assay thus requires labeled antigens, unlabeled antigens for the standard curve, a monoclonal antibody and/or an antiserum that specifically binds to its antigen, and, of course, specimens containing antigens.

If the concentration of free binding sites is steady, and the antibody concentration, the concentration of the labeled antigens, and the fluid volume in all the starting solutions are steady as well, the quantity of unlabeled antigens in the solution can be determined. The more unlabeled antigens present in the specimen and the more labeled antigens are displaced from the binding sites. Therefore, a high concentration of unlabeled antigens in the sample means a weak label signal in the found fraction and vice versa. In order for the competition principle to function, the free binding sites must be the limiting factor in

the solution. Ideally, the antibodies and labeled antigen are employed in such a way that about 50% of the labeled antigens are sufficient to occupy all binding sites. Figure 2.2 shows a typical standard curve of a competitive and sandwich assay [2]. The sigmoid course of the curve shows the reduction of the label signal in the bound fraction, with an increasing concentration of unlabeled antigens. In order to facilitate the analysis, one can transform this standard curve into a semi-logarithmic and/or a double-logarithmic representation.

A sandwich assay also referred to the noncompetitive immunoassays. Antigen in the unknown is bound to the antibody site, and then labeled antibody is bound to the antigen. The amount of labeled antibody on the site is measured and directly related to the amount of antigen. Unlike the competitive method, the results of the sandwich assay method will be directly proportional to the concentration of the antigen (Figure 2.2).

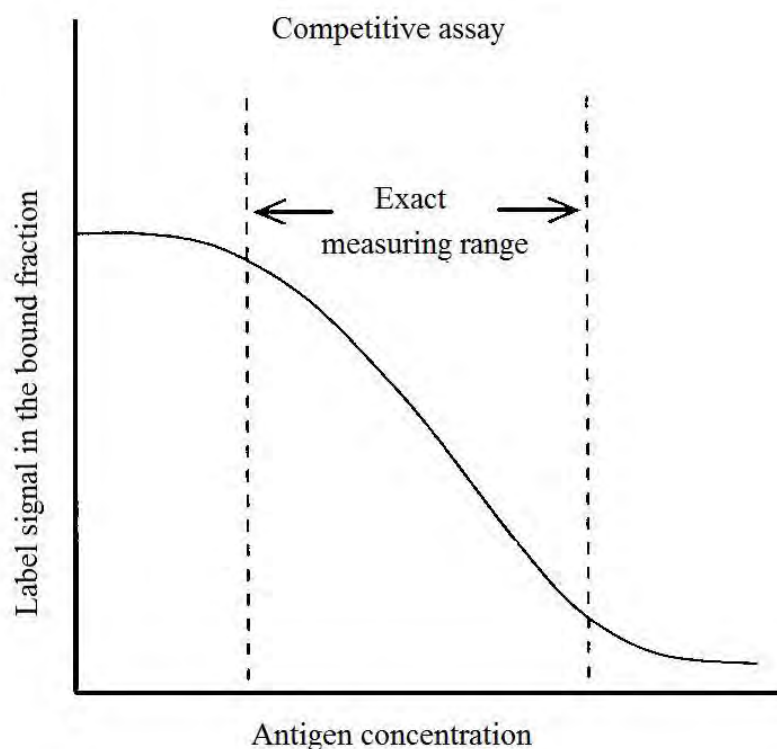


Figure 2.2 Comparative representations of typical standard curves of a competitive and a sandwich assay.

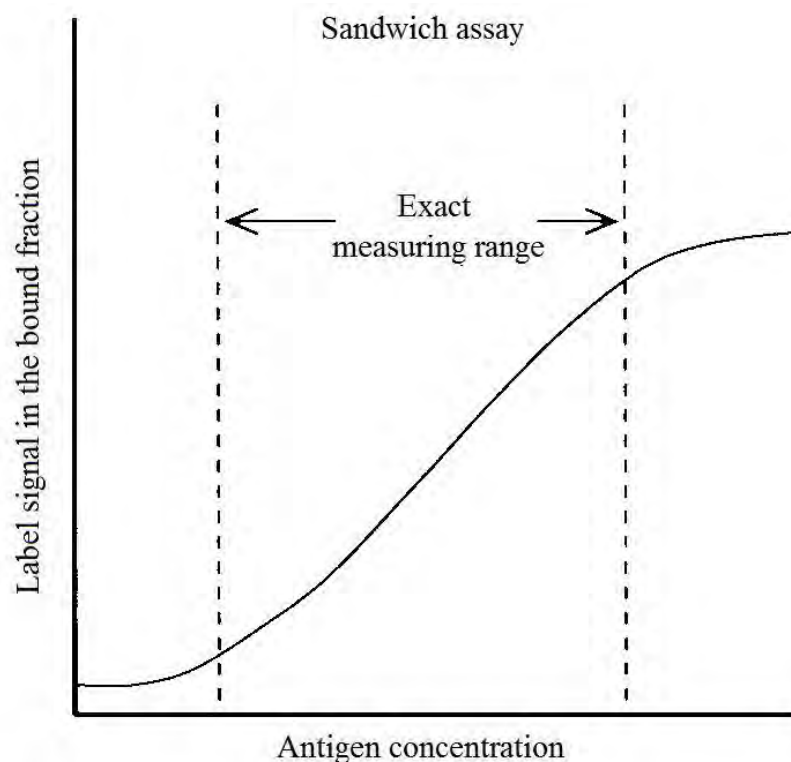


Figure 2.2 Comparative representations of typical standard curves of a competitive and a sandwich assay.

Immunoassays require a pure sample of antigen or antibody for labeling with an appropriate molecule. Such a molecule should retain high signal efficiency while its incorporation into the antigen or antibody should have no effect on their subsequent immunoreactivity. The most common labels are listed in Table 2.1.

Table 2.1 Detector system commonly used in immunoassay

Detector system	Molecules used in detection system
Radioisotopes	Iodine-125, Carbon-14, Tritium
Enzymes	Horseradish peroxidase, Alkaline phosphatase, β -Galactosidase
Chemiluminescence	Luminol, Acridinium esters, Adamantyl dioxetane
Fluorescence	Fluorescein, Rhodamine, Europium chelates

Detector system	Molecules used in detection system
Bioluminescence	Luciferase/Luciferin
Metal nanoparticles	Gold nanoparticles, Silver nanoparticles, Quantum dots

Enzyme and metal nanopertical label used in this work are described here. Enzyme labels are usually associated with solid-phase antibody in the technique known as enzyme-linked immunosorbent assay (ELISA). There are several variants of this technique employing both competitive and non-competitive systems. However, it is the best to use the combination with two monoclonal antibodies in the ‘two-site’ format in which an excess of antibody is bound to a solid phase such as a test-tube or microtitre plate; the test antigen is then added and is largely sequestered by the antibody. After washing to remove the remaining biological material a second, enzyme-labeled, monoclonal antibody is added which recognizes a different epitope on the antigen (the second site), thus the sandwich antigen between the enzyme-labeled and the solid-phase antibodies occurs. The excess enzyme-antibody is wash away before addition of a suitable substrate and development of a color which is measured either kinetically or as an end-point reaction.

The enzymes used should be capable of being covalently linked to the antigen or antibody without loss of either catalytic activity or immunoreactivity. The choice of enzymes is governed by the availability of substrate and the type of detector. Several substrates have been developed for use with alkaline phosphatase (ALP): 4-methoxy-4-(3-phosphate-phenyl)-spiro-(1,2-dioxetane-3,2'-adamantane) (AMPPD), 2-phospho-l-ascorbic acid, and 4-nitrophenol phosphate. In this work, ALP is used to react with AMPPD for chemiluminescence detection. The reaction between AMPPD and ALP is shown in Figure 2.3 [3].

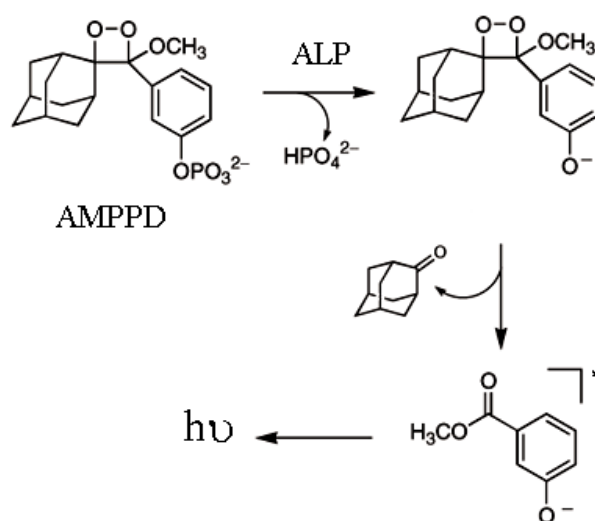


Figure 2.3 Reactions between ALP and AMPPD.

Metal nanoparticles act as a class of labels with many unique features, such as optical, electronic, and catalytic properties, that have been previously explored for potential applications in biomolecular detection. Metal nanoparticles are usually used in non-competitive system for the electrochemical detection because metal nanoparticle label can enhance the sensitivity of the electrochemical immunoassay technique. Amplified electrochemical detection of biological molecules was achieved by the dissolution of the metallic nanoparticles and by recording the subsequent electrochemical stripping of the dissolved ions. Gold-labeled antibodies are used in this work for the detection of antigens due to its electron density and long durability. The labeling of antibodies with colloidal gold occurs via the adsorption of the protein to the surface of the gold particles. The binding is stabilized by interactions between the negatively charged surface of the gold particles with the positively charged amino acid residues of the protein, as well as by hydrophobic interaction between the particle surface and the aromatic amino acid residues.

2.2 Electrochemical Method [4-7]

Electrochemistry is concerned with the interplay between electricity and chemistry, namely the measurements of electrical quantities, such as current, potential,

and charge, and their relationship to chemical parameters. Electrochemical methods are the important method for analytical chemistry which based on the monitoring of changes in an electrical signal occurring from the electrochemical reaction at an electrode surface. Such use of electrical signal measurements has provided many applications, including environmental monitoring, industrial quality control, and biomedical analysis. The two principal types of electrochemical methods are potentiometric and potentiostatic technique. Both types require at least two electrodes (conductors including working and reference electrode) and a contacting sample (electrolyte) solution, which construct the electrochemical cell. The reference electrode is of constant potential and the working electrode responds to the target analytes. Electrochemical cells can be classified as electrolytic cell when they consume electricity from an external source or galvanic cell when they are used to produce electric energy.

The first technique, potentiometric technique, is a static (zero current) technique in which the information about the sample composition is obtained from measurement of the potential established across membrane. Potentiometric techniques have been widely used for several decades for direct monitoring of ionic species such as protons or calcium, fluoride, and potassium ions in complex samples. The second one, potentiostatic technique, is based on dynamic (no zero current) situations. Here, the externally potential is used to drive an electron-transfer reaction, and the resultant current is measured. The current response related to the concentration of the target analyte is accomplished by monitoring the transfer of electrons during the redox process of the analyte:



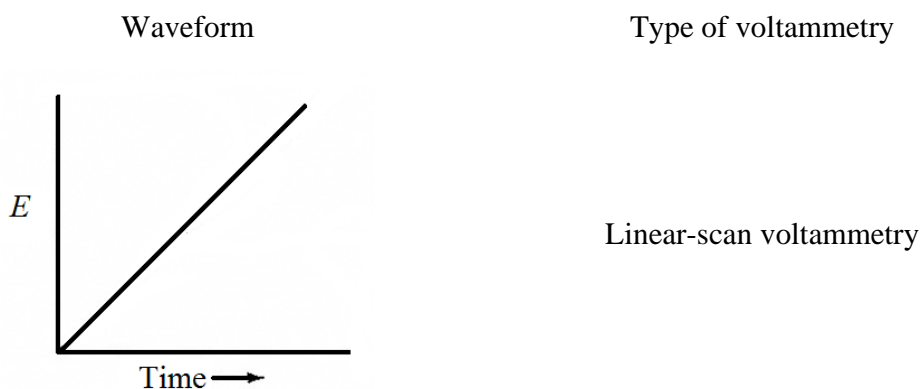
O and R are the oxidized and reduced forms, respectively, of the redox couple. Such reaction will occur in a potential region that makes the electron transfer thermodynamically or kinetically favorable. For systems controlled by the laws of thermodynamics, the potential of the electrode can be used to establish the concentration of the electroactive species at the surface represented by $C_O(0,t)$ and $C_R(0,t)$ according to the Nernst equation:

$$E = E^0 + \frac{2.3RT}{nF} \log \frac{C_{\text{O}}(0,t)}{C_{\text{R}}(0,t)} \quad (4)$$

E^0 is the standard potential for the redox reaction. R is the universal gas constant ($8.314 \text{ JK}^{-1}\text{mol}^{-1}$), T is the Kelvin temperature, n is the number of electrons transferred in the reaction, and F is the Faraday constant ($96,487 \text{ coulombs}$). On the negative side of E^0 , the oxidized form thus tends to be reduced, and the forward reaction (i.e., reduction) is more favorable. In this section some potentiostatic techniques used in this work including cyclic voltammetry, anodic stripping voltammetry, amperometry, and chronoamperometry are described respectively.

2.2.1 Voltammetry [4,7]

Voltammetry is that class of electroanalytical measurements, in which information about the analyte is derived from the measurement of current, as a function of applied potential. The signal, in the form of current as a function of potential obtained, is called voltammogram. The most common waveforms used in voltammetry are shown in Figure 2.4. The electrochemical cell is made up of three electrodes immersed in a solution containing the analytes and also an excess of nonreactive electrolytes called a supporting electrolyte.



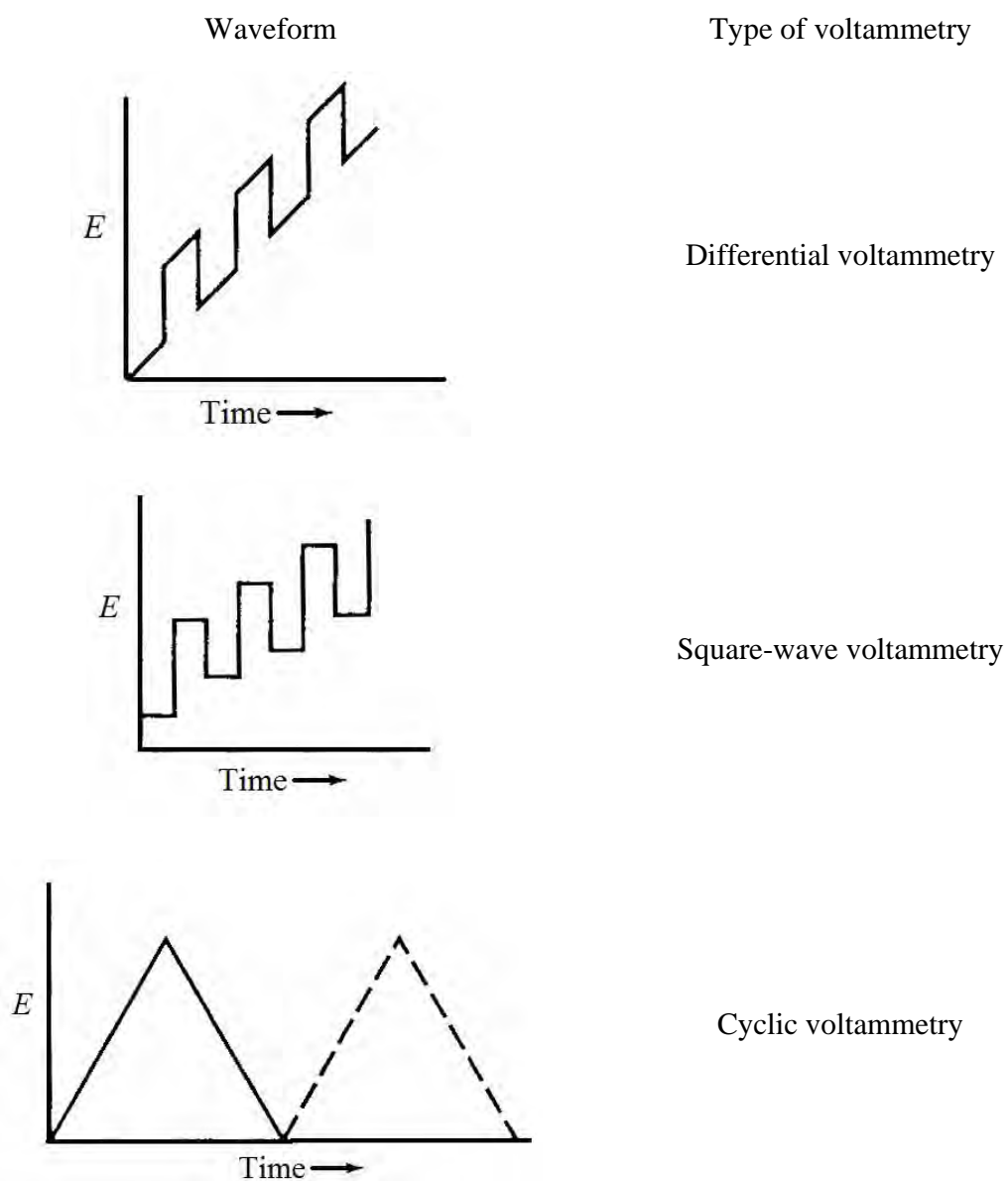


Figure 2.4 Potential excitation signals used in voltammetry [4].

2.2.1.1 Cyclic Voltammetry [4,5]

Cyclic voltammetry is the most widely used technique for acquiring qualitative information about electrochemical reactions but it is rarely used for quantitative determinations. The power of cyclic voltammetry results from its ability to rapidly

provide considerable information on the thermodynamic of redox processes and the kinetic of heterogeneous electrontransfer reaction, and on coupled chemical reactions or adsorption processes. In this work, cyclic voltammetry was used for the characterization of our developed electrochemical detection for paper-based Microfluidic devices.

Cyclic voltammetry consists of scanning linearly the potential of a stationary working electrode (in an unstirred solution), using a triangular potential waveform. Depending on the information sought, single or multiple cycles can be used. During the potential sweep, the potentiostat measures the current resulting from the applied potential. The resulting plot of current versus potential is termed a cyclic voltammogram. Figure 2.5 shows the expected voltammogram of a reversible redox couple during a single potential cycle. It is assumed that only the oxidized form (O) is present initially. Thus, a negative-going potential scan is chosen for the first half cycle, starting from a value where no reduction occurs. As the applied potential approaches the characteristic E^0 for the redox process, a cathodic current begins to increase, until a peak is reached. After traversing the potential region in which the reduction process takes place (at least $90/n$ mV beyond the peak), the direction of the potential sweep is reversed. During reverse scan, R molecules generated in the forward half cycle and accumulated near the electrode surface are reoxidized back to O as shown in an anodic peak results.

The voltammogram is characterized by a peak potential, E_p , at which the current reaches its maximum value and that value is called the peak current, i_p . The $i_{p,a}$ and $E_{p,a}$ are anodic peak current and anodic peak potential, respectively. The $i_{p,c}$ and $E_{p,c}$ are cathodic peak current and cathodic peak potential, respectively. The current peaks are commonly measured by extrapolating the preceding baseline current. The peak current for a reversible couple is given by the Randles-Sevcik equation:

$$i_p = (2.69 \times 10^5) n^{3/2} A C D^{1/2} v^{1/2} \quad \text{at } 25 \text{ }^\circ\text{C} \quad (5)$$

where i_p is in A, A (electrode area) is in cm^2 , D (diffusion coefficient) is in $\text{cm}^2 \text{ s}^{-1}$, C

(concentration of electroactive species) is in mol cm^{-3} , and ν (scan rate) is in V s^{-1} .

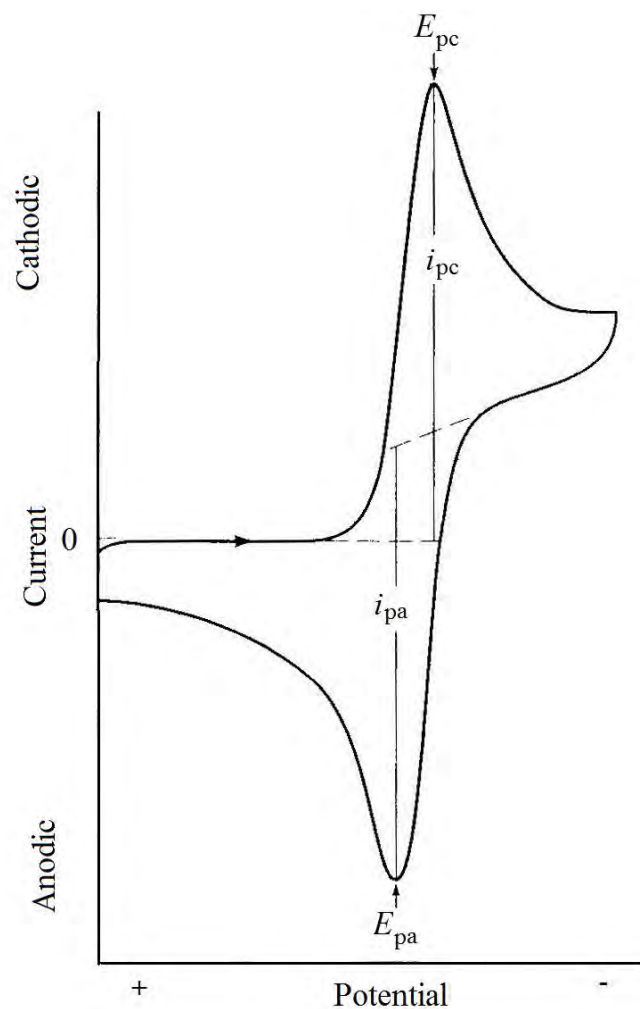


Figure 2.5 Typical cyclic voltammogram for a reversible redox process [4].

The ratio of the reverse-to-forward peak currents, $i_{p,a}/i_{p,c}$, is unity for a simple reversible couple. As will be discussed in the following sections, this peak ratio can be strongly affected by chemical reaction coupled to the redox process. The peak potential (E_p) is related to the formal potential of the redox process. The formal potential for a reversible couple is centered between $E_{p,a}$ and $E_{p,c}$:

$$E^0 = \frac{E_{p,a} + E_{p,c}}{2} \quad (6)$$

The separation between the peak potential for a reversible couple is given by:

$$\Delta E_p = E_{p,a} - E_{p,c} = 0.059/n \quad \text{V} \quad (7)$$

2.2.1.2 Stripping Voltammetry [6]

Stripping analysis is an extremely sensitive electrochemical technique for measuring trace metals. Its remarkable sensitivity is attributed to the combination of an effective preconcentration step with advanced measurement procedures that preconcentrated into electrode by factor of 100-1,000, detection limits are lowered by 2-3 orders of magnitude compared to solution phase voltammetric measurements. Essentially, stripping analysis is a two-step technique. The first, or deposition step, involves the electrolytic deposition of a small portion of the metal in solution into electrode surface to preconcentration the metals. This followed by the stripping step (the measurement step), which involves the dissolution (stripping) of the deposit. Different of stripping analysis can be employed, depending upon the nature of the deposition and measurement steps.

With the development of nanotechnology, various metal nanoparticles (i.e., gold, silver, copper) have been used as labels to enhance the sensitivity of the electrochemical immunoassay technique. Therefore, the anodic stripping voltammetry is among the best method for the detection of metal labels related to the amount of analyte. In anodic stripping methods, the metals are preconcentrated by electrodeposition on an electrode surface. The preconcentration is done by cathodic deposition at a controlled time and potential. The cathodic deposition potential is usually 0.3-0.5 V more negative than E^0 for the least easily reduced metal ion to be determined. Then, the deposited metals are dissolved into the solution by anodic potential. The potential-time sequence used in anodic stripping voltammetry, along with the resulting linear stripping voltammogram, is shown in Figure 2.6.

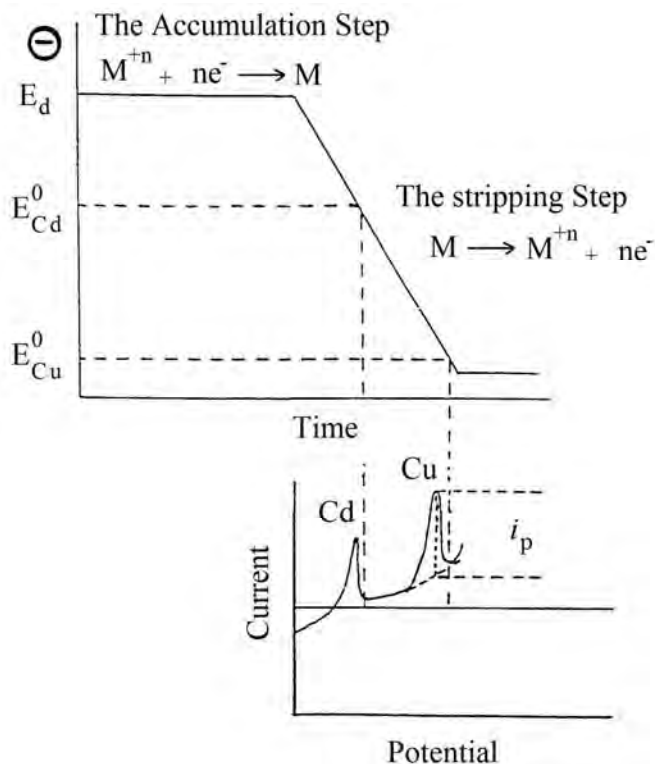


Figure 2.6 Anodic stripping voltammetry: the potential-time waveform (top), along with the resulting voltammogram (bottom) [6].

2.2.2 Chronomethods [4]

Chronomethods is the method in which the dependence of an electrical signal on time is measured. The electrical parameter measured may be current, charge, or potential as a function of time. In this thesis, the current was measured, in which the process is initiated by a potential step known as the chronoamperometry. The excitation signal, concentration profiles, and form of the observed output are shown in Figure 2.7. In chronoamperometric measurement, the initial potential is normally set sufficiently anodic (or cathodic) potential that the oxidation (or reduction) process occurs. As mass transport under these conditions is solely by diffusion, the current-time curve reflects the change in the concentration gradient in the vicinity of the electrode surface. The current that flows will then decay from infinity associated with the depletion of the reactant on the electrode

surface. The observed finite limit is because of the speed of response of the recording device used, as is the subsequent very rapid initial exponential decay.

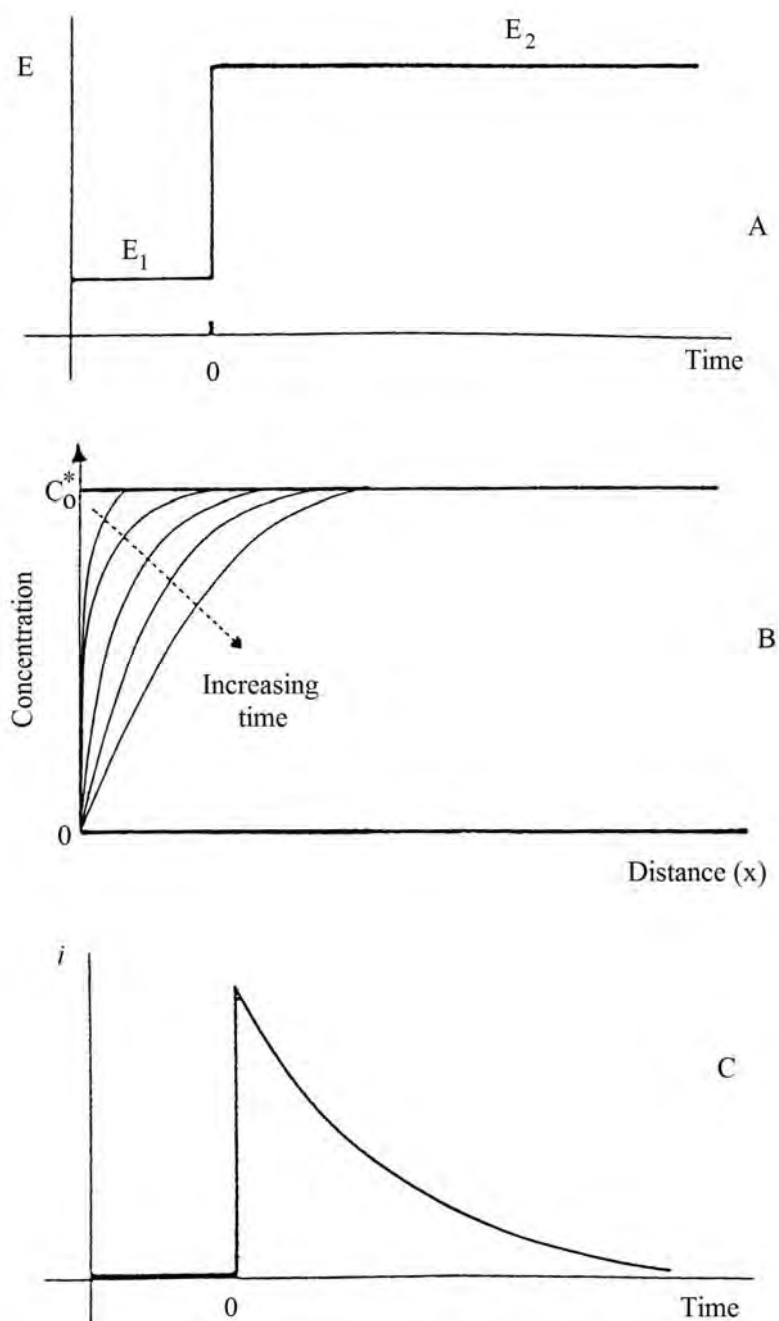


Figure 2.7 Chronoamperometry (A) Excitation potential step; (B) Concentration profiles for various times into the experiment; (C) Chronoamperometric response [4].

Accordingly, the current (at a planar electrode) decays with the time (Figure 2.7C), as given by the Cottrell equation:

$$i(t) = \frac{nFACD^{1/2}}{\pi^{1/2}t^{1/2}} = kt^{-1/2} \quad (8)$$

Chronoamperometry was used instead of cyclic voltammetry for many electrochemical biosensors because it gives a better signal to noise, can achieve lower detection limits, and. This technique is also an easier detection method to implement for immunoassay test strip in the long-term applicability.

2.3 Pathogenic Bacteria [8-12]

Pathogenic bacteria are bacteria that cause infectious diseases. This work deals with human pathogenic bacteria. Infectious diseases account for nearly 40% of the total 50 million annual estimated deaths worldwide. Infectious diseases occurring from pathogenic bacteria are the major cause of death in many developing countries. Increasing numbers of bacteria have been identified as important food-borne and water-borne pathogens. The yearly incidence of food-borne illness was found several million cases to 81 million cases in USA [8]. Food and drinking water are an essential part of the human diet, and contamination of municipal and other supplied food or water with pathogenic microorganisms constitutes a serious threat to public health [9]. Numerous examples of disease caused by the contamination of municipal food and water with microorganisms have been reported worldwide, including outbreaks in Albany, NY, USA, Canada, and Thailand [10,11]. So, these problems should be paid attention. One of the bacterial diseases with highest disease burden is tuberculosis, caused by the bacterium *Mycobacterium tuberculosis*, which kills about 2 million people a year, mostly in sub-Saharan Africa. Pathogenic bacteria contribute to other globally important diseases, such as pneumonia, which can be caused by bacteria such as *Streptococcus* and *Pseudomonas*, and foodborne illnesses, which can be caused by bacteria such as *Shigella*,

Campylobacter and *Salmonella*. Pathogenic bacteria also cause infections such as tetanus, typhoid fever, diphtheria, syphilis and leprosy.

Two broad qualities of pathogenic bacteria underlie the means by which they cause disease. The first, invasiveness is the ability to invade tissues. It encompasses mechanisms for colonization (adherence and initial multiplication), production of extracellular substances which facilitate invasion (invasins) and ability to bypass or overcome host defense mechanisms. The second one, toxigenesis is the ability to produce toxins. Bacteria may produce two types of toxins called exotoxins and endotoxins. Exotoxins are released from bacterial cells and may act at tissue sites, and are removed from the site of bacterial growth. Endotoxins are cell-associated substance. The term endotoxin refers to the lipopolysaccharide component of the outer membrane of Gram-negative bacteria. However, endotoxins may be released from growing bacterial cells by cell lysis that is a result of effective host defense (e.g. lysozyme) or the activities of certain antibiotics (e.g. penicillins and cephalosporins). Hence, bacterial toxins, both soluble and cell-associated, may be transported by blood and lymph and cause cytotoxic effect at tissue sites which remote from the original point of invasion or growth. Some bacterial toxins may also act at the site of colonization and play an important role in invasion.

The bacterial infections are usually diagnosed by specific laboratory tests that identify the causative organism. Table 2.2 shows the clinical characteristics of some pathogenic bacterium. Bacteria such as *Campylobacter*, *Salmonella*, *E. coli* O157 are found by culturing stool samples in the laboratory and identifying the bacteria that grow on the agar or other culture medium. Many bacterial infections are not identified by routine laboratory procedures but they require specialized, experimental, and/or expensive tests such as immunoassay, serological methods (i.e., slide agglutination and the Widal test), and polymerase chain reaction (PCR). Hence, the inexpensive, simple, and rapid method still need for the bacterial infections diagnosis. Immunoassay using electrochemical detection is an alternative attractive method for the bacteria pathogenic detection due to its high selectivity and sensitivity, inexpensive instrument and rapidity.

The utility and application of this method for the determination of *Salmonella typhi* were demonstrated in chapter III.

Table 2.2 The transmission, diseases, treatment, prevention and laboratory diagnosis of some pathogenic bacterium [12].

Species	Transmission	Diseases	Treatment	Prevention	Laboratory diagnosis
<i>Campylobacter</i>	<ul style="list-style-type: none"> • Fecal/oral from animals (mammals and fowl) • Contaminated meat (especially poultry) • Contaminated water 	Acute enteritis	<ul style="list-style-type: none"> • Symptomatically by fluid and electrolyte replacement • Ciprofloxacin in severe cases 	No available vaccine <ul style="list-style-type: none"> • Good hygiene • Avoiding contaminated water • Pasteurizing milk and milk products • Cooking meat (especially poultry) 	Finding campylobacter in feces
<i>Mycobacterium tuberculosis</i>	Droplet contact	Tuberculosis	Standard "short" course: <ul style="list-style-type: none"> • First 2 months, combination: <ul style="list-style-type: none"> ○ Isoniazid ○ Rifampicin ○ Pyrazinamide ○ Ethambutol • Further 4 months, combination: <ul style="list-style-type: none"> ○ Isoniazid ○ Rifampicin 	<ul style="list-style-type: none"> • BCG vaccine • Isoniazid 	<ul style="list-style-type: none"> • Ziehl-Neelsen stain showing acid-fast bacteria • Hybridization probes for DNA, succeeded by PCR • Culture on Lowenstein-Jensen agar

Species	Transmission	Diseases	Treatment	Prevention	Laboratory diagnosis
<i>Salmonella typhi</i>	Human-human <ul style="list-style-type: none"> Fecal-oral through food or water 	Typhoid fever	<ul style="list-style-type: none"> Ceftriaxone Fluoroquinolones, e.g. ciprofloxacin 	<ul style="list-style-type: none"> Ty21a and ViCPS vaccines Hygiene and food preparation 	<ul style="list-style-type: none"> Isolation from blood, feces, bone marrow, urine or rose spots on skin Colorless, non-lactose fermenting colonies on MacConkey agar Serology for antibodies against O antigen
<i>Staphylococcus aureus</i>	<ul style="list-style-type: none"> Human flora on mucosae in e.g. anterior nares and vagina, entering through wound 	Coagulase-positive staphylococcal infections: <ul style="list-style-type: none"> Localized skin infections Diffuse skin infection (Impetigo) 	<ul style="list-style-type: none"> Incision and drainage of localized lesions Nafcillin and oxacillin Vancomycin for Methicillin-resistant (MRSA) 	(no vaccine or preventive drug) <ul style="list-style-type: none"> Barrier precautions, washing hands and fomite disinfection in hospitals 	<ul style="list-style-type: none"> Microscopy showing strongly positive Gram stained cells in grape-like clusters Positive Catalase test and coagulase test

Species	Transmission	Diseases	Treatment	Prevention	Laboratory diagnosis
		<ul style="list-style-type: none"> • Deep, localized infections • Acute infective endocarditis • Septicemia • Necrotizing pneumonia • Toxinoses 			<ul style="list-style-type: none"> • Culture on enriched media producing deep yellow, hemolytic colonies
<i>Vibrio cholerae</i>	<ul style="list-style-type: none"> • Contaminated water and food, especially raw seafood 	Cholera	<ul style="list-style-type: none"> • Fluid and electrolyte replacement • e.g. doxycycline to shorten duration 	<ul style="list-style-type: none"> • Preventing fecal contamination of water supplies and food • Adequate food preparation 	<ul style="list-style-type: none"> • Culture on blood or MacConkey agar, enhanced by TCBS • Positive oxidase test

2.4 Paper-based microfluidic

A microfluidic device can be identified by the fact that it has one or more channels with at least one dimension less than 1,000 μm . The flow of a fluid through a microfluidic channel can be characterized by the Reynolds number (Re), defined as

$$\text{Re} = LV_{\text{avg}}\rho / \mu \quad (9)$$

where L is the most relevant length scale, μ is the viscosity, ρ is the fluid density, and V_{avg} is the average velocity of the flow. For many microchannels, L is equal to $4A/P$ where A is the cross sectional area of the channel and P is the wetted perimeter of the channel. Due to the small dimensions of microchannels, the Re is usually much less than 100, often less than $1.0 \text{ kg/Pa}\cdot\text{m}\cdot\text{s}^2$. In this Re regime, flow is completely laminar and no turbulence occurs. The transition to turbulent flow generally occurs in the range of Re $2000 \text{ kg/Pa}\cdot\text{m}\cdot\text{s}^2$. Laminar flow provides a means by which molecules can be transported in a relatively predictable manner through microchannels.

Microfluidic devices are suited to portable point-of-care (POC) diagnostics and on-site detection, hold great promise for improving global health, and other applications because the volume of fluids within these channels is very small, usually several nanoliters, the amount of reagents and analytes used is quite small. This is especially significant for expensive reagents. However, the fabrication techniques used to construct microfluidic devices are relatively the lithography based clean-room infrastructure. In addition, a plastic (or glass, silicon) used as substrate for the channel construct is complex and expensive material. Therefore, they are still not readily accessible to average users, particularly those in developing countries. Among the least expensive of the microfluidic devices are the recently introduced paper-based microfluidic devices. Paper-based microfluidic devices (μPADs) have the potential to be good alternatives for point-of-care testing over traditional glass and polymer based devices due to inexpensive material, less consumption of reagent and sample, disposability, and portability.

Paper, normally made of cellulose fibers, is abundant, inexpensive, sustainable, disposable, easy to use, store, and transport, easy to modify chemically and familiar to the public, but perhaps its most important advantage is that an enormous variety of inkjet printing techniques is available for its functionalization. For decades, paper strip tests are commercially available for pregnancy [13], diabetes [14,15], drugs of abuse [16,17], and biomarkers of pathogens test [18,19]. Most paper strip tests use visible color changes for qualitative analyte detection. In the assay, flow is directed along the paper matrix by capillary force, and the analyte is subsequently bound by the capture antibody at the test line. However, qualitative analysis is not sufficient when analyte levels are important for diagnosis or treatment. Much effort has therefore been directed towards the development of quantitative paper strip tests [20,21].

As an alternative to traditional paper-based immunochromatographic tests, Whitesides and coworkers recently introduced μ PAD, which represent the next generation of paper strip test devices [22-24]. This approach, which combines many advantages of paper strip tests with the utility of microfluidic devices, holds significant potential for point-of-care testing [22-27]. In their studies, hydrophobic polymers (e.g., polydimethylsiloxane) are photolithographically patterned [22] or printed using a desktop plotter [28] onto hydrophilic paper so that the millimeter-sized fluidic channels can be well-defined in the paper matrix as shown in Figure 2.8. Significantly, owing to the natural capillary action, biological fluids can flow along these channels without the external pumps that are required in the conventional microfluidic devices. The use of these patterned paper platforms not only minimizes the required sample volume, but also importantly makes multiplex analysis possible.

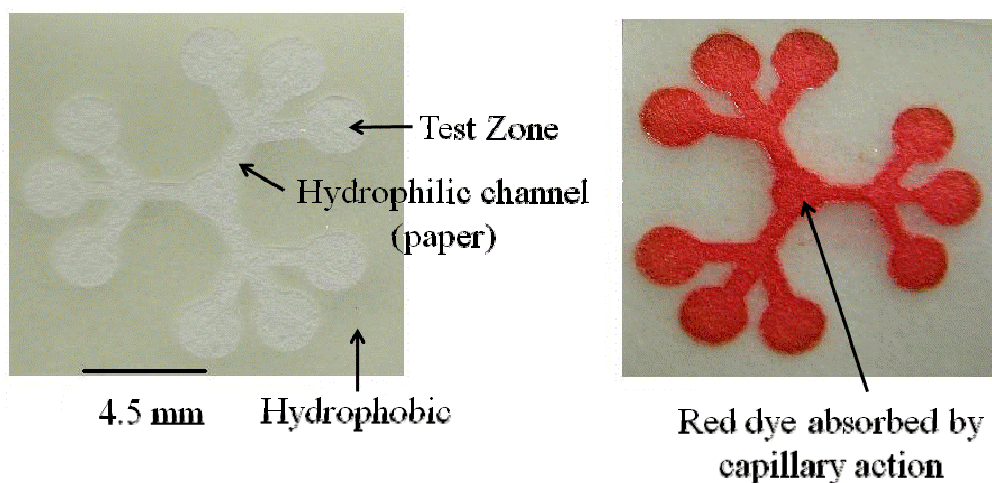


Figure 2.8 An example of a μ PAD with a central channel that wicks fluids into nine independent test zones.

One of our long term goals is to create portable clinical devices for the detection of pathogenic bacteria by electrochemical technique for home and bedside use in the developing country. In this work, low-cost fabrication method and electrochemical detection have been therefore developed for μ PADs to achieve our goal as described in chapter IV.

2.5 References

- [1] Holme, D. J.; Peck, H. Analytical Biochemistry. 3th ed. Malaysia: Prentice Hall, 1998.
- [2] Luttmann, W.; Bratke, K.; Kupper, M.; Myrtek, D. Immunology. 1st ed. German: Academic Press, 2006.
- [3] Bronstein, I.; Edwards, B.; Voyta, J. C. 1,2-Dioxetanes: Novel chemiluminescent enzyme substrates. Applications to immunoassays. J. Biolum. and Chemilumin. 4 (2005): 99-111.
- [4] Weng, J. Analytical Electrochemistry. 1st ed. United States of America: Wiley-VCH, 1994.

- [5] Douglas, S. A.; James, H. F.; Nieman, T. A. Principles of Instrumental Analysis. 5th ed. United States of America: Saunders Collage, 1998.
- [6] Weng, J. Stripping Analysis. United States of America: VCH, 1948.
- [7] Plambeck, J.A. Electroanalytical Chemistry. United States of America: John Wiley, 1982.
- [8] Archer, D. L.; Kvenberg, J. E. Incidence and cost of foodborne diarrheal disease in the United States. J. Food Protect 48 (1985): 887-894.
- [9] Ford, T. E. Microbiological Safety of Drinking Water: United States and Global Perspectives. Environ. Health Perspect. 107 (1999): 191-206.
- [10] Mackenzie, W. R.; Hoxie, N. J.; Proctor, M. E. A Massive Outbreak in Milwaukee of Cryptosporidium Infection Transmitted through the Public Water Supply. New Engl J. Med. 331 (1994): 161-167.
- [11] Centers for disease control and prevention. Outbreak of Escherichia coli O157:H7 and campylobacter among attendees of the Washington Country, Fair-New York. MMWR Morb Mortal Wkly Rep. 48 (1999): 803-805.
- [12] Bruce, F.; Richard, H. P.; Pamela, C. C. Lippincott's Illustrated Reviews: Microbiology. United States of America: Lippincott Williams & Wilkins, 2007.
- [13] One Step HCG Urine Pregnancy Test (Strip), AI DE Diagnostica Co. Ltd., Shandong, China (2009).
- [14] Hones, J.; Muller, P.; SurrIDGE, N. The technology behind glucose meters: test strips. Diabetes Technol. Ther. 10 (2008): S10-S26.
- [15] Kristensen, G. B. B.; Monsen, G.; Skeie, S.; Sandberg, S. Quality Assurance of Self-monitoring of Blood Glucose at the General Practitioner's Office. Point of Care. 5 (2006): 100-104.
- [16] Penttila, A.; Karhunen, P. J.; Pikkarainen, J. Alcohol screening with the Alcoscan test strip in forensic praxis. Forensic Sci. Int. 44 (1990): 43-48.
- [17] One Step Drugs of Abuse Test, Beijing China: Core Technology Co. Ltd., 2009.
- [18] Oberhofer, T. R.; Towle, D. W. Evaluation of the rapid penicillinase paper strip test for detection of beta-lactamase. J. Clin. Microbiol. 15 (1982): 196-199.

- [19] Mosley, L. M.; Sharp, D. S. The hydrogen sulphide (H₂S) paper strip test. SOPAC Technical Report 373 (2005).
- [20] Lin, Y. Y.; Wang, J.; Liu, G.; Wu, H.; Wai, C. M.; Lin, Y. A nanoparticle label/immunochromatographic electrochemical biosensor for rapid and sensitive detection of prostate-specific antigen. Biosens Bioelectron. 23 (2008): 1659-1665.
- [21] Mao, X.; Baloda, M.; Gurung, A. S.; Lin, Y.; Liu, G. Multiplex electrochemical immunoassay using gold nanoparticle probes and immunochromatographic strips. Electrochem Commun. 10 (2008): 1636-1640.
- [22] Martinez, A. W.; Phillips, S. T.; Butte, M. J.; Whitesides, G. M. Patterned Paper as a Platform for Inexpensive, Low-Volume, Portable Bioassays. Angew. Chem. Int. Ed. 46 (2007): 1318-1320.
- [23] Martinez, A. W.; Phillips, S. T.; Wiley, B. J.; Gupta, M.; Whitesides, G. M. FLASH: A rapid method for prototyping paper-based microfluidic devices. Lab Chip 8 (2008): 2146-2150.
- [24] Martinez, A. W.; Phillips, S. T.; Carrilho, E.; Thomas, S. W.; Sindi, H.; Whitesides, G. M. Simple Telemedicine for Developing Regions: Camera Phones and Paper-Based Microfluidic Devices for Real-Time, Off-Site Diagnosis. Anal. Chem. 80 (2008): 3699-3707.
- [25] Li, X.; Tian, J.; Nguyen, T.; Shen, W. Paper-Based Microfluidic Devices by Plasma Treatment. Anal. Chem. 80 (2008): 9131-9134.
- [26] Abe, K.; Suzuki, K.; Citterio, D. Inkjet-Printed Microfluidic Multianalyte Chemical Sensing Paper. Anal. Chem. 80 (2008): 6928-6934.
- [27] Dungchai, W.; Chailapakul, O.; Henry, C. S. Electrochemical Detection for Paper-Based Microfluidics. Anal. Chem. 81 (2009): 5821-5826.
- [28] Bruzewicz, D. A.; Reches, M.; Whitesides, G. M. Low-Cost Printing of Poly(dimethylsiloxane) Barriers To Define Microchannels in Paper. Anal. Chem. 80 (2008): 3387-3392.

CHAPTER III
ELECTROCHEMICAL IMMUNOASSAY

***Salmonella typhi* determination using voltammetric amplification of nanoparticles: a highly sensitive strategy for metalloimmunoassay based on a copper-enhanced gold label**

Wijitar Dungchai ^a, Weena Siangproh ^b, Wanpen Chaicumpa ^c,

Pongsri Tongtawe ^d, Orawon Chailapakul ^{a,*}

^a Sensor Research Unit, Department of Chemistry, Faculty of Science, Chulalongkorn University, Patumwan, Bangkok, 10330, Thailand

^b Department of Chemistry, Faculty of Science, Srinakharinwirot University, Sukhumvit 23, Wattana, Bangkok, 10110, Thailand

^c Department of Parasitology, Faculty of Medicine, Siriraj Hospital, Mahidol University, Bangkok, 10700, Thailand

^d Faculty of Allied Health Sciences, Thammasat University, Pathumthani, 12120, Thailand

* Corresponding author

Talanta (2008) 77:727-732

Abstract

A highly sensitive electrochemical amplification immunoassay for *Salmonella typhi* (*S. typhi*) determination has been developed for the first time by using a copper-enhanced gold nanoparticle label coupled with anodic stripping voltammetry. Monoclonal antibodies for *S. typhi* were first immobilized on polystyrene microwells and then captured by *S. typhi* bacteria. After an immunoreaction occurred, a polyclonal, antibody-colloidal gold conjugate was added to bind to the *S. typhi* bacteria. Next, a copper enhancer solution containing ascorbic acid and copper (II) sulfate was added into the polystyrene microwells. The ascorbic acid was employed to reduce the copper (II) ions to copper (0), which was subsequently deposited onto the gold nanoparticle tags. After the copper was dissolved in nitric acid, the released copper ions were detected by anodic stripping voltammetry. The amount of deposited copper was related to the amount of gold nanoparticle tag present, which was controlled by the amount *S. typhi* attached to the polyclonal antibody-colloidal gold conjugate. Therefore, the anodic stripping peak current was linearly dependent on the *S. typhi* concentration over concentration range of 1.30×10^2 cfu/mL to 2.6×10^3 cfu/mL in a logarithmic plot, with a detection limit as low as 98.9 cfu/mL. The influences of the relevant experimental variables, such as the concentration of copper and the reaction time of *S. typhi* with antibody, were investigated. We also successfully applied this method to determine the presence of *S. typhi* in human serum. Our results are a step towards developing more sensitive and reliable nanoparticle immunoassays.

3.1 Introduction

Typhoid fever is a serious problem for the public health of both underdeveloped and developing countries. It is a bacterial illness caused by *Salmonella typhi* (*S. typhi*), also known as *Salmonella enterica* serotype Typhi, a gram-negative rod found only in humans. Each year, around 16 million incidences of typhoid are reported worldwide, resulting in an estimated 600,000 deaths [1,2]. The transmission of typhoid fever may occur through several pathways, such as by contact with infected individuals and by eating food or by drinking water that is contaminated with typhoid bacteria. Following ingestion, the bacteria spread from the intestine via the bloodstream to the intestinal lymph nodes and other areas of the body where they multiply. The symptoms of this illness are characterized by the sudden onset of sustained fever, severe headache, loss of appetite, and either constipation or mild diarrhea. Samples of urine or blood are used to check the presence of *S. typhi*, which is the only way to ensure that the observed illness is typhoid fever [3]. Therefore, the determination of *S. typhi* in urine or blood plays an important role in clinical research and diagnosis of typhoid fever. Furthermore, a person who recovers from typhoid fever may still become an asymptomatic carrier who can infect others. Thus, the level of *S. typhi* in the patient's urine or blood after recovery should be continuously monitored in order to control the spread of this epidemic disease. Classical methods are usually used to detect *S. typhi*, including culturing [4,5], serological methods, such as slide agglutination and the Widal test [6], and polymerase chain reaction (PCR) [7,8]. Even though these methods can provide highly sensitive results for both qualitative and quantitative analysis, they are quite labor- and time-intensive to perform due to the pre-enrichment, isolation, and amplification steps of the bacterial cells.

With the above mentioned drawbacks, efforts to develop a method for *S. typhi* determination with increased sensitivity and selectivity and a reduction in analysis time have been proposed. Currently, alternative methods for biological molecular analysis are enzyme immunoassay [9,10], surface plasmon resonance [11], and electrochemical immunoassay [12-14]. In particular, the use of electrochemical immunoassay has attracted considerable interest for *S. typhi* determination because of its inherent

simplicity, high sensitivity, inexpensive instrumentation, and miniaturization. Although this method has a low detection limit and could be used in the diagnosis of typhoid fever, a sensitive and rapid method for analyzing and obtaining important information about the effectiveness of therapy, follow-up treatments, the epidemic disease, and protection is still needed. With the development of nanotechnology, various nanoparticles [15,16] and nano-quantum dots [17,18] have been used as labels to enhance the sensitivity of the electrochemical immunoassay technique. Amplified electrochemical detection of biological molecules was achieved by the dissolution of the metallic nanoparticles and by recording the subsequent electrochemical stripping of the dissolved ions. Gold nanoparticles act as a class of labels with many unique features, such as optical, electronic, and catalytic properties, that have been previously explored for potential applications in biomolecular detection. Based on these advantages, colloidal gold was used as an electrochemical marker or catalytic label for nanoparticle enlargement in order to elevate the sensitivity of the bioassay.

Recently, copper, silver, and gold-enhanced colloidal gold have been reported for immunoglobulin G (IgG) determination, which is the model of electrochemical immunoassay with detection limits as low as 0.5 ng/mL [19-21]. The metal-enhanced colloidal gold electrochemical stripping metalloimmunoassay combines the high sensitivity of stripping metal analysis with the remarkable signal amplification resulting from the catalytic precipitation of metals onto the gold nanoparticles [21-23]. Among these metals, the copper-enhanced protocol is better than the other metal-enhancing protocols because the copper enhancer solution, which contains ascorbic acid and copper sulphate, is easy to prepare and preserve. Furthermore, the copper determination by anodic stripping voltammetry is simple, and highly sensitive. However, metal-enhanced colloidal gold has not been previously applied to the detection of bacterial cells in real samples, especially for the detection of *S. typhi*. Therefore, we have employed the electrochemical stripping metalloimmunoassay based on a copper-enhanced gold nanoparticle label for the determination of *S. typhi* in real samples for the very first time, which will be useful in the diagnosis, follow-up treatment, and controlling in advance the epidemic disease of typhoid fever.

In this work, our ultimate aim was to develop an electrochemical metalloimmunoassay based on copper-enhanced gold nanoparticle label for *S. typhi* determination in real samples with a low limit of detection, high accuracy, and fast analysis time. The details of the optimization and the excellent performance of our proposed method are presented in the following sections.

3.2 Experimental Methods

3.2.1 Instrumentation

The stripping voltammograms were recorded using an Autolab Potentiostat 30 (Metrohm, Switzerland) with a three-electrode system. A glassy-carbon (GC) electrode (Bioanalytical System Inc., area 0.07 cm²) was used as the working electrode. Prior to use, the GC electrode was pretreated by sequential polishing with 1 and 0.3 μm of alumina/water slurries on felt pads, followed by rinsing with deionized water in order to remove the alumina impurities. A platinum wire and Ag/AgCl with a salt bridge were used as the counter and reference electrodes, respectively. The electrochemical equipment was housed in a Faraday cage to reduce electronic noise.

3.2.2 Materials and Methods

The polystyrene, 96-well, microtiter plates (high binding ELISA plates) were purchased from Ronbio (Shanghai, China). Polyclonal and monoclonal rabbit antibodies for polysaccharides of *Salmonella typhi* O901 and *Salmonella typhi* were obtained from Siriraj Hospital. Hydrogen tetrachloroaurate (III) and albumin bovine serum (BSA) were obtained from the Sigma Chemical Co. (St.Louis, MO). Nitric acid (65%), sodium chloride, sodium dihydrogen phosphate, disodium hydrogen phosphate, sodium carbonate, sodium bicarbonate, sodium citrate, copper (II) sulfate, and ascorbic acid were obtained from Merck (Germany).

The coating buffer for the microwells was 0.05 M NaHCO₃-Na₂CO₃ (pH 9.6). The incubation and washing buffer consisted of 0.01 M NaH₂PO₄-Na₂HPO₄ (pH 7.4) and 0.15 M sodium chloride. The copper enhancer solution was made from a 1:1 (v/v) ratio

of 0.10 M ascorbic acid and 0.2 M copper (II) sulfate. All of the solutions were prepared using Milli-Q 18 M Ω water (Millipore purification system).

3.2.3 Preparation of the antibody-colloidal gold conjugate

3.2.3.1 Preparation of gold nanoparticles

The gold nanoparticles were prepared according to the method reported in references [19,24] with slight modifications. Briefly, 1 mL of 1% HAuCl₄ solution was mixed with 100 mL of doubly distilled water and boiled under vigorous stirring. Then, 2.5 mL of 1% sodium citrate was added into solution under continuous heating and stirring for 15 minutes until the color of solution changed to wine red. The colloidal solution was left to cool at room temperature under stirring and was later stored in dark bottles at 4°C. The solution of colloidal gold particles was characterized by a UV-vis spectrophotometer and a transmission electron microscope (TEM).

3.2.3.2 Antibody-colloidal gold conjugate

The amount of coating antibody (polyclonal rabbit antibody for polysaccharides of *Salmonella typhi* O901) on the surface of the gold nanoparticles was optimized from 75 to 1200 mg/L. Solutions were prepared from 15,000 mg/L stock solutions of the rabbit antibody to *S. typhi*. An appropriate volume of stock solution was added into a centrifuge tube containing 2.0 mL of the colloidal gold solution. The pH solution was adjusted to 8.0 under stirring and was followed by incubation at room temperature for 1 hour. The absorbance at 519 nm of these samples was recorded and plotted versus the amount of coating antibody in order to determine the optimal amount of coating antibody.

After obtaining the optimal amount of coating antibody, the antibody-colloidal gold conjugate was prepared. The optimized amount of polyclonal rabbit antibody for the polysaccharides of *S. typhi* was added to 2 mL of the colloidal gold solution. The solution was then adjusted to pH 8.0 using Na₂CO₃ and was followed by incubation at room temperature for 1 hour under stirring. Next, 100 μ L of 3% BSA solution was added to minimize nonspecific adsorption, and the solution was incubated under stirring for an

additional hour at room temperature. The antibody-colloidal gold conjugate was centrifuged at 15,000 rpm for 10 min. The soft sediment was collected, washed and suspended in PBS solution, where the conjugate could be stored for more than 1 month at 4°C.

3.2.4 Immunoassay Procedure

The immunoassay procedure is shown in Figure 3.1. First, 50 µL of 125 mg/L monoclonal antibody was added into the polystyrene microwells and incubated at 37°C for 2 hours. Second, the solution was removed, and the microwells were washed with PBS (pH 7.4) for four times followed by the addition of 50 µL of 1% BSA solution to block the active sites of microwells from nonspecific adsorption. The microwells were incubated at 37 °C for 2 hours. The PBS (pH 7.4) washing step was repeated followed by the addition of 50 µL of *S. typhi* into the microwells. After incubating at 37°C for 1 hour followed by another PBS washing step, 50 µL of the antibody-colloidal gold conjugate was added to the solution, which was incubated at 37 °C for 1 hour in order to obtain the sandwich reaction. After performing four washing steps, 100 µL of copper-enhancer solution was added to the solution, which was incubated at room temperature for 10 min. After the microwells were washed four times with doubly distilled water, 100 µL of 1 M nitric acid solution was added to dissolve copper. Finally, the solution containing the released copper ions was transferred into an electrochemical cell and diluted to 3 mL with doubly distilled water. The experiments were carried out by anodic stripping voltammetry.

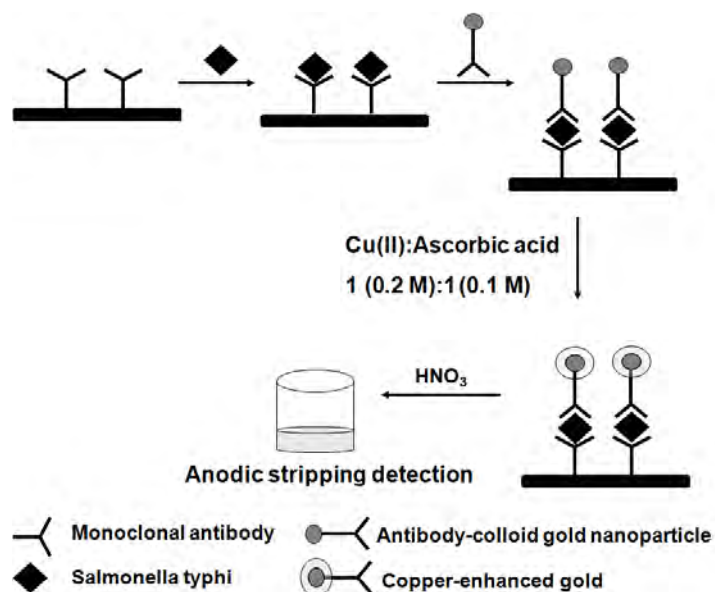


Figure 3.1 Schematic diagram of the proposed *S. typhi* immunoreactions.

3.3 Results and discussion

3.3.1 Preparation of the antibody-colloidal gold conjugate

3.3.1.1 Preparation of the gold nanoparticles

To characterize the gold nanoparticles, primary UV-vis spectra of the gold (III) ion and the gold nanoparticle solution were recorded. It was observed that the maximum absorbance of the gold nanoparticles occurred at a wavelength of 519 nm, which was similar to other reports [24]. This result indicated that the synthesis had yielded gold nanoparticles. From TEM measurements, the average gold nanoparticle size was 15 nm as shown in Figure 3.2.

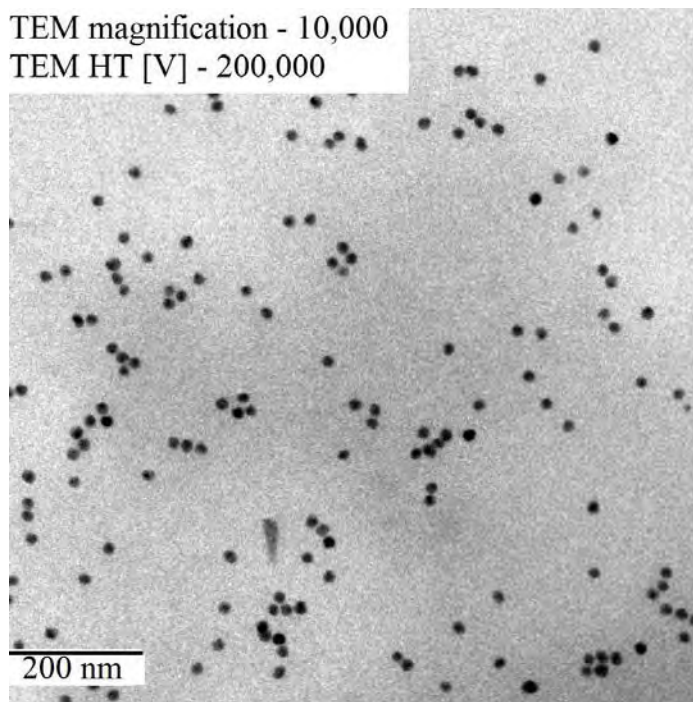


Figure 3.2 TEM images of the gold nanoparticles.

3.3.1.2 Preparation of the antibody-colloidal gold conjugate

Using the preparation procedure for antibody-colloidal gold conjugates as mentioned above, it was found that the antibodies could bind with the gold nanoparticles. The visible spectrum of antibody-colloidal gold conjugate displayed an absorption band at 519 nm, and there were no significant changes in the absorption spectrum of the gold nanoparticles. The result was shown in Figure 3.3. This could be explained if gold still exhibited the characteristics of a nanosized particle after binding. However, the antibody-colloidal gold conjugate generated a higher signal when compared to those of the gold nanoparticle at the same wavelength.

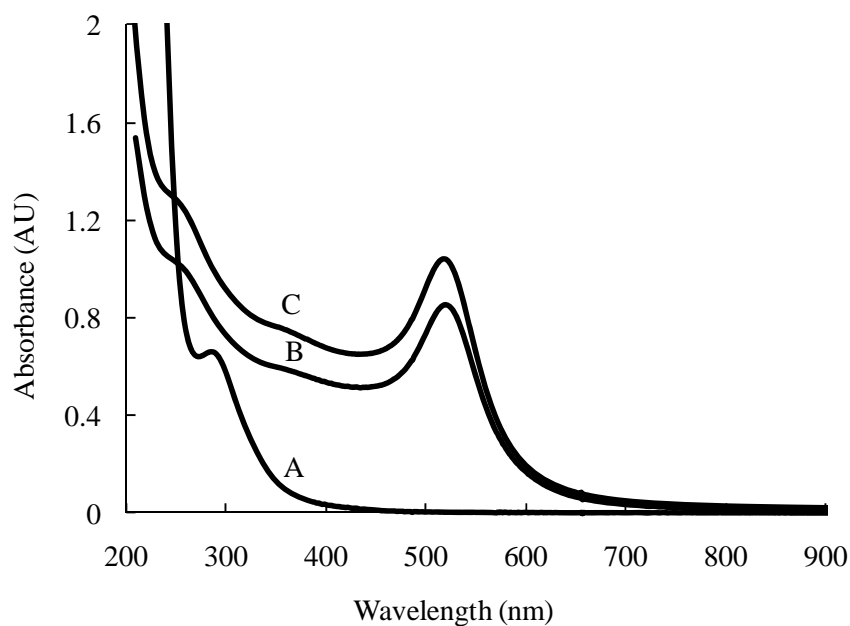


Figure 3.3 UV-vis absorption spectra of (A) Gold(III) solution; (B) Gold nanoparticles; (C) Antibody-colloidal gold conjugate.

The effect of the amount of coating antibody on the surface of the gold nanoparticles was examined in a range of 75-1200 mg/L. It could be seen that the absorbance increased with increasing the amount of coating antibody up to 450 mg/L. The absorbance decreased after the amount of coating antibody was higher than 450 mg/L (Figure 3.4). This indicated that a concentration of 450 mg/L was a suitable amount of coating antibody. Moreover, it was also effective in preventing aggregation.

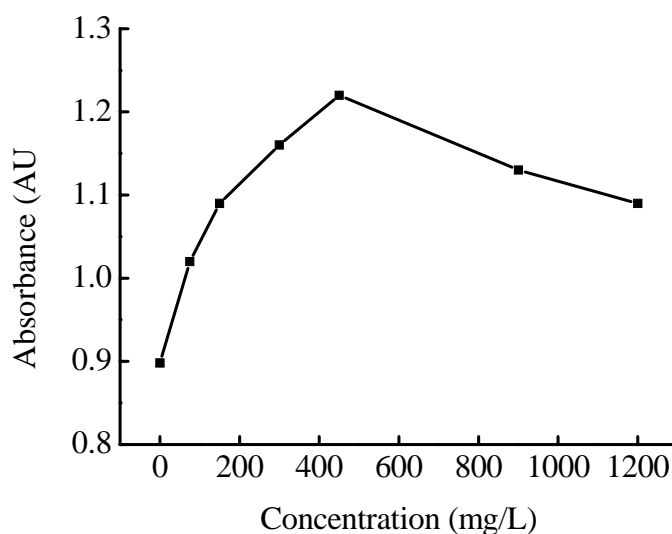


Figure 3.4 Relationship between absorbance and antibody concentration coated on the surface of the gold nanoparticles.

3.3.2 Determination of copper (II) ion at a glassy carbon electrode

In our proposed method, the copper-enhancer solution acts as a catalyst on the gold colloids. The amount of copper deposited on the gold nanoparticles is directly proportional to the amount of *S. typhi*. Therefore, the sensitivity of *S. typhi* determination is related to the sensitivity of the Cu (II) ion determination. Our goal was to evaluate the performance of the electrochemical assay for the determination of the copper (II) ion using a glassy carbon electrode. Several parameters were investigated in order to obtain suitable conditions for the Cu (II) ion determination.

3.3.2.1 The effect of the deposition potential

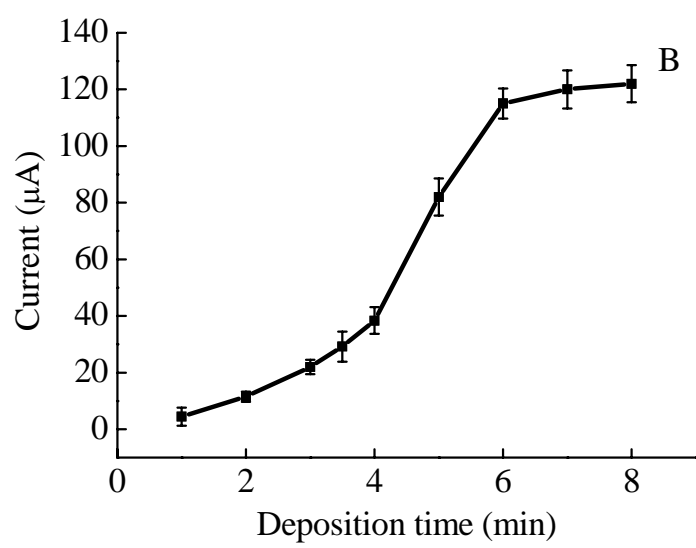
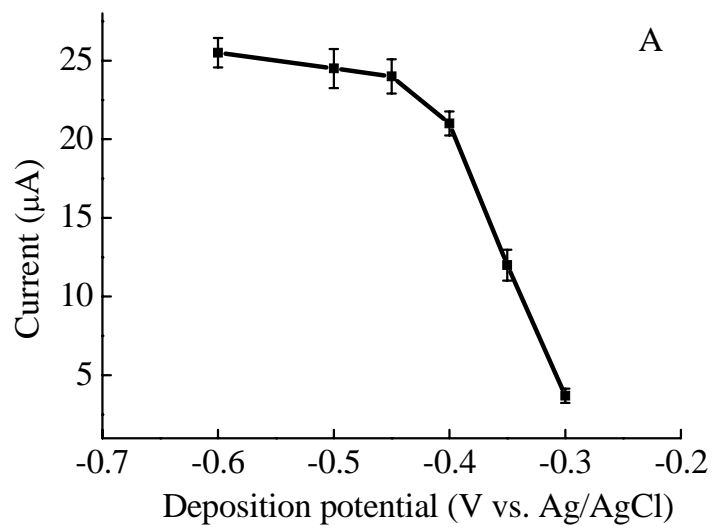
The effect of the deposition potential on the stripping peak current of the Cu (II) ion was studied from -0.3 V to -0.6 V. The anodic peak currents were increased rapidly from -0.3 V to -0.45 V, and no significant differences were observed for the anodic peak current between -0.5 V and -0.6 V as shown in Figure 3.5A. Therefore, a deposition potential of -0.5 V was selected in the experiment.

3.3.2.2 *The effect of the deposition time*

The deposition time of the Cu (II) ion at a glassy carbon electrode directly affects the sensitivity of the anodic stripping analysis. For this reason, the influence of the deposition time for the detection of copper was studied, with deposition times ranging from 1 min to 8 min. As shown in Figure 3.5B, when the deposition times were increased from 1 min to 6 min, the anodic peak currents also increased, and after 6 min, the current remained constant. Therefore, 6 min was chosen as the suitable deposition time.

3.3.2.3 *Linearity*

In order to judge the possibility of applying the assay for quantitative analysis, the linearity range was examined. Under optimal conditions, a good linearity in the anodic peak current with the copper (II) concentration over a range of 0.10 μM to 100 μM was obtained with a linear correlation coefficient of 0.9950 as shown in Figure 3.5C. The detectable limit, which was calculated as three times the standard deviation, was 0.0377 μM . It can therefore be concluded that anodic stripping voltammetry is a very highly sensitive method for Cu (II) ion determination, and therefore copper-enhanced gold nanoparticles can be effectively detected by this method.



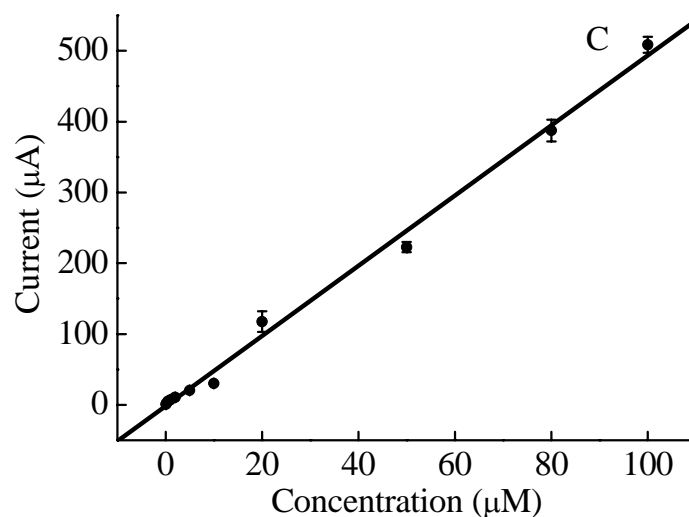


Figure 3.5 (A) The effect of the deposition potential of the Cu (II) ion under a 3 min deposition time with a concentration of Cu (II) 1×10^{-5} M in a 0.1 M nitric acid solution; (B) The effect of the deposition time of Cu (II) ion under a -0.5 V deposition potential with a concentration of Cu (II) 1×10^{-5} M in a 0.1 M nitric acid solution; (C) The calibration plots of the Cu (II) ion for a -0.5 V deposition potential and for a 6 min deposition time, $n = 3$.

3.3.3 Optimization of the immunoassay conditions

3.3.3.1 The effect of the concentration and the reaction time of copper enhancer solution

The sensitivity of the electrochemical immunoassay based on a colloidal gold-labeled antibody can be achieved by the catalytic precipitation of copper on the gold nanoparticles. The concentration of copper would therefore affect the amount of copper metal deposited on the gold nanoparticles. The copper concentration in the copper enhancer solution was investigated within the range of 0.10-0.40 M. The results demonstrated (Figure 3.6A) that the anodic peak current increased with increasing copper concentration along with the background signal. Therefore, the ratio of current between the *S. typhi* and the background signal was calculated as a function of the copper

concentration to determine the concentration which provided optimal sensitivity. The signal to background ratio reached a maximum value at a copper concentration of 0.20 M, as shown in Figure 3.6B. Hence, this concentration was selected for all subsequent experiments.

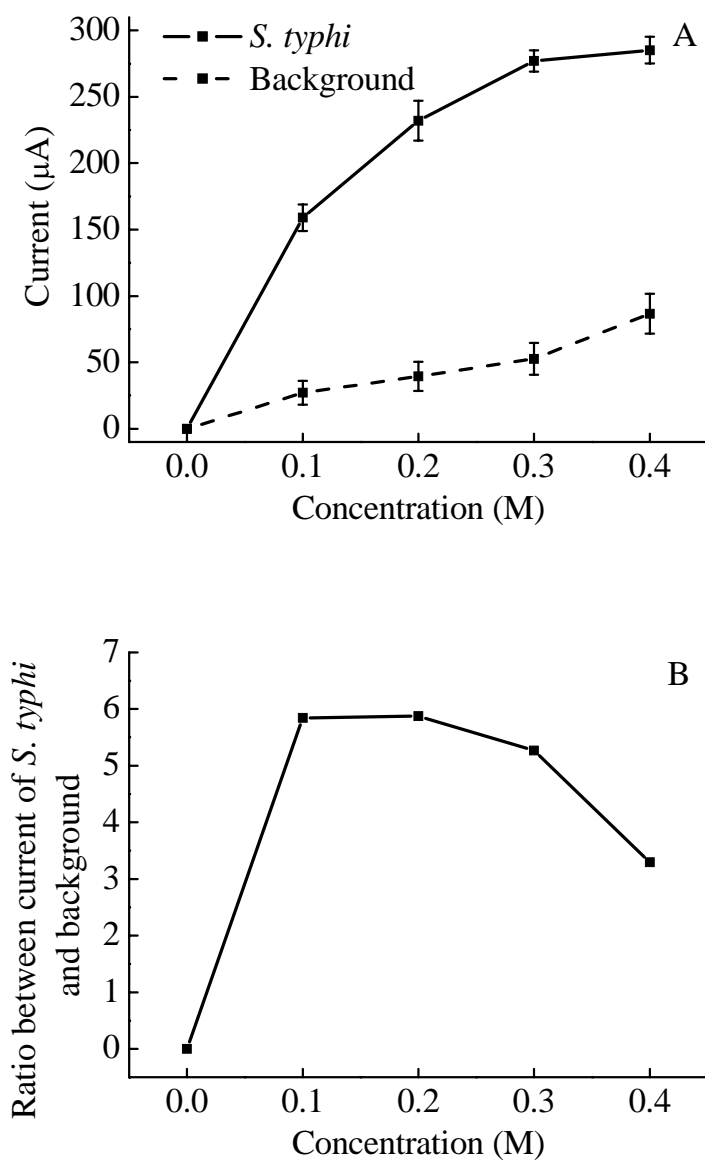
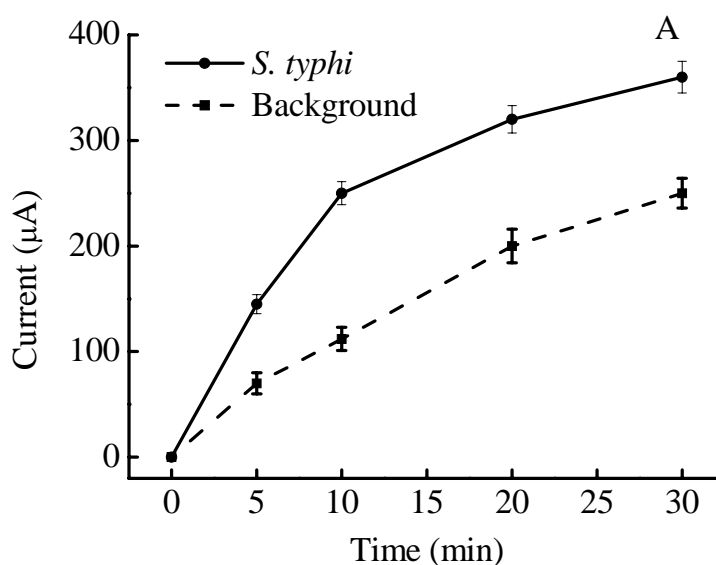


Figure 3.6 (A) The effect of the copper concentration and (B) the ratio between *S. typhi* signal and the background signal. The following conditions were used: 2.6×10^3 cfu/mL

of *S. typhi*, a 60 min incubation time for the *S. typhi* with the monoclonal antibody and the antibody-colloid gold conjugate, a 1:1 dilution ratio of the antibody-colloid gold conjugate, and a copper enhancement time of 10 min, $n = 3$.

The reaction time of the copper enhancer solution should also be optimized, since it is related to the amount of copper metal deposited on the gold nanoparticles. In this work, the reaction time was optimized over a range of 5-30 min. It was observed that the anodic peak current significantly increased with reaction time in the range of 5-10 min and then only slightly increased. However, the background also increased when the reaction time of copper enhancer solution increased. Therefore, the ratio of the signal between the *S. typhi* and the background was calculated as a function of the reaction time of the copper enhancer solution. A maximum of the signal with *S. typhi* to the background signal was obtained at a reaction time of 10 min, which was therefore chosen for the reaction time of copper enhancer solution in further experiments (Figure 3.7).



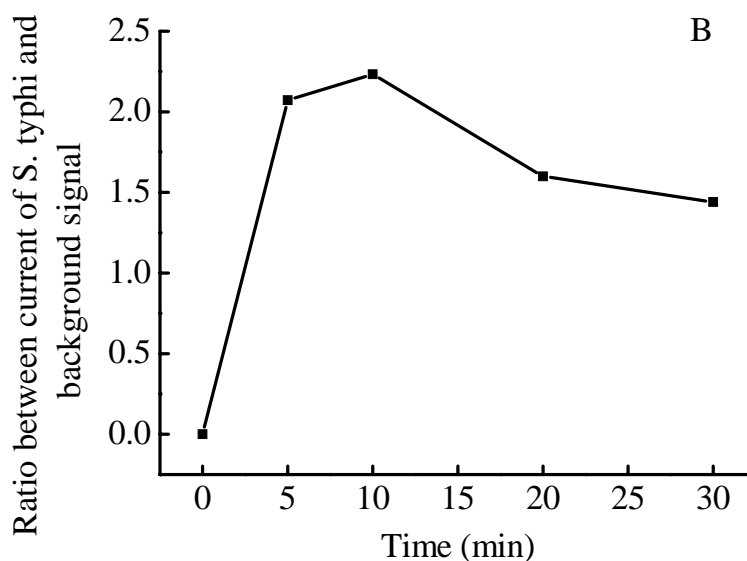


Figure 3.7 (A) The effect of the reaction time of the copper enhancer solution and (B) the ratio between *S. typhi* signal and the background signal. The following conditions were used: 2.6×10^3 cfu/mL of *S. typhi*, a 60 min incubation time for the *S. typhi* with the monoclonal antibody and the antibody-colloid gold conjugate, a 1:1 dilution ratio of the antibody-colloid gold conjugate, and the copper concentration 0.20 M, $n = 3$.

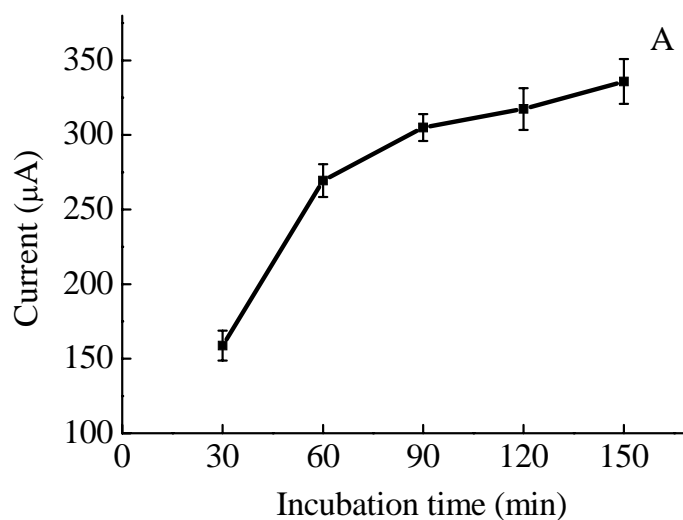
3.3.3.2 The effect of the immunoassay incubation time

The immunoreaction time between the *S. typhi* and the monoclonal antibody coated on the microwells was studied for times between 30-150 min. Figure 3.8A shows the results from the assay plotted as a function of the incubation time, and the current signal was found to increase with increasing incubation time. An incubation time of 60 min was selected since at longer incubation times, no significant changes in the signal were observed.

3.3.3.3 The effect of the dilution ratio and the incubation time of the antibody-colloidal gold conjugate

From the immunoassay procedure, *S. typhi* was bound with the antibody-colloidal gold conjugate in order that the amount of antibody-colloidal gold conjugate

added would directly affect the sensitivity of the *S. typhi* detection. In addition, the amount of bound antibody-colloidal gold conjugate also depends on the diffusion rate of the nanoparticle label. The diffusion rates of the nanoparticle label are smaller than that of the free antibody due to the bigger size of the nanoparticle label. Therefore, the antibody-conjugated particle binding could be the time-limiting step in the assay unless a high concentration of nanoparticles is used. However, the minimal amount of nanoparticle labels that can maintain an acceptable sensitivity is normally used in order to reduce the assay cost. Therefore, the dilution ratio and the incubation time of antibody-colloidal gold conjugate were optimized in this experiment. The results are shown in Figure 3.8B and 3.8C. The anodic stripping peak current was increased when the dilution ratio was increased up to 1:2. Therefore, a 1:2 of dilution ratio of the antibody-colloidal gold conjugate was selected. The peak current increased rapidly with the incubation time between 30-60 min and was found to remain constant for times greater than 60 min. Therefore, an incubation time of 60 min was chosen as a compromise between the analysis time and the sensitivity.



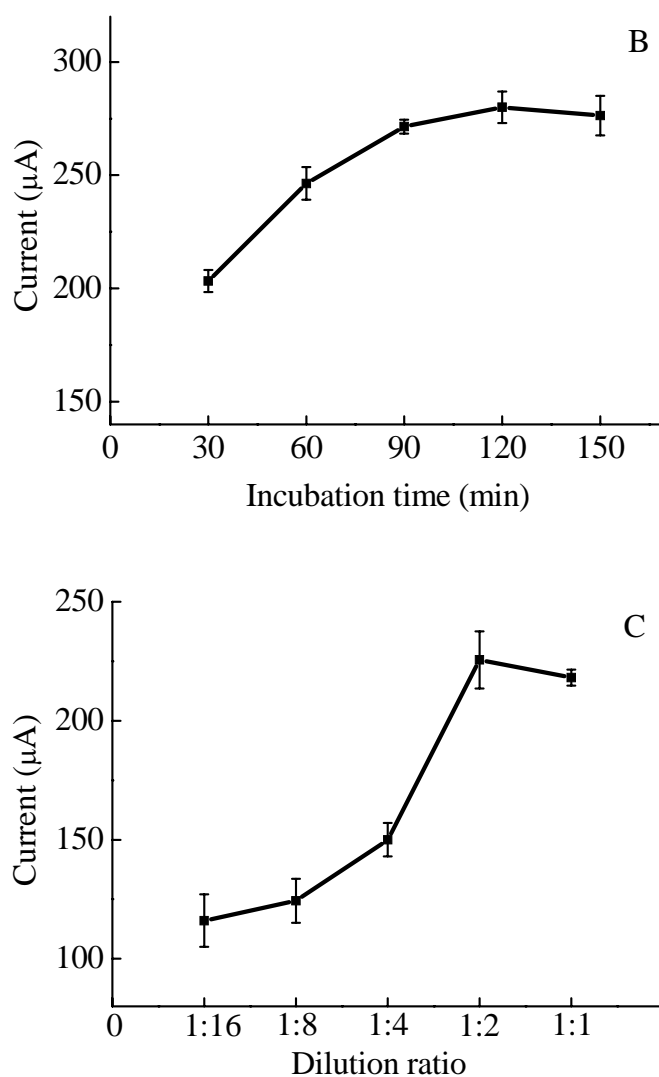


Figure 3.8 The effect of the incubation time between the *S. typhi* and either (A) the monoclonal antibody or; (B) the antibody-colloid gold conjugate; (C) The effects of antibody-colloidal gold conjugate dilution. The same conditions were used as those in Fig. 3, $n = 3$.

3.3.4 Analytical performance

Using the optimal conditions, the relationship between the anodic peak current of copper and the concentration of *S. typhi* is plotted in Figure 3.9 over a concentration

range of 0 - 4.30×10^3 cfu/mL. A linear relationship, $\log i_{pa} = 0.3053 \log C + 1.4489$, was observed with a correlation coefficient of 0.9961 for *S. typhi* concentrations between 1.30×10^2 to 2.6×10^3 cfu/mL. The data was plotted on a logarithmic scale in order to solve the curvature problem which resulted from the saturation of the probe binding site and particle aggregation (see insert of Figure 3.9) [22]. The detection limit was estimated to be 98.9 cfu/mL (based on a criterion of three times the standard deviation with $n = 8$), which is better than both the detection limit of 1.3×10^3 cfu/mL obtained from a direct-binding optical grating coupler immunosensor [25] and the detection limit of 5×10^3 cfu/mL obtained from a phage immobilized magnetoelastic sensor [26]. The reproducibility of our proposed method was studied by analyzing concentrations of *S. typhi* of 2.60×10^2 and 2.60×10^3 cfu/mL, where measurements were performed eight times during the same day on a single immoassay (intra-assay) and on three separate immunoassays over a three day period (inter-assay). A relative standard deviation (RSD) of the immunoassay of 14% was observed for both the intra- and inter-assays. The results are shown in Table 3.1.

Table 3.1 The reproducibility of the proposed method

Assay type	Concentration (cfu/mL)	%RSD
Intra-assay ($n = 8$)	2.6×10^2	11.4
	2.6×10^3	7.7
Inter-assay ($n = 3$)	2.6×10^2	13.7
	2.6×10^3	8.4

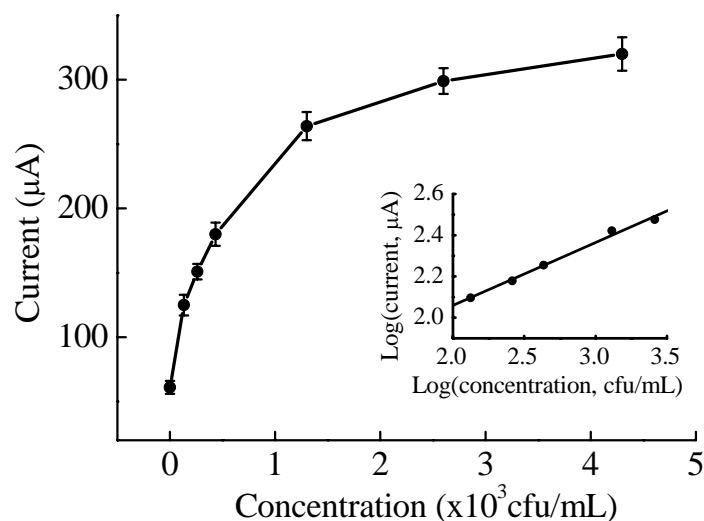


Figure 3.9 The relationship between the anodic stripping peak current and concentration of *S. typhi* (with concentrations of 0 and 1.30×10^2 to 4.30×10^3 cfu/mL). The calibration plot for the *S. typhi* determination (1.30×10^2 – 2.60×10^3 cfu/mL) is shown in the insert, $n = 3$.

3.3.5 Analytical applications

The proposed method was also applied to determine the level of *S. typhi* in human serum. In order to determine the accuracy of our method, normal human serum was spiked with different concentration of *S. typhi* and analyzed by using a calibration method without any pretreatment. Recoveries of *S. typhi* were in the range of 80-101%. The results (as shown in Table 3.2) demonstrated that this method can be used to efficiently determine *S. typhi* in human serum without any sample preparation.

Table 3.2 Results of *S. typhi* in human serum sample

Concentration (cfu/mL, $n = 3$)		Recovery (%)
Added	Found	
260	223.3 ± 28.6	85.9
433	352.1 ± 37.5	81.3
1300	1305.3 ± 115.8	100.4
2600	2541.5 ± 216.1	97.7

3.4 Summary

For the first time, we have successfully developed an electrochemical metalloimmunoassay, which is based on a copper-enhanced gold nanoparticle label, for *S. typhi* determination with high sensitivity, specificity, and reproducibility. The electrochemical stripping metalloimmunoassay combines the inherent signal amplification of stripping metal analysis with a biospecific interaction. The proposed method was also applied with satisfactory recovery results for *S. typhi* determination in human serum. The coupling of gold nanoparticles with the advantages of electrochemical stripping analysis can easily be extended for detecting other bacterial cells in real samples with high accuracy and sensitivity.

3.5 References

- [1] Ivanoff, B.; Levine, M. M.; Lambert, P. H. Vaccination against typhoid fever present status. Bull World Health Organ. 72 (1994): 957-971.
- [2] Parry, C. M.; Hien, T. T.; Dougan, G.; White, N. J.; Farrar, J. J. Typhoid fever. New Engl. J. Med. 347 (2002): 1770-1782.

- [3] National Center for Immunization and Respiratory Diseases: Division of Bacterial Diseases. Typhoid fever. <http://www.cdc.gov/nczved/dfbmd>: Centers for Disease Control and Prevention, 2005.
- [4] Wain, J.; Diep, T. S.; Ho, V. A.; Walsh, A. M.; Hoa, N. T. T.; Parry, C. M.; White, N. J. Quantitation of bacteria in blood of typhoid fever patients and relationship between counts and clinical features, transmissibility, and antibiotic resistance. J. Clin. Microbiol. 36 (1998): 1683-1687.
- [5] Swaminathan, B.; Feng, P. Rapid detection of food-borne pathogenic bacteria. Annu. Rev. Microbiol. 48 (1994): 401-426.
- [6] Myron, M. L.; Oscar, G.; Robert, H. G.; William, E. W.; Rene, S. P.; William, W. Diagnostic Value of the Widal Test in Areas Endemic for Typhoid Fever. Am. J. Trop. Med. Hyg. 27 (1978): 795-800.
- [7] Huang, H. S.; Garcia, M. M.; Brooks, B. W.; Nielsen, K.; Ng, S. P. Evaluation of culture enrichment procedures for use with Salmonella detection immunoassay. Int. J. Food Microbiol. 51 (1999): 85-94.
- [8] Hein, I.; Flekna, G.; Krassnig, M.; Wagner, M. Real-time PCR for the detection of Salmonella spp. in food: An alternative approach to a conventional PCR system suggested by the FOOD-PCR project. J. Microbiol. Methods 66 (2006): 538-547.
- [9] Chaichupa, W.; Ruangknaporn, Y.; Burr, D.; Chongsanguan, M.; Echeverria, P. Diagnosis of Typhoid Fever by Detection of Salmonella typhi Antigen in Urine. J. Clin. Microbiol. 30 (1992): 2513-2515.
- [10] Chaicumpa, W.; NgrenNgarmert, W.; Kalambaheti, T.; Ruangknaporn, Y.; Chongsanguan, M.; Tapchaisri, P.; Desakorn, V.; Suthienkul, O. Monoclonal antibody-based dot-blot ELISA for the detection of Salmonella in foods. Asian Pac J Allergy Immunol 13 (1995): 159-166.
- [11] Mazumdar, S. D.; Hartmann, M.; Kampfner, P.; Keusgen, M. Rapid method for detection of Salmonella in milk by surface plasmon resonance (SPR). Biosens. Bioelectron. 22 (2007): 2040-2046.

- [12] Rao, V. K.; Rai, G. P.; Agarwal, G. S.; Suresh, S. Amperometric immunosensor for detection of antibodies of *Salmonella typhi* in patient serum. *Anal. Chim. Acta* 531 (2005): 173-177.
- [13] Suye, S.; Matsuura, T.; Kimura, T.; Zheng, H.; Hori, T.; Amano, Y.; Katayama, H. Amperometric DNA sensor using gold electrode modified with polymerized mediator by layer-by-layer adsorption. *Microelectron. Eng.* 81 (2005): 441-447.
- [14] Huang, T. S.; Tzeng, Y.; Liu, Y. K.; Chen, Y. K.; Walker, K. R.; Guntupalli, R.; Liu, C. Immobilization of antibodies and bacterial binding on nanodiamond and carbon nanotubes for biosensor applications. *Diamond Relat. Mater.* 13 (2004): 1098-1102.
- [15] Dequaire, M.; Degrand, C.; Limoges, B. An electrochemical metalloimmunoassay based on a colloidal gold label. *Anal. Chem.* 72 (2000): 5521-5528.
- [16] Zhang, S. B.; Wu, Z. S.; Guo, M. M.; Shen, G. L.; Yu, R. Q. A novel immunoassay strategy based on combination of chitosan and a gold nanoparticle label. *Talanta*. 71 (2007): 1530-1535.
- [17] Wu, H.; Liu, G. D.; Wang, J.; Lin, Y. H. Quantum-dots based electrochemical immunoassay of interleukin-1 alpha. *Electrochem. Commun.* 9 (2007): 1573-1577.
- [18] Thurer, R.; Vigassy, T.; Hirayama, M.; Wang, J.; Bakker, E.; Pretsch, E. Potentiometric immunoassay with quantum dot labels. *Anal. Chem.* 79 (2007): 5107-5110.
- [19] Mao, X.; Jiang, J. H.; Luo, Y.; Shen, G. L.; Yu, R. Q. Copper-enhanced gold nanoparticle tags for electrochemical stripping detection of human IgG. *Talanta*. 73 (2007): 420-424.
- [20] Chu, X.; Fu, X.; Chen, K.; Shen, G. L.; Yu, R. Q. An electrochemical stripping metalloimmunoassay based on silver-enhanced gold nanoparticle label. *Biosens. Bioelectron.* 20 (2005): 1805-1812.
- [21] Liao, K. T.; Huang, H. J. Femtomolar immunoassay based on coupling gold nanoparticle enlargement with square wave stripping voltammetry. *Anal. Chim. Acta* 538 (2005): 159-164.

- [22] Wang, J.; Xu, D. K.; Kawde, A. N.; Polsky, R. Metal nanoparticle-based electrochemical stripping potentiometric detection of DNA hybridization. Anal. Chem. 73 (2001): 5576-5581.
- [23] Wang, J.; Polsky, R.; Xu, D. Silver-Enhanced Colloidal Gold Electrochemical Stripping Detection of DNA Hybridization. Langmuir 17 (2001): 5739-5741.
- [24] Katherine, C. G.; GrWith, F.; Michael, B. H.; Michael, J. N. Preparation and characterization of Au colloid monolayer. Anal. Chem. 67 (1995): 735-743.
- [25] Kim, N.; Park, I. S.; Kim, W. Y. Salmonella detection with a direct-binding optical grating coupler immunosensor. Sens. Actuators, B 121 (2007): 606-615.
- [26] Lakshmanan, R. S.; Guntupalli, R.; Hu, J.; Petrenko, V. A.; Barbaree, J. M.; Chin, B. A. Detection of Salmonella typhimurium in fat free milk using a phage immobilized magnetoelastic sensor. Sens. Actuators, B 126 (2007): 544-550.

CHAPTER IV

PAPER-BASED MICROFLUIDICS

There are three parts for this Chapter. Part A presents the invention of electrochemical detection for paper-based microfluidic devices. Part B gives the improvement of visual discrimination using multiple colorimetric indicators for semi-quantitative analysis. Part C reports the novel fabrication method for implementation in developing countries.

PART A**Electrochemical Detection for Paper-Based Microfluidics**

Wijitar Dungchai ^a, Orawon Chailapakul ^{a,*}, Charles S. Henry ^{b,*}

^a Sensor Research Unit, Department of Chemistry, Faculty of Science, Chulalongkorn University, Patumwan, Bangkok, 10330, Thailand

^b Department of Chemistry, Colorado State University, Fort Collins, CO, 80523-1872, USA

*Corresponding author

Analytical Chemistry (2009) 81: 5821–5826

Abstract

We report the first demonstration of electrochemical detection for paper-based microfluidic devices. Photolithography was used to make microfluidic channels on filter paper, and screen-printing technology was used to fabricate electrodes on the paper-based microfluidic devices. Screen-printed electrodes on paper were characterized using cyclic voltammetry to demonstrate the basic electrochemical performance of the system. The utility of our devices was then demonstrated with the determination of glucose, lactate, and uric acid in biological samples using oxidase enzyme (glucose oxidase, lactate oxidase, and uricase, respectively) reactions. Oxidase enzyme reactions produce H_2O_2 while decomposing their respective substrates and therefore a single electrode type is needed for detection of multiple species. Selectivity of the working electrode for H_2O_2 was improved using Prussian Blue as a redox mediator. The determination of glucose, lactate, and uric acid in control samples was performed using chronoamperometry at the optimal detection potential for H_2O_2 (0 V versus the on-chip Ag/AgCl reference electrode). Levels of glucose and lactate in control serum samples measured using the paper devices were 4.9 ± 0.6 and 1.2 ± 0.2 mM (level I control sample), and 16.3 ± 0.7 and 3.2 ± 0.3 mM (level II control sample), respectively and were within error of the values measured using traditional tests. This study shows the successful integration of paper-based microfluidics and electrochemical detection as an easy-to-use, inexpensive, and portable alternative for point of care monitoring.

4.1 Introduction

The development of microfluidic devices has been spurred at least in part by the desire to produce low-cost point-of-care diagnostics and environmental monitoring devices [1,2]. For point-of-care applications, the goal is to provide a total answer where a sample is introduced to the device and data is generated that can be used to make an informed decision. A variety of devices meeting these requirements have been demonstrated. The most common example, by far, has been for DNA analysis where complex functions such as DNA capture, amplification, and separation on a single device have been demonstrated [3-7]. The Burns group has successfully generated a device with integrated microchannels, heaters, temperature sensors, and fluorescence detectors used to analyze nanoliter-size DNA samples on a single glass and silicon substrate. The device is capable of mixing the solution together, amplifying or digesting the DNA, then separating and detecting those DNA [3-7]. In another example from the Landers group, a two-stage microfluidic device consisting of C₁₈ reversed-phase monolithic column for DNA extraction efficiency on a single glass slide (3 x 2.5 cm) was coupled with a device that was able of performing polymerase chain reactions (PCR) and DNA separations [6]. While these examples show the power of microfluidic devices and their potential for solving complex problems, a significant portion of the world's population could never afford the cost of such advanced devices. To this end, there is a growing push to generate microfluidic devices that are extremely low cost (<\$1 US) and require minimal external instrumentation for obtaining quantitative information.

Among the least expensive of the microfluidic devices are the recently introduced paper microfluidic devices. Paper-based microfluidic devices have the potential to be good alternatives for point-of-care testing over traditional glass and polymer based devices because they are easy to use, inexpensive, require small volumes of reagents and sample, provide rapid analysis, are disposable, can be made from renewable substrate materials, and are portable [8-13]. These devices have been used for the simultaneous determination of glucose and protein on a single piece of patterned paper [8]. The results of the assay were quantified by visually comparing the color intensity of the reaction

spots with the developed color intensity. Matching color and color intensity by the naked eye is complicated by many factors including different visual perception of color from one person to another, lighting, and the difference between the colors of a dry printed color on label stock and the colors seen in a reacted (i.e., wetted) paper. In an effort to conduct quantitative analysis for diagnostic tests based on paper microfluidics, several authors have used cameras or scanners to record the color intensity. Using this approach, glucose, pH, and protein levels were simultaneously determined by paper-based microfluidic devices [13]. Camera phones and portable scanners are an attractive format because they can be used by unskilled personnel and provide more accurate results as compared to visual inspection. However, the transmission of data from on-site to experts is still required to analyze the data. Moreover, the intensities of digital images from the camera are affected by lighting conditions and a calibration curve using standards of known color and intensity is necessary for processing data of each imaging device. Finally, camera phones and portable scanners lack the sensitivity and selectivity of traditional analytical instrumentation. Therefore, a detector with high sensitivity and selectivity is still needed for determination of low levels of analytes in biological samples and complex sample matrixes such as blood and plasma.

Electrochemical detection (ECD) is an attractive alternative detection scheme for paper-based microfluidics due to its small size, portability, low cost, high sensitivity, and high selectivity by proper choice of detection potential and/or electrode material [14-19]. An additional advantage of ECD is simplicity of the instrumentation resulting in low electrical power requirements for in-field use [19]. These advantages have led to the almost universal use of electrochemical detection in handheld glucometers for monitoring diabetes. Finally, screen-printed carbon electrodes have many attractive advantages for ECD including low cost, disposability, flexibility in design, ease of chemical modification, and ability to produce with minimal outside technology [20-22]. Here, we present electrochemical based detection for paper-based microfluidic devices for simultaneous determination of glucose, lactate, and uric acid in biological samples. Electrodes modified with Prussian Blue (PB) for improved selectivity for H_2O_2 detection were characterized to show the viability of the combined approach. Electrodes were

subsequently modified with appropriate enzymes for the detection of small molecule markers in urine and blood samples. Experimentally determined levels measured using the paper microfluidic devices were within error of the levels measured for the same samples done using traditional clinical diagnostic assays.

4.2 Experimental Methods

4.2.1 Materials and equipment

D-(+)-glucose, sodium L-lactate, uric acid, glucose oxidase (from *Aspergillus niger*, 215 U/mg) and uricase (from *Bacillus fastidiosus*, 9 U/mg) were purchased from Sigma-Aldrich (St. Louis, MO). Lactate oxidase (from *Aerococcus viridians*, 38 U/mg) was obtained from A.G. scientific, INC (San Diego, CA). Potassium phosphate was purchased from Fisher Scientific (Pittsburgh, PA). Acetone was obtained from Mallinckrodt chemicals (Phillipsburg, NJ). SU-8 3025 negative photoresist was purchased from MicroChem Corp. (Newton, MA). Whatman filter paper 1 was obtained from Cole-parmer (Vernon Hills, Illinois). Carbon ink mediated with Prussian blue (C2070424D2) was purchased from Gwent group (Torfaen, United Kingdom). Silver chloride ink (Electrodag 7019) was obtained from Acheson colloids company (Port Huron, MI). All chemicals were used as received without further purification. Electrochemical measurements were made using a potentiostat (CHI 1207A, CH Instruments, Austin, TX) at room temperature ($22 \pm 1^\circ\text{C}$).

4.2.2 Preparation of paper-based microfluidic devices

Photolithography was used to pattern Whatman filter paper 1 according to previously reported methods [8-12]. Briefly, SU-8 3025 photoresist was poured on the center of the paper and spread over the paper using a spin-coater. The photoresist-covered paper was baked at 95°C for ~ 10 min. The paper was then covered with transparency film photomask generated using a standard laser printer and irradiated with a UV lamp. After baking at 95°C for 1-3 min, unpolymerized photoresist was removed from the paper by submerging the paper in acetone for 1 min, and by rinsing the paper with acetone. Next, the paper was dried under ambient conditions for 1 hr. Prior to use,

paper microfluidic devices were exposed to air plasma (Harrick PDC-32G) for 30 s. Areas covered with photoresist remained hydrophobic while areas without photoresist were hydrophilic.

4.2.3 Design and preparation of electrochemical detector for paper-based microfluidic devices

The electrodes were screen-printed in house using carbon ink containing PB as the working (WE) and counter electrode (CE) and silver/silver chloride ink as the reference electrode (RE) and conductive pads. The screen-printing emulsion was designed with Corel Draw 9 software and generated by Chaiyaboon Co. (Bangkok, Thailand). The electrode design is shown in Figure 4.1. The working electrode was designed to be as close as possible to the reference electrode to minimize the effect of uncompensated resistance between the WE and RE (spacing about 0.15 mm). The counter electrode (geometric area about 7.5 mm^2) was designed to be larger than the working (geometric area 1.3 mm^2) and reference electrodes (geometric area 1.2 mm^2) to allow unlimited current transfer in the circuit. All electrodes were designed with the working portion of the electrode on the hydrophilic portion of the paper and the contact pads on the hydrophilic portion of the paper. The screen printing process consisted of two layers. The first layer was applied with the silver/silver chloride ink and served as the reference electrode and conductive pads. Next, carbon ink containing PB was screened on the paper. Both layers were subsequently cured for 30 min at $65 \text{ }^\circ\text{C}$ and allowed to cool at room temperature.

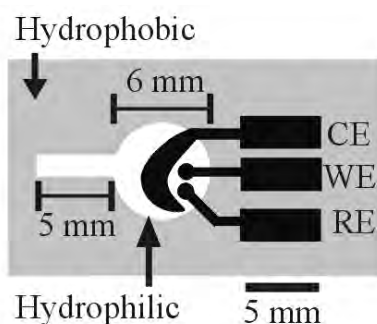


Figure 4.1 Basic design of the electrochemical detection cell for paper-based microfluidic devices. WE: working electrode, RE: reference electrode, CE: counter electrode.

4.2.4 Design and preparation of paper-based microfluidic devices for multianalyte determination

The characterization of electrochemical detection for paper-based microfluidic devices was firstly studied by dropping 5 μL of 0.1 M potassium phosphate buffer solution (pH 6) on the end of the paper at the detection zone. The solution flowed directly through the electrode zone and cyclic voltammetry was performed using a CH Instruments 1207A potentiostat. The scan rate dependence was studied at the carbon electrode containing PB. In addition to single analyte devices, multianalyte systems were fabricated using the method described above. A photograph showing the design is shown in Figure 4.2. Each reaction area was spotted with different enzymes for the specific analytes of interest. The glucose, lactate, and uric acid test zones were prepared by spotting 0.3 μL of glucose oxidase solution (645 U/mL), lactate oxidase (114 U/mL), and uricase solution (27 U/mL), respectively into the respective test zones. The paper was allowed to dry at room temperature for 10 min. All standard and enzyme solutions were prepared in 0.1 M potassium phosphate buffer (pH 6). For analysis, 5 μL of standard or sample solution was dropped on the center of paper and subsequently flowed to each test zone. Direct current chronoamperometry were then used for analysis at the screen-printed carbon PB-mediated electrode. The sampling rate for all chronoamperometric analyses was 10 Hz.

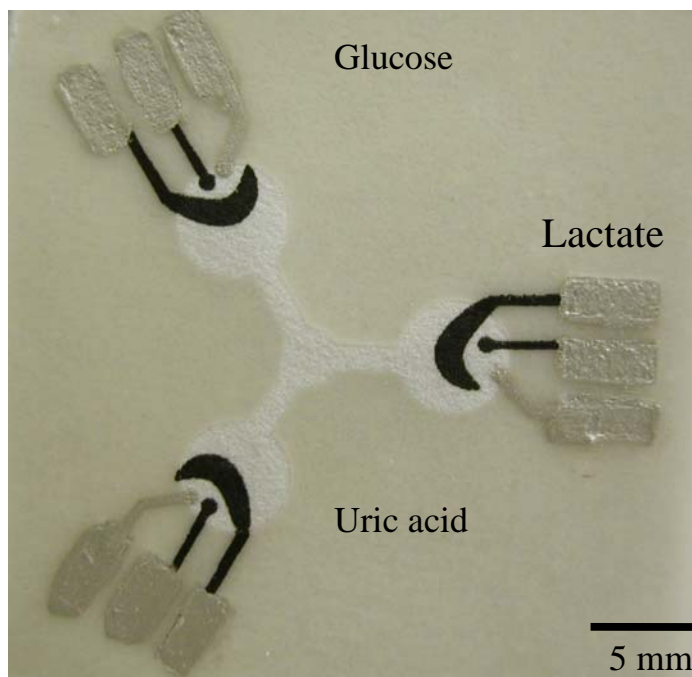


Figure 4.2 Picture of a three electrode paper-based microfluidic devices. The hydrophilic area at center of the device wicks sample into the three separate test zones where independent enzyme reaction occur. The silver electrodes and contact pads are made from Ag/AgCl paste with the black electrode portions are the PB-modified carbon electrodes. The device size is 4 cm x 4 cm.

4.2.5 Human serum sample

Human control serum samples (levels I and II) were obtained from Pointe Scientific (Canton, MI). Levels of analytes were provided by the supplier. All samples were analyzed using electrochemical detection for paper-based microfluidic without any pretreatment.

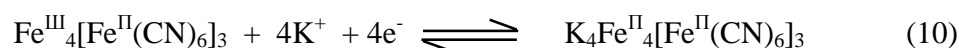
4.3 Results and discussion

The recent development of paper microfluidics has generated considerable excitement because of their ease of use, very low cost, and portability for point-of-care monitoring. To date, all reported systems have used colorimetric detection. While

colorimetric detection is the simplest detection mode, it has several significant problems as discussed previously. Here we report the development of an electrochemical detection scheme for quantitative analysis in paper microfluidics. Electrochemical detection, while more expensive than visual-based colorimetric detection, is still very low cost and requires minimal instrumentation. Here we demonstrate characterization of screen printed electrodes fabricated on paper microfluidic devices followed by their use for the measurement of clinically relevant analytes in a biological matrix using enzyme modified electrodes.

4.3.1 Characterization of electrochemical detection for paper-based microfluidic devices

Before using the devices for measuring analytes in biological samples, the functionality of the electrodes was established. The electrodes were screen-printed on the hydrophilic and hydrophobic area of paper with the working area of the electrodes on the hydrophilic portion of the device. To demonstrate proper electrode functionality and isolation of the leads by the hydrophobic photoresist underlayer characterization of the PB electrodes using cyclic voltammetry of buffer samples was performed. After dropping solution at the entrance of the microfluidic channel and allowing the test solution to wet the electrode area, cyclic voltammetry was performed. The redox reaction for PB is as follows:



The characteristic voltammograms as a function of scan rate for PB (Iron (III) hexacyanoferrate (II)) [23] are shown in Figure 4.3. These results agree well with published results for PB electrodes [23]. Next, the dependence of the PB peak current on the scan rate was studied for the electrochemical system on paper. Figure 4.4 shows anodic and cathodic peak currents were directly proportional to the square root of scan rate between 2.5 and 100 mV/s. It should be noted that the slopes of the forward and reverse sweeps are not identical as would be found at most traditional electrode materials.

The differences in slope could be the result of the use of a surface confined redox species (Prussian Blue) coupled with the expected non-ideal behavior of these carbon electrodes [23]. The linearity however indicates the mass transfer in this system is a diffusion controlled process similar to the behavior of traditional electrochemical cells [23-27]. A diffusion controlled process in this system represents the diffusion of potassium ions within the PB lattice in the plating phase of electrode [26-27].

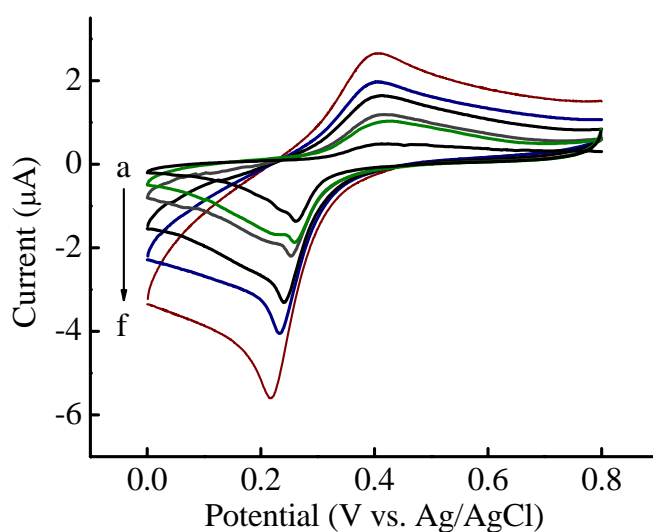


Figure 4.3 Representative cyclic voltammograms of the PB-modified carbon electrodes at various scan rates (a: 2.5, b: 5, c: 10, d: 25, e: 50, f: 100 mV/s) in 0.1 M potassium phosphate buffer (pH 6).

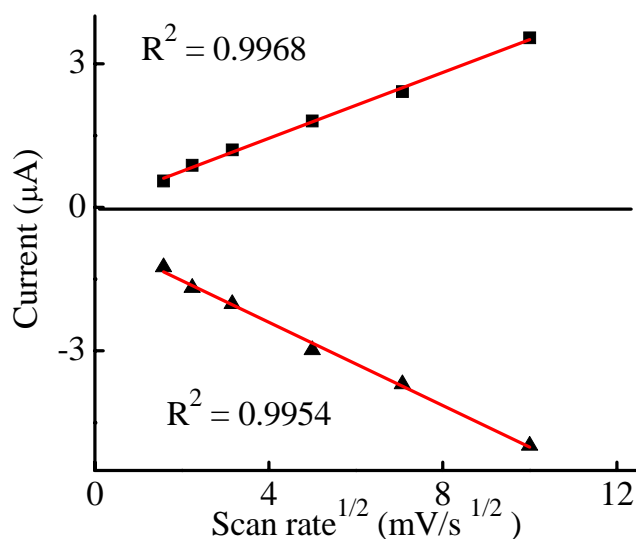


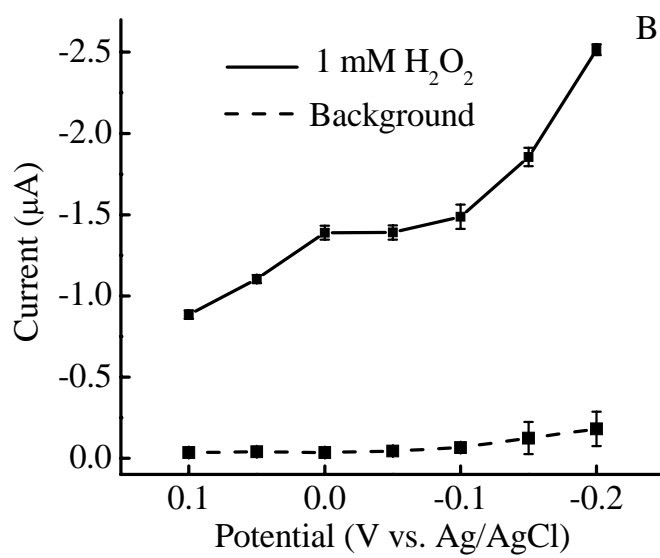
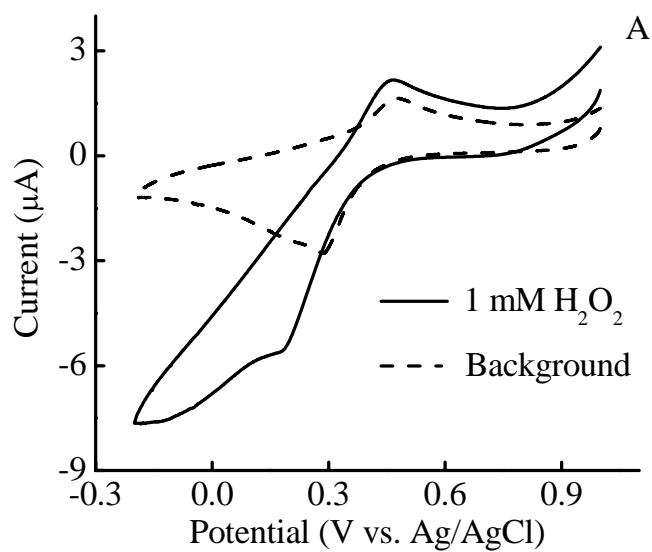
Figure 4.4 The relationship between anodic and cathodic currents and the square root of scan rate.

4.3.2 Choice of detection potential for hydrogen peroxide

The utility of our system was next demonstrated for different oxidase enzymes. Oxidase enzymes catalyze the oxidation of a substrate such as glucose, uric acid, or lactate while reducing oxygen to hydrogen peroxide (H_2O_2). Many electrochemical biosensors using enzymes rely on detection of peroxide for quantification of the analyte. Therefore, it is necessary to have methods for the detection of hydrogen peroxide at a low oxidation potential where few biologically relevant analytes will interfere. The most common electrochemical method is the anodic oxidation of H_2O_2 at a platinum electrode [28-30]. However, platinum is expensive and requires advanced patterning methods that dramatically increase the cost of fabrication [30]. Alternatively, screen-printed carbon electrodes that are significantly cheaper to produce can be used, however the high overpotential and subsequent interference from matrix species such as ascorbic acid and uric acid represents a significant problem for plain carbon electrodes [31]. One way to minimize the problem is by using the cathodic reduction of H_2O_2 aided by a catalytic redox mediator (e.g., Prussian Blue (PB) [23], cobalt hexacyanoferrate [32], or

horseradish peroxidase) [20,33-35]. For the current study, PB was used as the mediator on the electrode because it has been shown to be a selective catalyst for H_2O_2 reduction [36,37]. The catalytic reaction occurs in a relatively low potential region (-0.2 to 0.2 V versus Ag/AgCl) where interferences from endogenous compounds such as uric and ascorbic acid are minimal. Moreover, PB is an inexpensive material that is easy to incorporate with the paper-based screen-printed electrode.

The modified electrode was first characterized in the absence of H_2O_2 (Figure 4.5A, dashed line), and provided the characteristic anodic and cathodic peak of Prussian blue. Next, the catalytic nature of this electrode to the reduction of H_2O_2 was studied. Figure 4.5A (solid line) clearly shows a larger cathodic peak in the presence of 1 mM H_2O_2 relative to the background electrolyte. After characterizing the modified electrodes with cyclic voltammetry, a detailed investigation was conducted using chronoamperometry to optimize the detection potential, generate calibration data, and apply the proposed method to real samples. Chronoamperometry was used instead of cyclic voltammetry because it is a more sensitive, can achieve lower detection limits, and, for long-term applicability, is an easier detection method to implement. Hydrodynamic voltammetry (HDV) was first employed to optimize the detection potential for H_2O_2 in the range of 0.1 to -0.2 V. Analyte solution containing H_2O_2 was deposited in the microfluidic channel and the current measured at a fixed time with different potentials. The cathodic current of the H_2O_2 significantly increased as the detection potentials increased; however, the background current also increased as shown in Figure 4.5B. Therefore, ratios between H_2O_2 and background current (S/B) were considered. Figure 4.5C shows S/B ratio at each potential. The ratio signal had a maximum of 0 V versus the on-chip Ag/AgCl reference electrode so a detection potential of 0 V was selected for further studies. Higher potentials were not investigated because of the concern over interfering reactions with endogenous compounds.



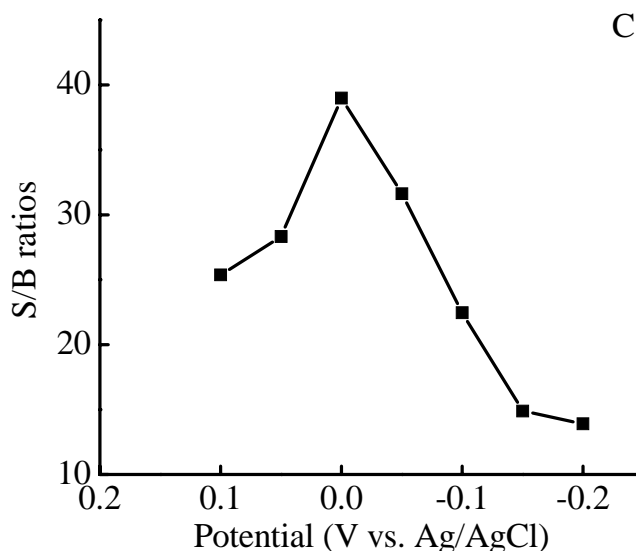


Figure 4.5 (A) Cyclic voltammograms of the carbon mediator Prussian blue electrode in the absence (dashed line) and presence of 1 mM H₂O₂ (solid line) at a 100 mV/s scan rate. (B) Hydrodynamic voltammograms of 1 mM H₂O₂ (solid line), and background (dashed line) for 100 s sampling time, from 3 separate devices. (C) Hydrodynamic voltammogram of signal-to-background ratios extracted from the data shown in B.

Moreover, analytical performance of H₂O₂ using our devices was demonstrated under the optimal detection potential. It obtained that a linear calibration curve between H₂O₂ concentration and the anodic current was between 0 to 0.1 mM (cathodic current, $\mu\text{A} = -1.265 (\text{H}_2\text{O}_2 \text{ conc.}, \text{mM}) - 0.082$, $R^2 = 0.9945$). The limit of detection (LOD) and limit of quantitation (LOQ) were found at 3.6 ± 0.3 and $11.9 \pm 1.1 \mu\text{M}$ (conc. $\pm\text{SD}$, $n = 3$), respectively as shown in Figure 4.6.

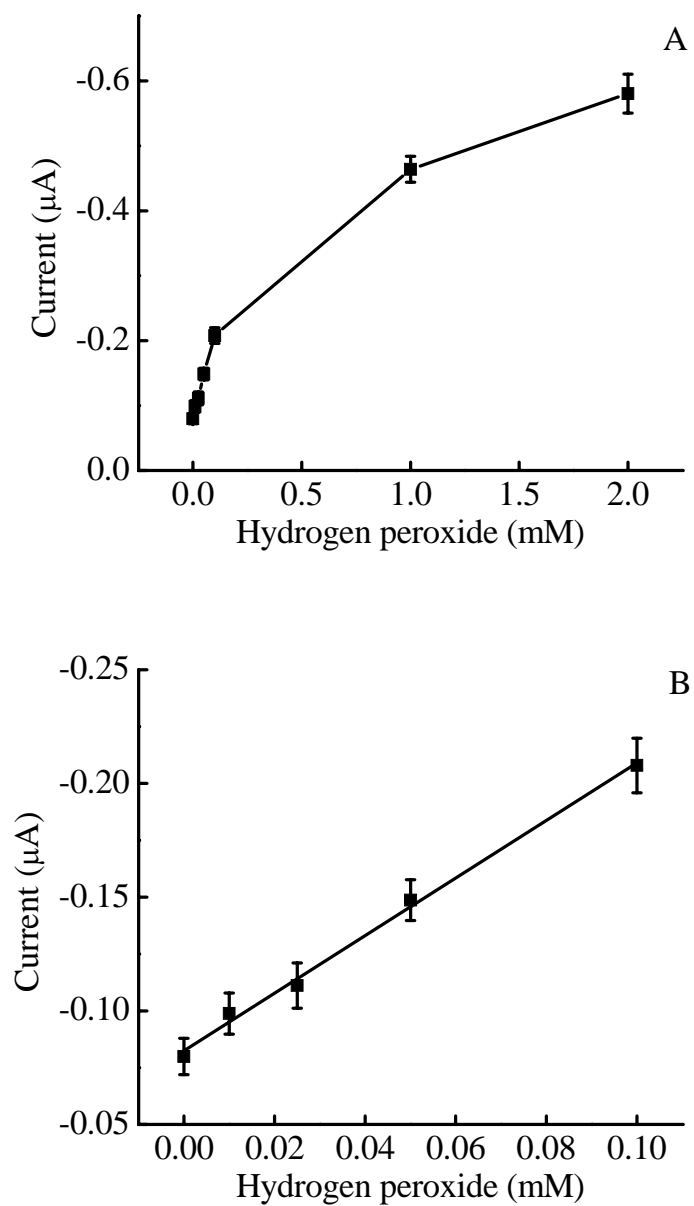
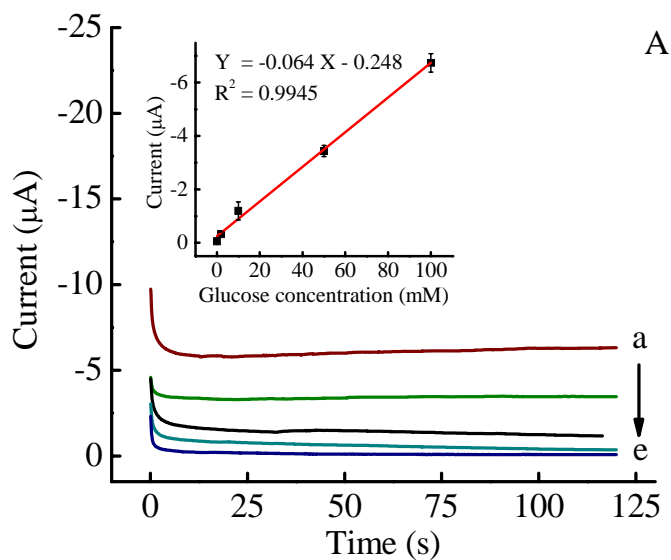


Figure 4.6 The relationship between cathodic current and hydrogen peroxide concentration in the range 0-2 mM (A) and 0-0.10 mM (B).

4.3.3 Analytical performance

After determining the optimal detection potential, the anodic current was recorded at 100 s, the apparent steady state current, to generate a linear calibration curve for a three

electrode system consisting of glucose, lactate, and uric acid oxidase on each of three electrodes (Figure 4.7). The average and standard deviation in Figure 4.7 are the mean and relative standard deviation, respectively, from 3 separate devices. The relative standard deviations of all concentrations of glucose, lactate, and uric acid was less than 14% ($n=3$), demonstrating acceptable reproducibility for this type of device. Calibrations of the anodic current against concentrations generated linear functions for all of the analytes within a range between 0 and 100 mM, and the coefficients of determination (R^2) were higher than 0.993. The limits of detection (LOD) and limit of quantitation (LOQ) were calculated as the concentration which produced the signal at three and ten times, respectively the standard deviation of a blank ($n = 10$) are summarized in Table 4.1.



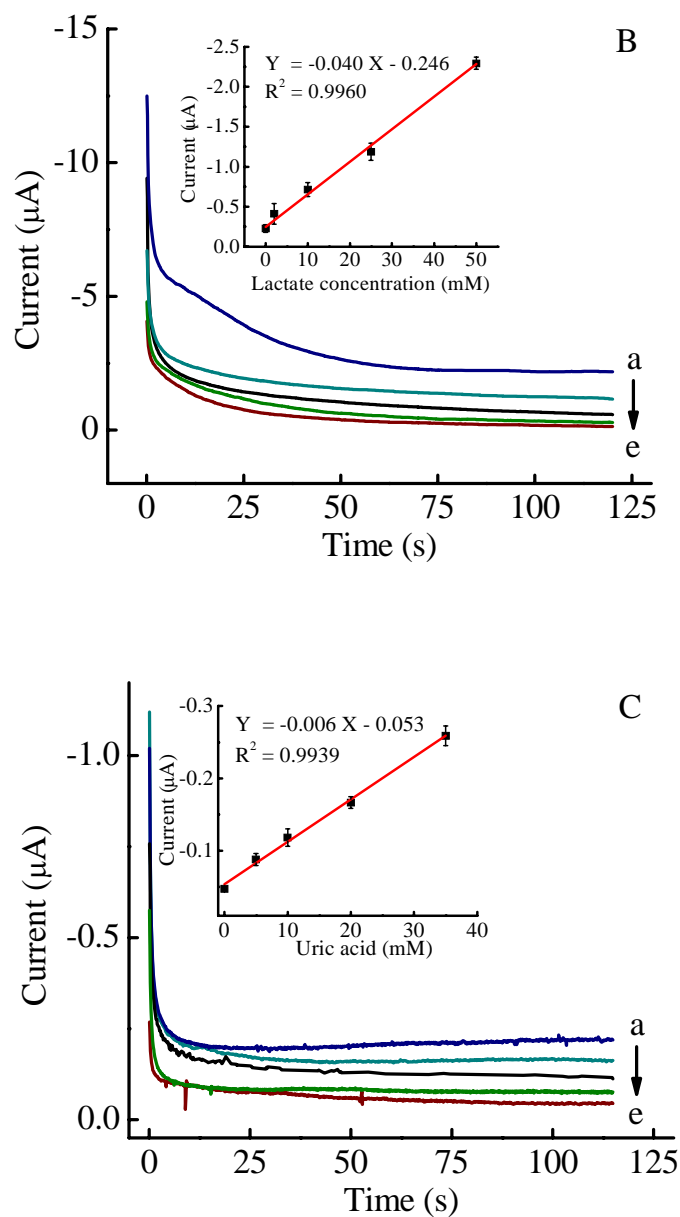


Figure 4.7 Chronoamperograms of (A) glucose (a: 100, b: 50, c: 10, d: 2 mM, e: Background), (B) lactate (a: 50, b: 25, c: 10, d: 2 mM, e: Bg), and (C) uric acid (a: 35, b: 20, c: 10, d: 5 mM, e: Bg) determination at 0 V versus an on-chip Ag/AgCl. The calibration plot of anodic currents at 100 s of sampling time for determination of three analytes are shown in the insert, $n = 3$.

Table 4.1 Linear dynamic range, limit of detection and limit of quantification of the proposed method

Analyte	Linear dynamic range (mM)	LOQ (mM)	LOD (mM)
Glucose	0-100	0.7	0.2
Lactate	0-50	1.2	0.4
Uric acid	0-35	4.6	1.4

The LOD for glucose was found to be substantially lower (0.2 mM) than the camera detection method (0.5 mM) [13]. The normal level of glucose is 3.5-5.3 mM in whole blood, 2.5-5.3 mM in serum, and 0.1-0.8 mM in urine [38]. Conventional blood glucometers can detect levels as low as 1.7 mM [39], while more modern glucometers can detect glucose as low as 0.6 mM in urine [30]. Our device should therefore be comprehensive for the determination of glucose in all biological samples including serum, blood and urine. The LOD of lactate was found to be 0.4 mM. Even though our LOD is higher than the LOD of conventional lactate kit (0.02 mM) [40], it is sufficient for clinical diagnostics where the normal concentration of lactate is 0.7-1.7 mM in blood, 0.5-1.7 mM in serum, and 5.5-22 mM in urine [38]. Uric acid had a measured LOD of 1.4 mM. Commercially available uric acid assay kits can detect as low as 13 μ M [41]. The normal level of uric acid is 0.1-0.4 mM in serum and 1.5-4.4 mM in urine [38]. Further improvements in the LOD for uric acid and the other markers can be obtained by improving the enzyme loading on the paper.

4.3.4 Analytical applications

In order to evaluate the electrochemical paper microfluidic system with real samples, three replicate determinations of glucose, lactate, and uric acid in clinical control samples were carried out using the optimized conditions. The control samples are common systems for determining the accuracy of diagnostic tests in a biologically

relevant matrix without worry of blood borne pathogens. The results are shown in Table 4.2. The paired *t*-test was used to validate our method versus the control levels for glucose and lactate. No significant difference was found at the 95% confidence level. Thus, the analyzed values of glucose and lactate in human serum can be accepted. We also tried to measure uric acid in the control samples, but the 0.4 mM concentration was below our LOD (1.4 mM). Therefore, we measured uric acid in spiked samples. The control samples (level I) were spiked with uric acid at 5 and 10 mM and analyzed without any additional treatment. The 5 and 10 mM uric acid spiked samples were measured to contain 5.9 ± 0.7 and 10.6 ± 1.3 mM, respectively. After subtracting the level of uric acid in control samples (level I: 0.4 mM), recoveries of uric acid were obtained in the range of 102-110%. Although our method cannot detect uric acid in the control serum samples, it can be successfully applied to the determination of uric acid in spiked control samples.

Table 4.2 Determination of glucose, lactate, and uric acid in control samples

Analyte	Concentration (mM \pm SD ^a)			
	Human serum level I		Human serum level II	
	Certified Value	Proposed method	Certified Value	Proposed method
Glucose	5.3 ± 0.3	4.9 ± 0.6	16.5 ± 0.7	16.3 ± 0.7
Lactate	1.4 ± 0.1	1.2 ± 0.2	3.5 ± 0.1	3.2 ± 0.3
Uric acid	0.4 ± 0.1	ND ^b	0.6 ± 0.1	ND ^b

^a SD: standard deviation ($n=3$), ^b ND: not detectable

4.4 Summary

We demonstrate here for the first time the coupling of electrochemical detection and paper microfluidics to provide rapid quantitative measurement of critical health markers in blood. In this work, the biological sample matrix and sample color have negligible effect on the glucose, lactate, and uric acid determination in real sample due to both selectivity of enzyme reaction and the working electrode material and detection

potential (0 V versus Ag/AgCl). Paper-based microfluidic devices have not been previously applied to real biological samples therefore we have employed electrochemical detection for paper-based microfluidic devices for the determination of glucose and lactate in real world samples for the very first time, which demonstrates the feasibility of using paper microfluidic devices in medical diagnosis.

PART B**Use of multiple colorimetric indicators for paper-based microfluidic devices**

Wijitar Dungchai^a, Orawon Chailapakul^{a,b}, Charles S. Henry^{c,*}

^a Sensor Research Unit, Department of Chemistry, Faculty of Science, Chulalongkorn University, Patumwan, Bangkok, 10330, Thailand

^b Department of Chemistry, Colorado State University, Fort Collins, CO, 80523-1872, USA

* Corresponding author

Abstract

We report here the use of multiple indicators for a single analyte for paper-based microfluidic devices (μ PADs) in an effort to improve the ability to visually discriminate between analyte concentrations. In existing μ PADs, a single dye system is used for the measurement of a single analyte. In our approach, devices are designed to simultaneously quantify analytes using multiple indicators for each analyte improving the accuracy of the assay. The use of multiple indicators for a single analyte allows for different indicator colors to be generated at different analyte concentration ranges as well as increasing the ability to better visually discriminate colors. The principle of our devices is based on the oxidation of indicators by hydrogen peroxide produced by oxidase enzymes specific for each analyte. Each indicator reacts at different peroxide concentrations and therefore analyte concentrations giving an extended range of operation. To demonstrate the utility of our approach, the mixture of 4-aminoantipyrine and 3,5-dichloro-2-hydroxy-benzenesulfonic acid, *o*-dianisidine dihydrochloride, potassium iodide, acid black, and acid yellow were chosen as the indicators for simultaneous semi-quantitative measurement of glucose, lactate, and uric acid on a μ PADs. Our approach was successfully applied to quantify glucose (0.5–20 mM), lactate (1–25 mM), and uric acid (0.1–7mM) in clinically relevant ranges. The determination of glucose, lactate, and uric acid in control serum and urine samples was also performed to demonstrate the applicability of this device for biological sample analysis. Finally results for the multi-indicator and single indicator system were compared using untrained readers to demonstrate the improvements in accuracy achieved with the new system.

4.5 Introduction

Point-of-care testing (POCT) has become relatively commonplace in the developed nations as a way to augment traditional medicine and increase patient compliance [42]. POCT is also needed in the developing world because it can reduce the number of clinical visits, decrease costs to the patient and healthcare system, increase patient satisfaction, improve clinical outcomes, and provide clinical services for people in low resource settings [43-46]. Paper strip tests, termed lateral-flow immunochromatographic tests, are currently used in these scenarios [47]. Paper strip tests are commercially available for pregnancy [48], diabetes [49,50], drugs of abuse [51,52], and biomarkers of pathogens test [53,54]. Most paper strip tests use visible color changes for qualitative analyte detection. In the assay, flow is directed along the paper matrix by capillary force, and the analyte is subsequently bound by the capture antibody at the test line. However, qualitative analysis is not sufficient when analyte levels are important for diagnosis or treatment. Much effort has therefore been directed towards the development of quantitative paper strip tests but these devices still required instrumentation and trained personnel for use and are limited to a single analyte [55,56].

As an alternative to traditional paper-based immunochromatographic tests, Whitesides and coworkers recently introduced paper-based microfluidics (μ PAD), which represent the next generation of paper strip test devices [8,10-13]. This approach, which combines many advantages of paper strip tests with the utility of microfluidic devices, holds significant potential for POCT due to its low cost, multianalyte capability, low sample volume, and inherent portability [8,10-13,57]. To date, μ PADs have been developed for glucose, protein, lactate, uric acid, and cholesterol determination [8,57]. The results of the assay were quantified by comparing the color intensities generated by unknowns to those generated for known analyte concentrations. Matching color and intensity by eyes can be complicated by many factors, however, including different color perception, differences in lighting, and the difference between the colors of a dry printed color and those seen in wetted paper. In an effort to conduct quantitative analysis for diagnostic tests based on paper microfluidics, several authors have used cameras or scanners to record the color intensity [13]. Camera phones and portable scanners can be used by unskilled personnel in remote areas but require transmission of data from on-site to

remote experts, delaying the decision making process. Moreover, the intensities of digital images from a camera are affected by the lighting.

One approach to overcome the limitations of colorimetric approaches for μ PADs is to use multiple indicators for a single analyte. Greater visual discrimination is possible when more than one color is developed as opposed to different hues or intensities of a single color [58]. Hence, multiple indicators should provide more accurate results as compared to single color tests by allowing differences in hue and intensity to be averaged across multiple detection spots for the same analyte. In addition, the improved accuracy should allow for diagnosis by untrained personnel without the need to transmit the results to a central laboratory. Here, we report the development of a novel multiple-indicator approach for μ PADs that allows simultaneous detection using iodide [8], the mixture of 4-aminoantipyrine and 3,5-dichloro-2-hydroxy-benzenesulfonic acid [59], *o*-dianisidine [60], acid yellow and acid black for each of the three analytes. The devices share advantages of previous μ PADs, while allowing for more accurate quantitative analysis of glucose, uric acid, and lactate without external instrumentation. The colorimetric assays in this work utilize oxidase enzymes to decompose analytes and produce hydrogen peroxide [59,61]. Hydrogen peroxide then oxidizes the indicators to generate a visible color change. Each indicator yields a different color and will also change color at different analyte concentrations, allowing a greater dynamic range to be achieved [62-64]. Here, the volume of reagent and sample spotted on the devices was first optimized. Dynamic ranges were then investigated. Our approach was successfully applied to quantify glucose (0.5-20 mM), lactate (1-25 mM), and uric acid (0.1-7 mM) in clinically relevant ranges. Finally, the devices were successfully applied to the analysis of control serum and urine samples. To demonstrate the improvements in accuracy of measurement for clinical samples, 10 random untrained individuals were asked to screen μ PADs comparing single indicator versus multiple indicators. Tests using multiple indicators yielded a statistically significant improvement in accuracy of the measurement compared to tests performed with a single indicator color.

4.6 Experimental methods

4.6.1 Materials and equipments

D-(+)-glucose (99.5%), sodium L-lactate (98%), uric acid (99%), glucose oxidase (from *Aspergillus niger*, 215 U/mg), uricase (from *Candida Sp.*, 2 U/mg), peroxidase Type I (from *Horseradish*, 113 U/mg), 4-aminoantipyrine (reagent grade), 3,5-dichloro-2-hydroxy-benzenesulfonic acid (sodium salt, 99%), and *o*-dianisidine dihydrochloride (purified grade for use with peroxidase reaction) were purchased from Sigma-Aldrich (St. Louis, MO). Lactate oxidase (from *Aerococcus viridians*, 38 U/mg) was obtained from A.G. Scientific, Inc (San Diego, CA). Potassium phosphate (ACS grade), potassium iodide (ACS grade), sodium hydroxide (ACS grade) and acid yellow 34 (Indicator grade) were purchased from Fisher Scientific (Pittsburgh, PA). Acid Black 1 (Indicator grade) was purchased from Acros Organic (Geel, Belgium). Trehalose dehydrate (HPLC grade) was obtained from Calbiochem (Gibbstown, NJ). Acetone (AR grade) was obtained from Mallinckrodt chemicals (Phillipsburg, NJ). SU-8 3025 negative photoresist was purchased from MicroChem Corp. (Newton, MA). Whatman #1 filter paper was obtained from Cole-Parmer (Vernon Hills, IL). All chemicals were used as received without further purification. A digital camera (coolpix5000, Nikon corp.) was used to photograph results.

4.6.2 Preparation of paper-based microfluidic devices

Photolithography was used to pattern the filter paper according to previously reported methods [47, 57]. Briefly, SU-8 3025 photoresist was poured on the center of the paper and distributed using a spin-coater (Laurell Technologies Corp., WS-400A-6NPP/LITE). The photoresist-covered paper was baked at 95 °C for ~5 min. The paper was then covered with a patterned transparency film generated using a standard laser printer and irradiated with a UV lamp at 100% intensity (400 W) for 7 s (Uvitron international, Intelli-RAY 400). After baking at 95 °C for ~3 min, unpolymerized photoresist was removed from the paper by submerging in acetone for 1 min, followed by rinsing with acetone. After that, the paper was dried under ambient conditions for approximately 1 hr. Prior to adding the reagents, the paper microfluidic devices were exposed to an air plasma (Harrick PDC-32G) at 18 W for 30 s. Areas covered with photoresist remained hydrophobic while areas without photoresist were hydrophilic.

4.6.3 Design of multiple oxidative indicators for paper-based microfluidic devices

For the current experiments, the dendritic flow channels terminating in nine detection zones (giving position number 1-4, 5-7, and 8-9 of the detection zones for glucose,

lactate, and uric acid detection, respectively) connected to a central sample deposition spot were created as shown in Figure 4.8. Each detection zone was spotted with a different indicator in addition to the appropriate enzyme. The indicators used here were the mixture of 4-aminoantipyrine (AAP) and 3,5-dichloro-2-hydroxy-benzenesulfonic acid (DHBS) in the mole ratio of 1:2 abbreviated to AB, *o*-dianisidine dihydrochloride (OD), potassium iodide (KI), acid yellow 34 (Y), and acid black 1 (B). AB, OD, and KI oxidized will change from colorless to red [64,70], green-brown [66,67], and yellow-brown colors [8,68,69] while Y and B oxidized will change from yellow and black color to colorless, respectively. For detection, sample was added to sample deposition spot and flowed outward via capillary forces to the detection zones.

4.6.4 Effect of reagent and sample volume

Varying volumes of red food dye (0.4, 0.5, and 0.6 μL) were dropped into the detection zone to optimize the volume of reagent. The effect of sample volumes was studied by dropping 5.0, 7.0, 9.0, and 11 μL of red food dye into the center of devices using a micropipette. The micropipette which was used to transfer and control the sample volume into device may not be available in the field. In our effort to conduct quantitative analysis for self-monitoring diagnostic tests based on paper microfluidic devices without external equipment, the assays of known volume of level 4 standard solution (11 μL) containing 5 mM glucose, 10 mM lactate, and 4.5 mM uric acid were compared with unknown volume dropped by dropper. Images of fully developed tests were captured with a digital camera for additional characterization.

4.6.5 Preparation of multiple oxidative indicators for paper-based microfluidic devices

For a given analyte, positions 1-4, 5-7, and 8-9 were spotted with glucose oxidase, lactate oxidase, and uricase enzyme, respectively and the different indicators. The glucose assay was prepared by spotting 0.5 μL of mixture each oxidative indicator, glucose oxidase solution (645 U/mL), *Horseradish* peroxidase (339 U/mL), and 0.3 M trehalose into the four detection areas of glucose. Trehalose is added to stabilize the enzyme according to prior reports [70]. The three lactate and two uric acid test zones were created with the different component of indicators and the same amount of *Horseradish* peroxidase and trehalose but the specific enzymes used were lactate oxidase (114 U/mL), and uricase (80 U/mL), respectively. The indicator composition of each test zone is shown in Figure 4.8. After spotting the reagent solution, the

paper was allowed to dry at room temperature (~22°C) for 10 min. All standard and enzyme solutions were prepared in 0.1 M potassium phosphate buffer (pH 6) except for 15 mM of uric acid stock solution which prepared in 20 mM sodium hydroxide. 6 levels of standard solution containing with glucose, lactate, and uric acid and a negative control consisting of buffer were used to study the multiple indicator approach. The concentrations of glucose, lactate, and uric acid in each level of standard solution are shown in Table 4.3.

Table 4.3 Concentrations of glucose, lactate, and uric acid in each level of standard solution

Std. level	Glucose Conc. (mM)	Lactate Conc. (mM)	Uric acid Conc. (mM)
0	0	0	0
1	0.5	1	0.1
2	1.5	2.5	1
3	3	5	2.5
4	5	10	4.5
5	10	20	6
6	20	25	7

4.6.6 Human serum sample

Human control serum and urine samples (levels I and II) were obtained from Pointe Scientific (Canton, MI) and Quantimetix Corporation (Redondo Beach, CA), respectively. These complex samples are intended to mimic biological fluids and are used to validate clinical assays commercially. Analyte concentrations were provided by the supplier. All samples were analyzed using multiple oxidative indicators for paper-based microfluidic devices without pretreatment. To test the hypothesis of improved accuracy, results from urine and serum samples were interpreted by 10 randomly selected, untrained individuals who are not familiar with this assay from the varieties of faculty such as education, veterinary, science at Colorado State University for both single and multiple indicator systems.

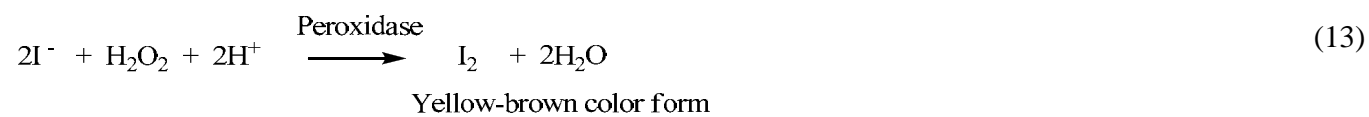
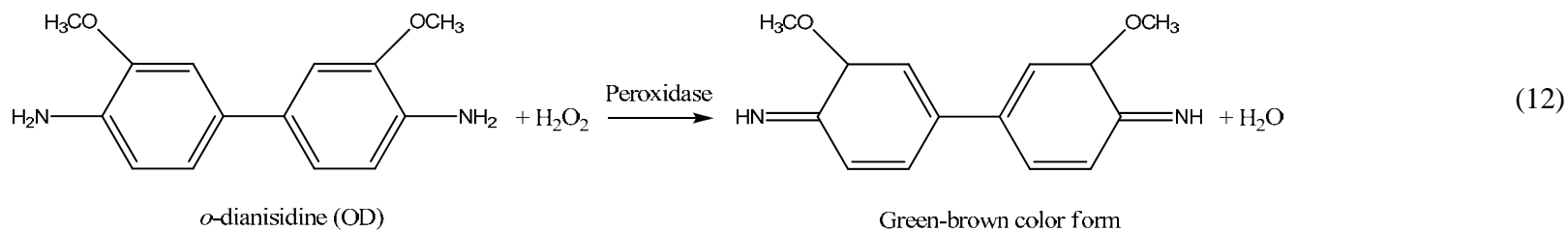
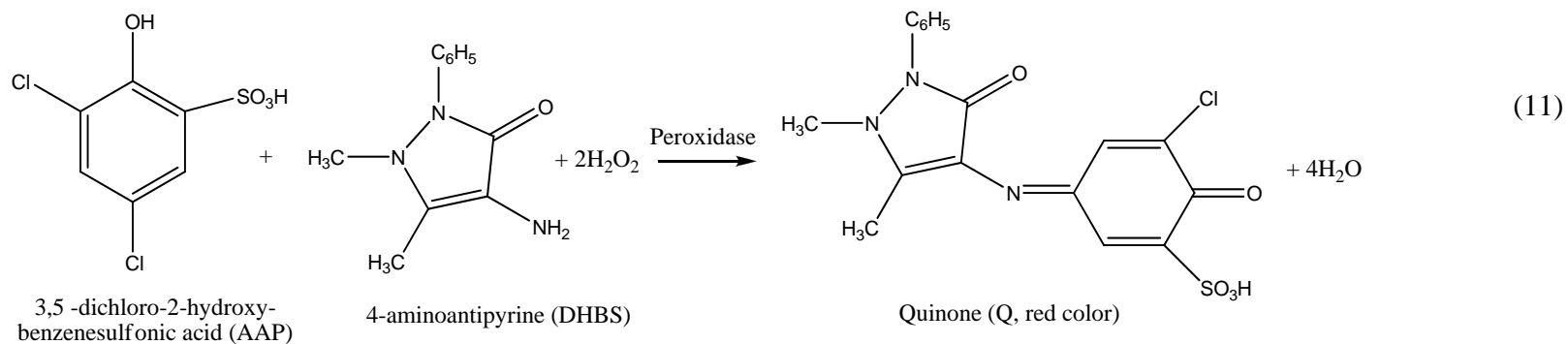
4.6.7 Lifetime of the devices

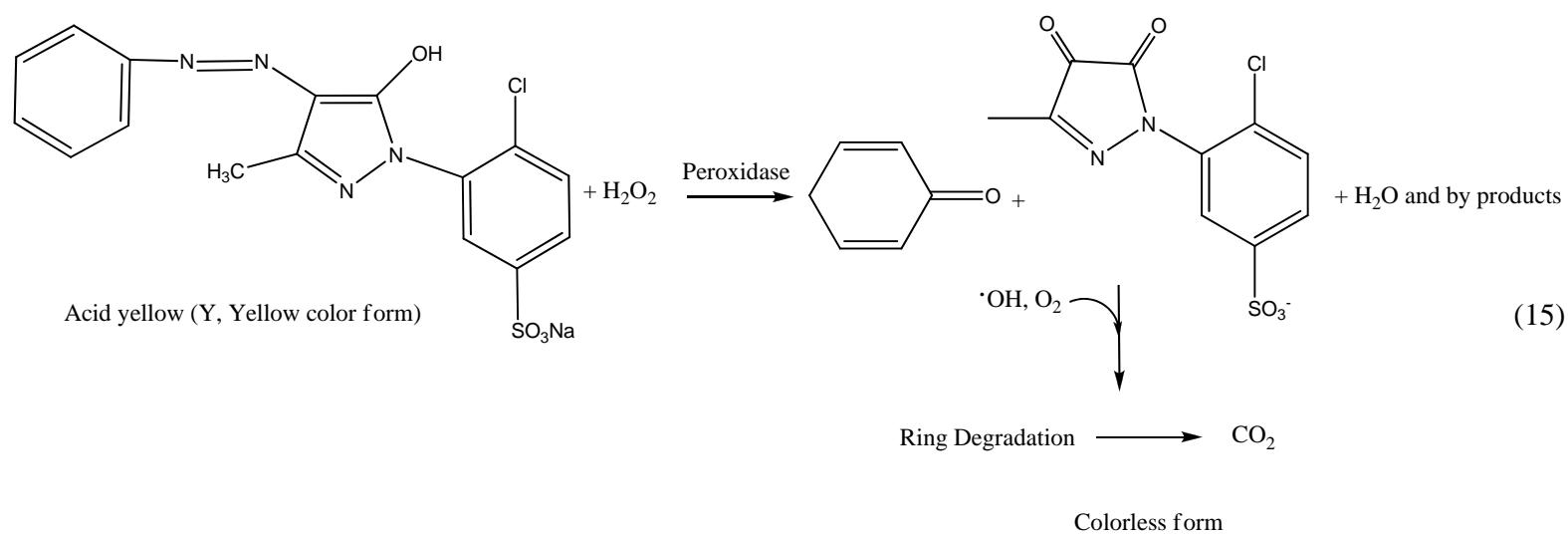
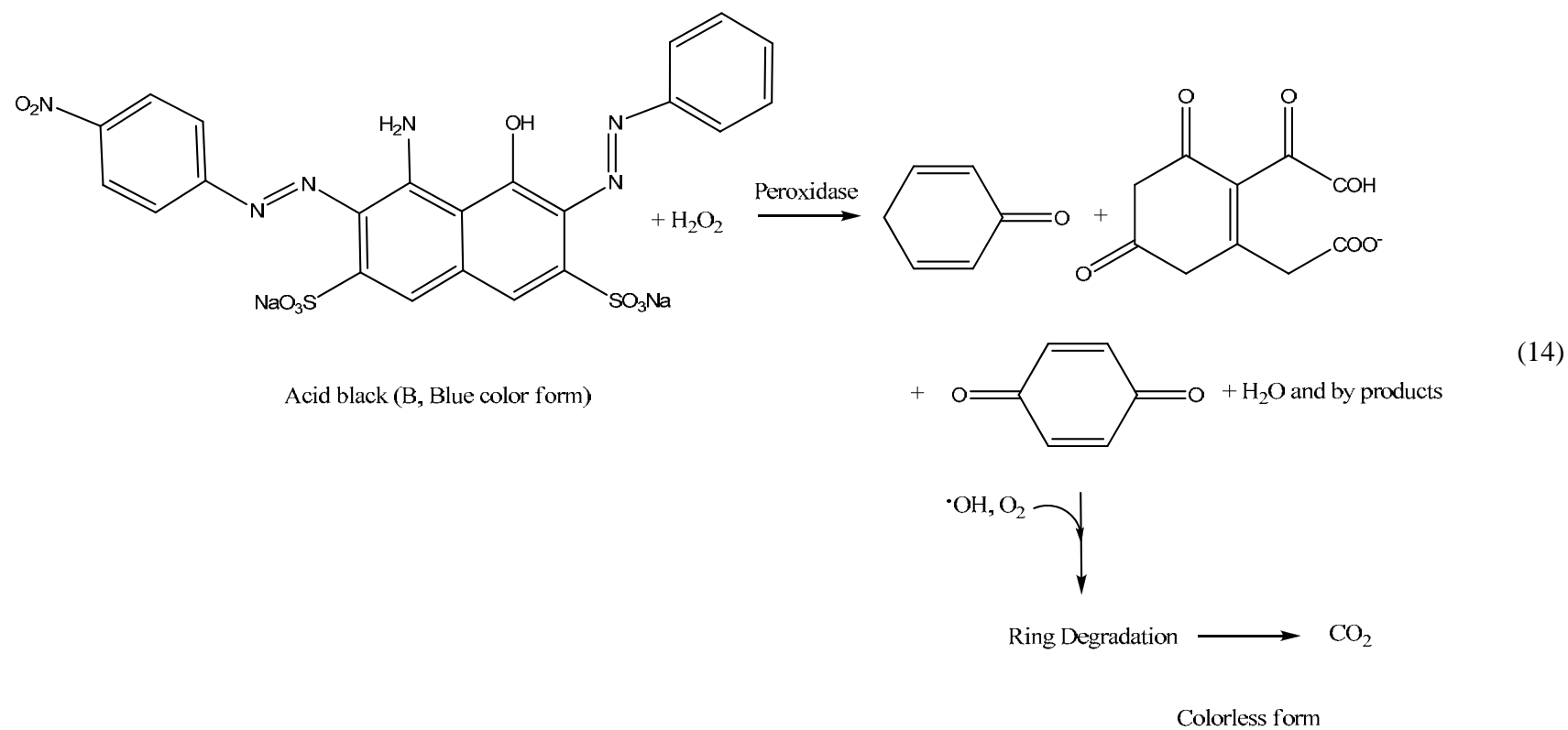
The devices spotted with oxidase enzyme and indicators solution were kept at 8 °C, room temperature (~22 °C), and 40 °C for multiple days to determine lifetime. Stored devices were tested for lifetime using the standard mixtures (Table 4.3) every four days.

4.7 Results and discussion

4.7.1 Colorimetric bioassays

The goal of this work was to test the hypothesis that multiple indicators for a single analyte would improve the accuracy of the data interpretation in colorimetric μ PAD assays. Three analytes of clinical relevance (glucose, lactate, and uric acid) were tested using multiple indicators (AB, OD, KI, Y, and B) for each analyte. The device design is shown in Figure 4.8. The combination of indicators is needed for this assay because it provides the greater visual discrimination than one color. Two types of indicators were used. The first type generated a stable color on oxidation. AAP and DHBS produced a red quinone product on reaction with peroxide. In a similar fashion, green-brown and yellow-brown stable colors were generated from the reaction of H_2O_2 with OD and KI. The second type of indicator was selected to lose color when oxidized. Here, we used Y (yellow color) and B (blue color) as indicators because they are colorless when oxidized. The reactions between peroxide and these indicators were shown in below equations.





The first indicator shade in oxidized form will be mixed with the other indicator shade at each test zone so the gradient of shade and intensity color occurs at the different levels of analyte. For example, we used the mixture of AB as the first indicator and Y as the second indicator at position number 1 of device for the glucose test. At two levels of glucose, we will get two shades as orange (mixture of yellow and red color) and red colors whereas the previous approach using one indicator obtains only one shade at the different color intensities providing more difficult visual distinction than the indicators combination. Our proposed method was therefore expected to provide a larger difference in color hues and intensities, allowing greater visual discrimination and therefore accuracy. All case of the mixture of first and second indicator was studied to demonstrate the dynamic range between the changing of shade and glucose, lactate, and uric acid concentration but we found only 4, 3, and 2 cases of the mixture changed the shade of indicator for glucose, lactate, and uric acid assay, respectively. Therefore, our design needed 4, 3, and 2 wells for glucose, lactate, and uric acid assay as shown in Figure 4.8.

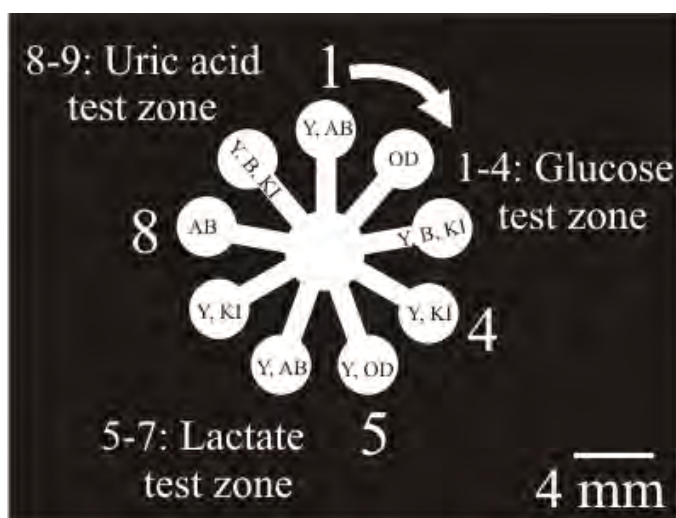


Figure 4.8 Design of multiple oxidative indicators for paper-based microfluidic devices which determine three analytes simultaneously with nine test zones. Back and white colors refer to hydrophobic and hydrophilic area, respectively. The device size is 2 cm x 2 cm. Position numbers 1–4: glucose test zones, 5–7: lactate test zones, 8–9: uric acid test zones.

4.7.2 Effect of reagent and sample volume

We first determined the volume of reagent and sample required for analysis. In existing paper test strips, the major cost comes from reagents. Hence, we designed the reaction zones to be small (3 mm diameter) for reduced reagent consumption while still making it large enough to be visible to the naked eye. Reaction zone diameters smaller than 3 mm were studied. Even though the reagent consumption can be reduced with a small detection zone, dispensing less than 0.2 μL is difficult with standard micropipettes. We next determined the reagent volume necessary to wet the entire detection zone by dropping red food dye in the range of 0.4 to 0.6 μL into the detection zones. As the results show in Figure 4.9A, 0.4 μL of reagent solution cannot completely wet the detection zones whereas 0.6 μL spread outside the detection zones. Therefore, we selected 0.5 μL of reagent solution for the further experiments. The minimum sample volume that can spread through the entire device was also studied by spotting red food dye into the center of the device. It was found that 11.0 μL of sample is required to fill all detection zones (Figure 4.9B-E). In many situations a micropipette may not be available to apply an accurate sample volume. Hence, the effect of sample volume on the assays reaction was determined by dropping a standard solution level 4 containing 5 mM glucose, 10 mM lactate, and 4.5 mM uric acid into the center of the device with 11.0 μL . In addition, an unknown volume was dispensed with a disposable transfer pipet to simulate real field-testing. The results with controlled volumes (Figure 4.9F) were compared with results from unknown volumes (Figure 4.9G and 4.9H). We found that the color hue of the three indicators was the same regardless of the sample volume added, meaning tight control of sample volume was not necessary. In the field, the samples can therefore be directly dropped into our devices using simple transfer pipettes and similar spotting devices.

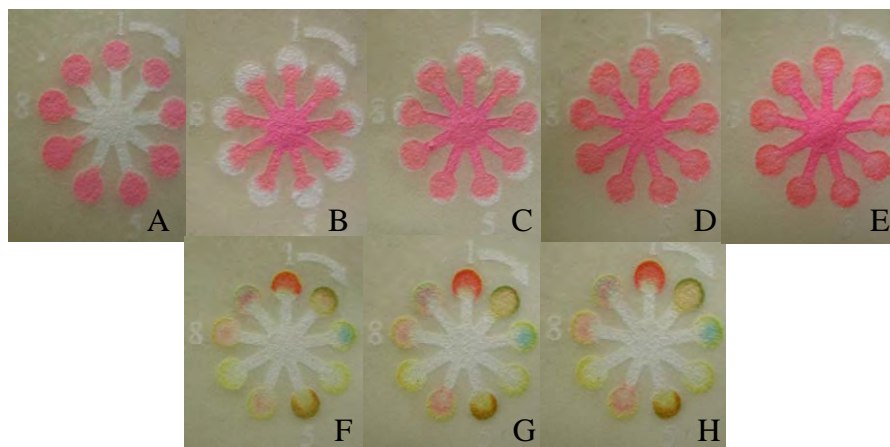


Figure 4.9 (A) Paper-based microfluidic devices after spotting red food dyes of various volumes (0.4, 0.5, and 0.6 μL into the position numbers 1–3, 4–6, and 7–9, respectively of the detection zones). (B–E) Paper-based microfluidic devices after spotting 5 (B), 7 (C), 9 (D), and 11 μL (E) of red food dye respectively into the central of devices. (F–H) Multiple oxidative indicator for paper-based microfluidic devices after spotting level 4 of standard solution including 5 mM glucose, 10 mM lactate, and 4.5 mM uric acid with 11 μL of controlled standard volume (f) and unknown of standard volume (G and H).

4.7.3 Simultaneous measurement of three analytes

The principle of our proposed method is to use the color change of each oxidative indicator and the color intensity at different analyte concentrations to improve the accuracy and extend the linear range of colorimetric μPAD assays. To demonstrate the multiple indicator systems, we studied the dynamic range of glucose, lactate, and uric acid on a single device. The results were captured with a digital camera for visualization (Figure 4.10). Glucose at 0.5 mM generated an orange color (position number 1). Glucose at 1.5 mM showed orange and green-brown colors, while glucose between 3 and 5 mM gave red and green-brown colors (position number 1 and 2, respectively). Glucose concentrations ≥ 10 mM glucose gave red, green-brown, and brown colors (position number 1-4). Moreover, the intensity of red, green-brown increased when glucose concentrations increased. Hence, the difference of hue and intensity of multiple indicators can be used to identify glucose concentration. The normal level of glucose is 2.5-5.3 mM in serum, and 0.1-0.8 mM in urine [38]. Given the dynamic range of the color changes, our devices could be used in a variety of biological matrices such as serum, plasma, and urine.

Our device also gave multiple color hues for different concentrations of lactate. Lactate at 1 mM gave brown and orange colors, while lactate concentrations between 5 and 20 mM gave green-brown and red colors at positions 5 and 6, respectively. Moreover, lactate concentrations ≥ 25 mM showed three colors, green-brown, red, and brown at positions 5, 6, and 7, respectively. These devices are therefore sufficient for clinical diagnostics where the normal concentration of lactate is 0.5-1.7 mM in serum, and 5.5-22 mM in urine [38].

Uric acid detection zones also exhibited color changes as a function of concentration. Concentrations at 0.1 mM gave orange color at position number 8, while concentrations between 1 and 2.5 showed orange and red colors at position number 8 and 9, respectively. At uric acid concentrations ≥ 2.5 mM, both position number 8 and 9 were red. The normal level of uric acid is 0.1-0.4 mM in serum and 1.5-4.4 mM in urine [38]. These results clearly suggest the ability to visually discriminate between different concentrations using multiple indicators for a single analyte.


Std. level	0	1	2	3	4	5	6
Conc. (mM)							
Glucose	0	0.5	1.5	3	5	10	20
Lactate	0	1	3	5	10	20	25
Uric acid	0	0.1	1	2.5	4.5	6	7

Figure 4.10 Multiple oxidative indicators system designed on paper-based microfluidic devices for the simultaneous semi-quantitative analysis of glucose, lactate, and uric acid. Pictures were captured after spotting varying concentration of three analytes for 10 min.

The reproducibility of our proposed method was also studied by spotting each level of standard solution into three paper devices in the same day (intra-day assay) and three different days (inter-day assay) (Figure 4.11). At each test zone, the change in color intensity as a function of analyte concentration was obtained with high reproducibility.




































Std.	Intra-day			Inter-day	
	1 st	2 nd	3 rd	2 nd	3 rd
0					
1					
2					
3					
4					
5					
6					

Figure 4.11 Multiple oxidative indicators system designed on paper-based microfluidic devices for the simultaneous semi-quantitative analysis of glucose, lactate, and uric acid. Pictures were captured after spotting varying concentration of three analytes for 10 min.

4.7.4 Semi-quantitative measurement of three analytes in real samples

The multi-indicator μ PAD devices were next evaluated for glucose, lactate, and uric acid analysis in clinical control samples. The control samples are used for determining the accuracy of diagnostic tests in a biologically relevant matrix without worry of blood borne pathogens. The results are shown in Figure 4.12. We found that level I serum and urine samples gave significantly different color patterns than the level II samples. The results indicated that glucose concentrations were between 5-10 mM in serum level I (control level: 5.6 mM), and 3-5 mM (control level: 3.3) in urine level I, whereas 20 mM glucose was determined in both serum and urine samples level II (control serum and urine level: 16.8 and 16.5 mM, respectively). For the lactate test, we obtained brown and orange colors for both serum sample levels I and II. This indicated lactate levels in both serum sample levels were between than 1-2.5 mM. Moreover, the intensities of brown color from standard lactate can be used to identify lactate concentration of 1 mM in level I (control level: 1.2 mM) and 2.5 mM (control level: 3.3 mM). In these cases, both the color intensity and hue can be used to confirm our results. Lactate test zones of both urine sample levels show insignificant difference of the color changing comparing with buffer solution (Std. level 0). Therefore, we can indicate both urine samples in the absence of lactate correlated with the certificated concentration. Uric acid concentrations in samples were determined to be 0.1 mM for level I serum and urine samples (control level: 0.2 mM in serum and 0.5 mM in urine) and 1 mM for level II serum and urine samples (control level: 0.7 mM in serum and 1.1 mM in urine) by comparing the differences in color intensity.





Samples		Certified Concentration (mM)	Our proposed method (mM)	
Serum Level I	Glucose	5.6		5-10
	Lactate	1.2		1
	Uric acid	0.2		0.1
Serum Level II	Glucose	16.8		20
	Lactate	3.3		2.5
	Uric acid	0.7		1
Urine level I	Glucose	2.9		3-5
	Lactate	Not labeled		ND
	Uric acid	0.5		0.1
Urine level II	Glucose	16.5		20
	Lactate	Not labeled		ND
	Uric acid	1.1		1

Figure 4.12 Multiple oxidative indicators system designed on paper-based microfluidic devices for the simultaneous semi-quantitative analysis of glucose, lactate, and uric acid in real biological samples.

To demonstrate our method comparing with a single indicator system in terms of accuracy, the highest sensitivity single dye indicators including Y+AB, Y+OD, and AB for the glucose, lactate, and uric acid test, respectively were selected for single indicator systems as showed in Figure 4.13. We also compared the percentage of correct answer obtained from 10 untrained individuals using single and multiple indicator tests (Figure 4.14). The results indicated that our devices were successfully applied for glucose, lactate, and uric acid screening

tests by the naked eye. As can be seen in Figure 4.13, there is a clear difference between the two sets of data in terms of colors generated. Furthermore, Figure 4.14 shows the increase in accuracy for the tests using multiple indicators. The single indicator system had an accuracy of ~70%, while the multi-indicator system had an accuracy of over 90%. The results suggest our approach provides a more accurate result when compared to a single indicator system.

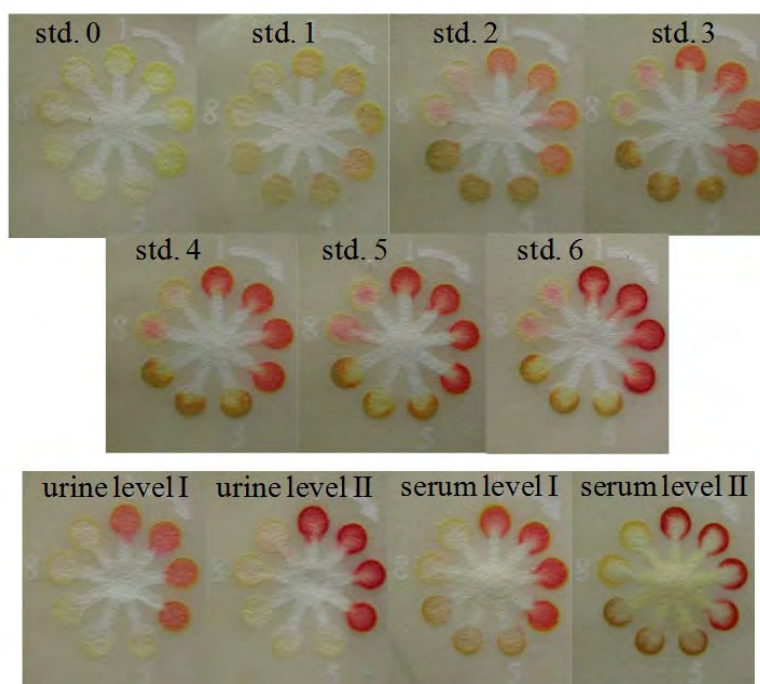


Figure 4.13 Single indicator system designed on paper-based microfluidic devices for the simultaneous semi-quantitative analysis of glucose, lactate, and numbers 1–4: glucose test zones using Y +AB indicator, 5–7: lactate test zones using Y +OD indicator, 8–9: uric acid test zones using AB indicator.

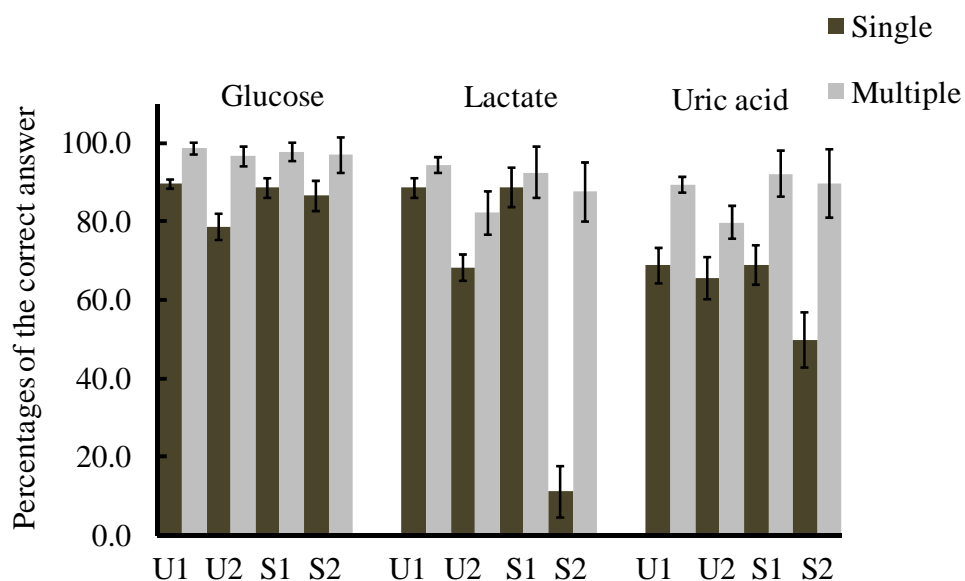


Figure 4.14 Comparison of percentages of the correct answer where a corrected answer was determined to be within ± 0.5 mM of the certified concentration between single and multiple-indicator systems ($n = 10$). U1: level I urine human, U2: level II urine human, S1: level I serum human, S2: level II serum human, error bar: standard deviation ($n = 3$).

4.7.5 Lifetime of the devices

Diagnostic devices must remain stable for weeks to be useful in the field for use in developing countries. Hence, the performance of devices was studied after storing the prepared paper devices for multiple days at varying temperatures. To test stability, prepared paper devices were dried at ambient condition before storage at either 8 °C, room temperature (~ 22 °C), or 40 °C. Oxidase enzymes can degrade, aggregate, or unfold during dry storage [38]. Non-reducing sugars such as sucrose and trehalose, and polyols such as mannitol have been used to stabilize dried proteins during storage [70,71-73]. Here, trehalose was added to oxidase enzymes solution during devices preparation to improve stability of the enzyme during storage. The lifetime of these devices was observed over a period of several days as shown in Figure 4.15. We found that multiple indicators, which were generated at all detection zones of all standard solution levels, exhibited no significant difference from day to day at all temperatures.

At 12 storage days at room temperature and 40 °C, an observable signal decrease was noted. The results indicated the devices can be kept for 8 day without loss of activity but longer storage time requires refrigeration (Figure 4.16). Future work will focus on methods to increase the lifetime of these devices to allow months of storage at elevated temperatures.

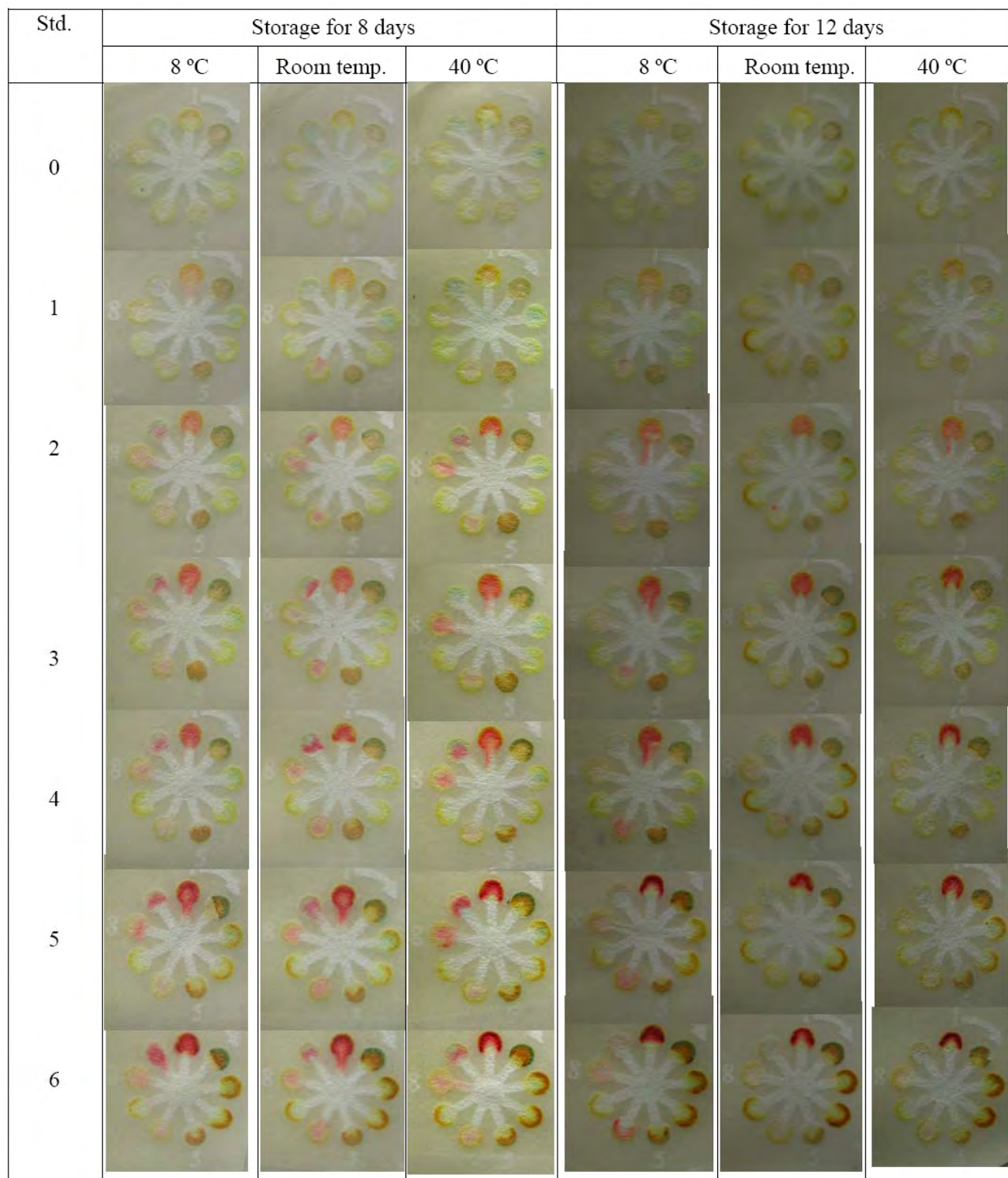


Figure 4.15 Lifetime of our devices kept at 8 °C, room temp. (~22 °C), and 40 °C.

Background signals were obtained by spotting 0.1 M of phosphate buffer solution while standard test signals were obtained by spotting all levels of standard solution.

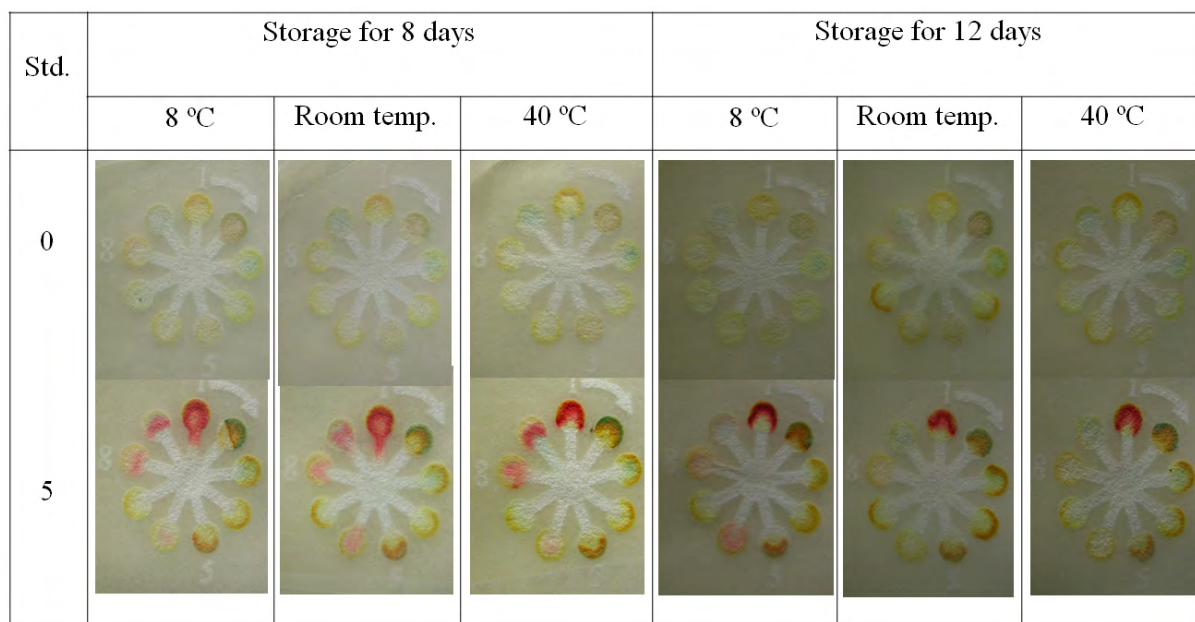


Figure 4.16 Lifetime of our devices kept at 8 °C, room temperature (~22 °C), and 40 °C. Background signals were obtained by spotting 0.1 M of phosphate buffer solution while standard test signals were obtained by spotting 10 mM glucose, 20 mM lactate, and 6 mM uric acid.

4.8 Summary

This paper demonstrates the use of multiple indicators for a single analyte as part of a multianalyte μ PAD. Multiple indicators improve accuracy of detection by improving the ability to visually discriminate between different concentrations. While different concentrations of the same dye could also be used to achieve a similar result, using different colors provides increase visual discrimination capability. Furthermore, different indicators generate colors at different analyte concentrations, which should provide more accuracy than different shades or intensities of a single color. Our devices were also successfully applied to the simultaneous semi-quantitative analysis of glucose, lactate, and uric acid in biologically relevant samples. These results demonstrate the feasibility of using multiple oxidative indicators for paper-based

microfluidic devices as an easy-to-use, inexpensive, and portable alternative device for point of care testing and self-monitoring diagnosis.

PART C**A low-cost, simple, and rapid fabrication method for paper-based microfluidics using wax screen-printing**

Wijitar Dungchai,^a Orawon Chailapakul,^{a,b} Charles S. Henry^{c,*}

^a Sensor Research Unit, Department of Chemistry, Faculty of Science, Chulalongkorn University, Patumwan, Bangkok 10330, Thailand.

^b National Center of Excellence for Petroleum, Petrochemicals, and Advanced Materials, Chulalongkorn University, Patumwan, Bangkok 10330, Thailand.

^c Department of Chemistry, Colorado State University, Fort Collins, CO 80523-1872, USA.

* Corresponding author

Analyst (2010) *in press*

Abstract

Wax screen-printing as a low-cost, simple, and rapid method for fabricating paper-based microfluidic devices (μ PADs) is reported here. Solid wax was rubbed through a screen onto paper filters. The printed wax was then melted into the paper to form hydrophobic barriers using only a hot plate. We first studied the relationship between the width of a hydrophobic barrier and the width of the original design line. We also optimized the heating temperature and time and determined the resolution of structures fabricated using this technique. The minimum width of hydrophilic channel and hydrophobic barrier is 650 and 1300 μm , respectively. Next, our fabrication method was compared to a photolithographic method using the reaction between bicinchoninic acid (BCA) and Cu^{1+} to demonstrate differences in background reactivity. Photolithographically defined channels exhibited a high background while wax printed channels showed a very low background. Finally, the utility of wax screen-printing was demonstrated for the simultaneous determination of glucose and total iron in control human serum samples using an electrochemical method with glucose oxidase and a colorimetric method with 1,10-phenanthroline. This study demonstrates that wax screen-printing is an easy-to-use and inexpensive alternative fabrication method for μ PAD, which will be especially useful in developing countries.

4.9 Introduction

μ PADs were recently introduced as alternative devices for point-of-care testing because they have attractive features including low cost, ease of use, low consumption of reagent and sample, portability, and disposability [74]. Several fabrication methods for μ PADs have been reported including photolithography [8,12,13,57,75-77], polydimethylsiloxane (PDMS) plotting [78], inkjet etching [10], plasma etching [11], cutting [79], and wax printing [80]. Each fabrication method has its own advantages and limitations. The first reported method was based on photolithography and provided high resolution between hydrophilic and hydrophobic areas (~ 200 μm of minimal barrier line width) [12]. However, this method requires organic solvents, expensive photoresists, and photolithography equipment. An oxygen plasma treatment is also required to create hydrophilic areas. The PDMS plotting method does not need organic solvent and expensive photoresists and also overcomes the problem of physical inflexibility of devices made using photolithography. Unfortunately, this method requires a customized plotter [78]. The inkjet etching method allowed for the simultaneous creation of patterned substrates and the dispensing of chemical reagents. However, this method requires a customized and potentially expensive inkjet printer [10]. Most recently, a wax printing method utilizing a commercially available wax printer was reported for the production of μ PADs [80]. Although wax printing has a lower resolution than photolithography (~ 850 μm of minimal barrier line width), the hydrophilic areas are never exposed to photoresists or other polymers; hence, wax printing methods do not require external processing steps to create the hydrophilic areas. This method does, however, require an expensive wax printer and the accompanying consumables.

One common limitation of the aforementioned fabrication methods is the need for tools that are rare in laboratories of developing countries such as spin coaters, plasma oxidizers, and wax printers [74]. Moreover, trained personnel are required to use and maintain these tools. The aim of this study was to develop low-cost, simple, and rapid fabrication methods requiring minimal external instrumentation for implementation in developing countries. Our proposed fabrication method consists of two simple steps: 1) printing patterns of solid wax on the surface of paper using a simple screen-printing method and common household supplies, and 2) melting the wax into paper to form complete hydrophobic barriers using a hot plate. The overall approach is

shown schematically in Figure 4.17. Screen printing is a well-known, inexpensive method for printing images on clothing and other everyday materials as well as creating electrodes [81-83]. Printing screens are cheap (~\$5US or 200 Thai Baht per 100 cm²) and widely available around the world. In addition, wax is inexpensive, can be purchased anywhere in the world, and is environmentally friendly. Finally, the wax screen-printing method is accomplished without the use of a clean room, UV lamp, organic solvents, or sophisticated instrumentation. Another advantage of our method over previous methods is that it requires only a hot plate (or similar heated surface) making it ideal for fabrication of μ PADs in developing countries. We first studied the spreading of wax in paper and determined the minimum dimensions achievable for the width of hydrophobic barriers and hydrophilic channels. Next, we studied the background reactivity of wax versus photolithography methods, and demonstrate a clear reduction in background signal when using the wax printing method. Finally, applications of colorimetric and electrochemical detection on patterned paper using the wax screen-printing method are presented.

4.10 Experimental

4.10.1 Materials and equipment

D-(+)-glucose (99.5%) and glucose oxidase (from *Aspergillus niger*, 215 U/mg) were purchased from Sigma-Aldrich (St. Louis, MO). Ascorbic acid (AR grade) was obtained from Mallinckrodt Baker Inc. (Paris, KY). 1,10-phenanthroline monohydrate (ACS grade) was purchased from Acros organics (Morris Plains, NJ). Potassium phosphate (ACS grade), iron chloride hexahydrate (FeCl₃·6H₂O, ACS grade), and calcium nitrate (ACS grade) were obtained from Fisher Scientific (Pittsburgh, PA). The bicinchoninic acid (BCA) assay kit was purchased from Pierce (Rockford, IL). Solid wax was obtained from a local candle making supply shop. Whatman #1 filter paper was purchased from Cole-Parmer (Vernon Hills, IL). Carbon ink mediated with Prussian blue (C2070424D2) was purchased from Gwent group (Torfaen, United Kingdom). Silver chloride ink (Electrodag 7019) was obtained from Acheson colloids company (Port Huron, MI). All chemicals were used as received without further purification. Electrochemical measurements were made using a potentiostat (CHI 1207A, CH Instruments,

Austin, TX) at room temperature (22 ± 1 °C). A digital camera (12.1 megapixels, PowerShot SD960 IS), which was used to obtain pictures, was purchased from Canon.

4.10.2 Wax screen-printing method

For screen-printing, a mask was created using CorelDraw and printed on a transparency film using a laser printer. Black areas of the mask generate a hydrophobic area on the paper, while colorless areas yield hydrophilic features. The screens were built by a local screen-printing shop and were based on the transparency. Solid wax was rubbed through the screen (200 mesh of Nylon on an aluminum frame) onto the paper. The printed wax was then melted on a hot plate at 100 °C for 60 s, absorbing into the paper to form hydrophobic barriers (Figure 4.17). The patterned paper was ready for use after removing the paper from the hot plate and allowing it to cool to room temperature (<10 s). The screen was placed on tissue paper on a hot plate and heated for 60 s to remove the residual wax.

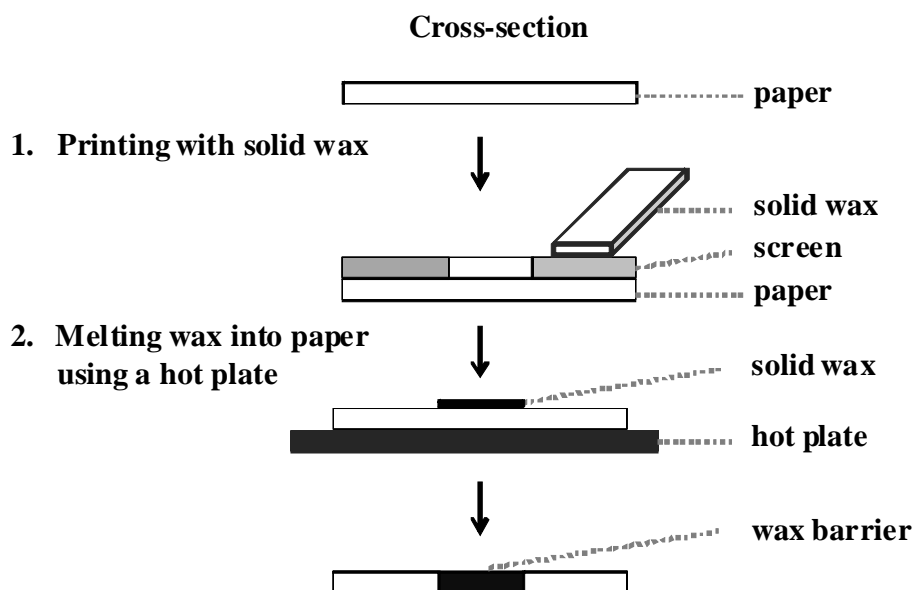


Figure 4.17 Schematic diagram of the fabrication step for wax screen-printing method.

4.10.3 Study of molten wax spreading in paper

In the melting step, wax on the paper surface melts and spreads both vertically and horizontally into the paper. To determine the extent of wax spreading, the melting temperature and time were varied from 100-120 °C and 10-60 s, respectively, and resulted in hydrophobic barrier widths of 200-1,200 μm . After red food dye was dropped onto the patterned paper, the final width of the hydrophobic barriers was measured by first capturing a digital image and then converting this to size using Adobe Acrobat™. These widths were compared to the widths of the printed masks, and a simple linear equation was generated to select the optimal melting temperature and time.

4.10.4 Wax screen-printing resolution

To determine the resolution of our method, the final widths of hydrophobic barrier and hydrophilic channel were studied in the range of 1,200-1,800 μm and 550-1,000 μm , respectively at the optimal melting temperature and time. After fabrication, red food dye was added to the paper devices to visualize the hydrophobic and hydrophilic properties.

4.10.5 Applications

To evaluate the impact of reagent residues on the background signal in paper microfluidics, the BCA assay was used. Results generated on paper devices patterned both by our method and the photolithographic methods were compared. A solution of 0.5 μL each of BCA and Cu^{2+} was dropped at the colorimetric test zone. The paper was then allowed to dry at room temperature for 10 min. For analysis, 12 μL of potassium phosphate buffer or uric acid solution was added and flowed to the measurement zone.

The utility of μPADs fabricated by the wax screen-printing was demonstrated using electrochemical and colorimetric detection for glucose and total iron using the design shown in Figure 4.18. Electrodes were constructed on paper devices using a previously reported screen-printing method [57,77]. Glucose oxidase (1 μL of 645 U/mL solution) was added to the electrode region. Ascorbic acid (0.5 μL of 1 mM solution) and 1,10-phenanthroline (0.5 μL of 0.25 M solution) was spotted in the colorimetric test zone for total iron detection [84]. The paper was allowed to dry at room temperature for 10 min. For analysis, 12 μL of a standard or sample solution was dropped onto the colorimetric test zone and subsequently flowed to the

electrochemical test zone. Direct current chronoamperometry was used for analysis at the screen-printed carbon Prussian Blue-mediated electrode. The sampling rate for all chronoamperometric analyses was 10 Hz. Additionally, the red color intensity relating to the concentration of total iron was measured using Adobe Photoshop™.

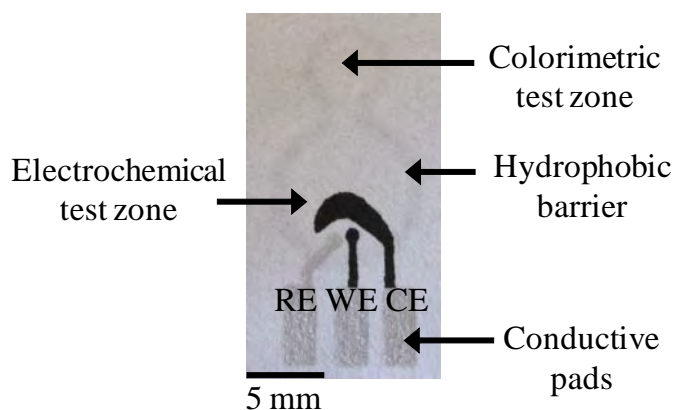


Figure 4.18 Picture of μ PAD for the dual electrochemical/ colorimetric method (WE: working electrode; RE: reference electrode; CE: counter electrode)

4.10.6 Human serum sample

Human control serum samples (levels 1 and 2) were obtained from Pointe Scientific (Canton, MI). Levels of analytes were provided by the supplier. All samples were analyzed using electrochemical and colorimetric detection for μ PADs after protein precipitation with 1.4 M hydrochloric acid (HCl) and 10% (w/v) trichloroacetic acid. For the protein precipitation, 3 mL of sample was added to 1 mL HCl and heated in a water bath at 100 °C for 5 min. After cooling, 2 mL of 10% trichloroacetic acid was added and the resulting suspension centrifuged at 14,500 rpm (Minispin Plus, Eppendorf) for 5 min [85-87]. Supernatant was diluted in 0.1 M potassium phosphate buffer (pH 6) in a 1:1 ratio to adjust the solution pH prior to analysis.

4.11 Results and discussion

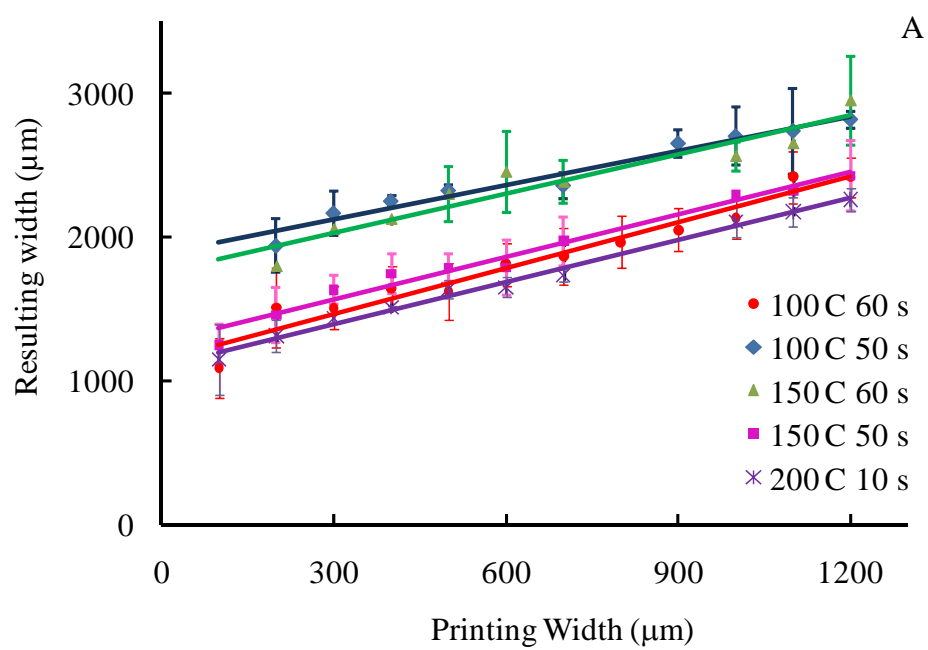
4.11.1 Wax screen-printing

Screen-printing is a technique in which a design is generated on a screen of silk or other fine mesh, with blank areas (areas where no transfer is intended) coated with an impermeable film. Patterns are transferred by forcing ink through the mesh onto the printing surface. Screen-printing is well established for the fabrication of biosensors and chemical sensors because of advantages such as miniaturization, versatility, low cost, and the possibility of mass production [88-90]. Various types of printing surfaces can be used including glass, ceramic, paper, and cotton or similar fabrics. The type of ink also depends on the printing surface and the application. Typically, printing materials include liquid inks and dyes. We reported here the use of solid wax as a printing material for screen-printing hydrophobic barriers on paper (wax screen-printing method) as shown in Figure 4.17. Wax is environmentally friendly and much cheaper and easier to obtain than photoresist or PDMS. Moreover, our fabrication method is accomplished without the use of a clean room, UV lamp, organic solvents, or sophisticated instrumentation. From previous reports, wax printing needs a wax printer (~\$2,500US) but printing screens required for our method are cheap (<\$5US) and widely available around the world [80]. Although hand drawing with a wax pen in the previous report needs only a common hot plate, it lacks the reproducibility and is difficult to fabricate small channels in high-throughput [91]. The major advantage of our method over previous methods is that it requires only a common hot plate (or similar surface) and a common printing screen that can be produced any place in the world.

4.11.2 Wax spreading

The melting temperature and time impact the spreading and penetration of wax into paper, playing an important role in the final patterns dimensions. It was found that melting times ranging from 10-40 s at 100 and 150 °C were not adequate for wax penetration into the paper. Additionally, melting times in the range of 30-60 s at 200 °C can burn the paper. Hence, 50 and 60 s melting time at 100 and 150 °C, as well as 10 s melting time at 200 °C were considered. A plot of the resulting hydrophobic barrier widths versus the line width from the mask is shown in Figure 4.19. The slope and intercept of these plots are shown in Table 4.4. The intercept represents the width of the smallest hydrophobic barrier (~1,100-1,800 μm). The lowest intercept values were seen for 100 °C for 60 s and 200 °C for 10 s indicating these two conditions resulted in lines most similar to the mask line width. Melting conditions of 100 °C

for 60 s were chosen as optimal because they maintained the integrity of the printed features better than 200 °C for 10 s.



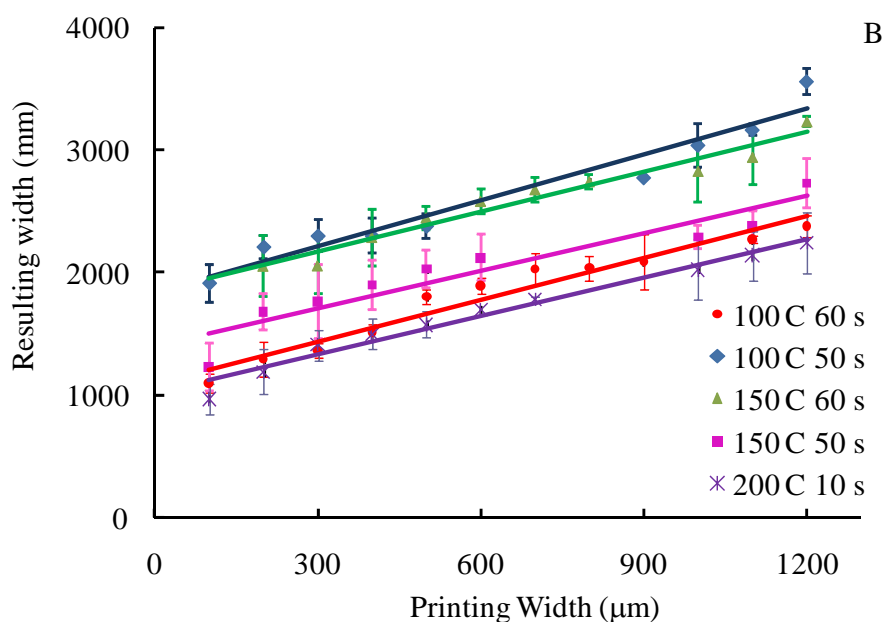


Figure 4.19 Plot of the width of the resulting hydrophobic barriers after melting the wax as a function of the printed width line of wax in a) front and b) back of paper devices.

Table 4.4 Slope, intercept and R^2 of the linearity curve and the matching percentage of slope and intercept between hydrophobic barrier width at front and back of paper devices.

Melting temp : time	Slope		Intercept		R^2		% matching	
	Front	Back	Front	Back	Front	Back	Slope	Intercept
50 s : 100 °C	0.961	1.250	1786.1	1835.9	0.978	0.947	76.9	97.3
60 s : 100 °C	1.081	1.071	1136.3	1128.0	0.984	0.981	100.9	100.7
50 s : 150 °C	1.018	1.067	1243.8	1382.5	0.985	0.937	95.4	90.0
60 s : 150 °C	1.145	1.118	1630.1	1826.2	0.939	0.979	102.4	89.3
10 s : 200 °C	0.996	1.050	1090.6	1012.6	0.995	0.971	94.9	107.7

Using the optimal melting temperature and time, the resulting width of hydrophobic barriers (W_{RB}) was calculated using the linear equation $W_{RB} = 1.081 W_{PB} + 1136.3$, where W_{PB} is the printed line width. The resulting width of hydrophilic channels (W_{RC}) was then calculated with equation 1 and 2, where L is the length of wax spreading from the original wax line, and W_{PC} is the printed width of the channel. Figure 4.20 demonstrates these variables in a schematic.

$$2L = W_{RB} - W_{PB} \quad (1)$$

$$W_{RC} = W_{PC} - 2L \quad (2)$$

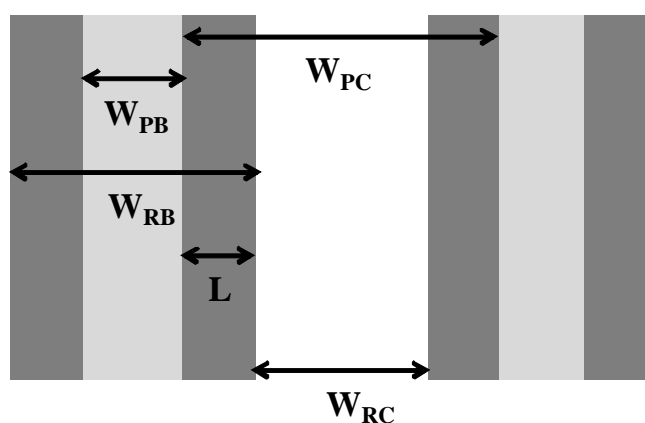


Figure 4.20 Schematic representation of the spreading of wax in paper and definition of variables: W_{PC} is the printed width of the channel, W_{PB} is the printed width of the wax hydrophobic line, W_{RC} is the resulting width of hydrophilic channel after melting of wax, W_{RB} is the resulting width of hydrophobic barrier after melting of wax, L is the spreading of wax from the original edge of wax line.

4.11.3 Wax screen-printing resolution

At the optimal melting temperature and time, the width of the hydrophobic barrier from 1,200-1,800 μm was studied in steps of 100 μm (Figure 4.21) to demonstrate the resolution of this method. A minimum hydrophobic barrier of $1,300 \pm 104 \mu\text{m}$ was determined. The width of the hydrophilic channel from 550-1,000 μm in 50 μm steps was also studied (Figure 4.22). The smallest channel width allowing solution to flow the entire length of a 12 mm channel was found to be $650 \pm 71 \mu\text{m}$ ($n = 10$) (Figure 4.22). The resolution of our method is currently

limited by the thickness, porosity, and orientation of paper fibers as well as the smallest features printable on the screen. Here, only Whatman #1 filter paper (180 μm thickness and 11 μm particle retention rating at 98% efficiency) was used; and it is anticipated that some differences will exist for different printing surfaces.

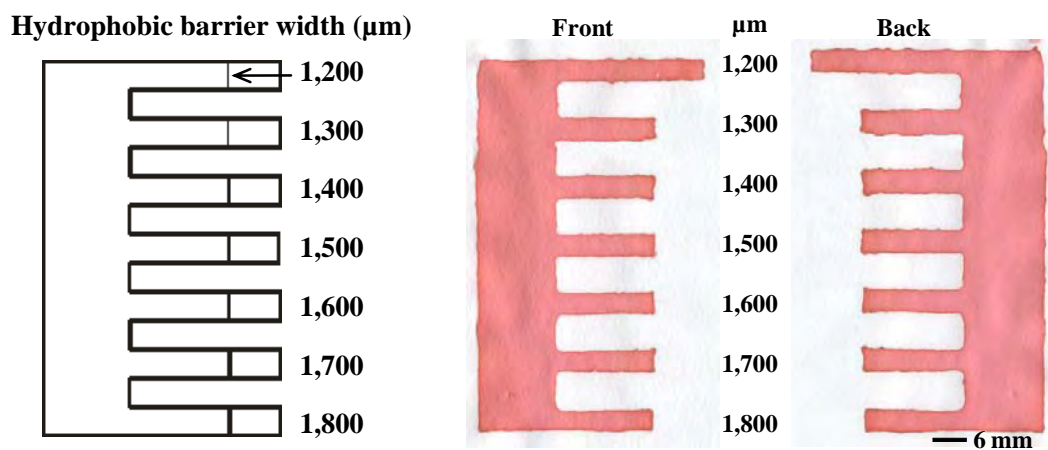


Figure 4.21 Resolution of the wax screen-printing method showing the smallest hydrophobic barrier width.

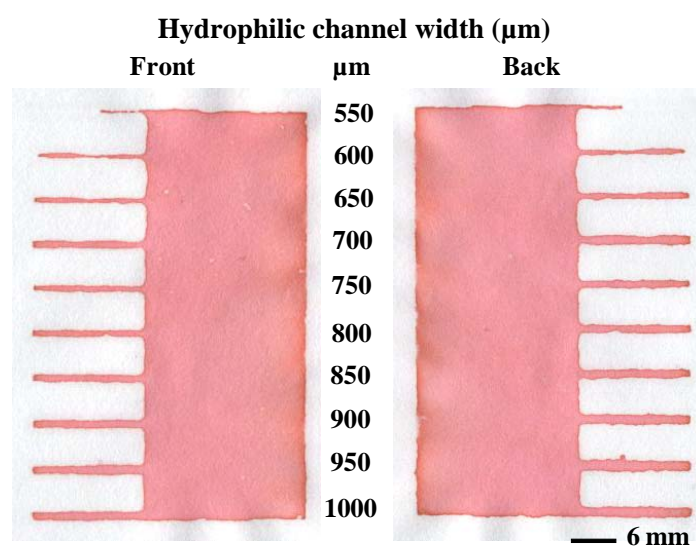






Figure 4.22 Resolution of the wax screen-printing method showing the smallest hydrophilic channel width.

4.11.4 Applications

To demonstrate the effect of the patterning method on the background signal, a total reducing agents analysis using the reaction between bicinchoninic acid (BCA) and Cu^{1+} reaction as a model. Cu^{2+} ion is converted to Cu^{1+} by the reducing agents such as uric acid, vitamin E and ascorbate. Cu^{1+} is chelated with BCA giving an intense violet color, proportional to the total reducing agents. No reaction was seen when the BCA and Cu^{2+} solution was carried out on devices patterned with the wax screen printing method; however, a positive result was obtained when using paper devices patterned by photolithography (Figure 4.23). This result indicates that the patterning method can give rise to false signals. It has been shown in a previous report that photoresist residues can also interfere with amperometric detection in paper-based microfluidic devices [76].

(A) Photolithography

After drop BCA and Cu^{2+} solution	After drop uric acid (mM)		
	0	0.5	1
			

(B) Wax screen printing

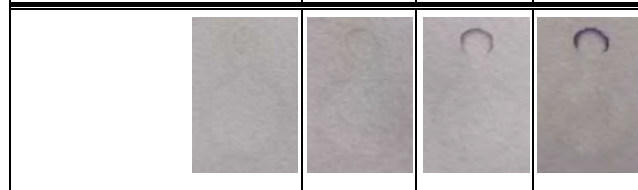
After drop BCA and Cu^{2+} solution	After drop uric acid (mM)		
	0	0.5	1
			

Figure 4.23 Cross reaction test with BCA assay (A) paper devices fabricated by our method and (B) photolithography.

In order to evaluate the utility of wax screen-printed μ PADs, the simultaneous determination of glucose and total iron in control human serum samples was performed. The design of the paper device is shown in Figure 4.18. Total iron was analyzed by a colorimetric method involving the formation of a red-colored complex between 1,10-phenanthroline and iron (II). The color intensity increased with iron concentration (Figure 4.24). Color intensity calibrations were done using Adobe PhotoshopTM in gray scale mode within a range of 0 and 200 μM , generating coefficients of determination (R^2) greater than 0.999 (Figure 4.25). The relative standard deviations of all iron concentrations were less than 17% ($n = 3$), demonstrating acceptable reproducibility for this type of device. Improvements in the reproducibility could potentially be achieved using a reaction that generated a more intense color.

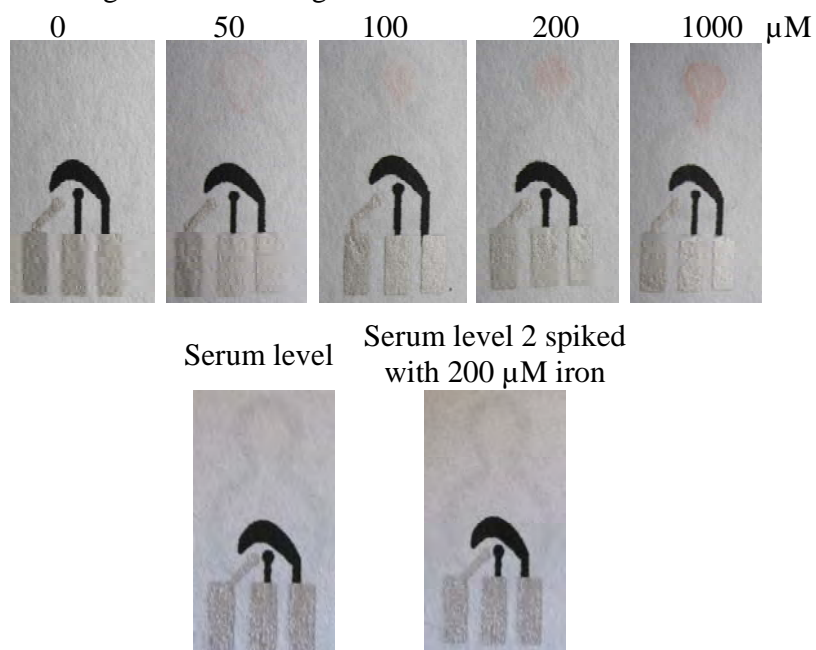


Figure 4.24 Photographs of the result for the total iron analysis using colorimetric method.

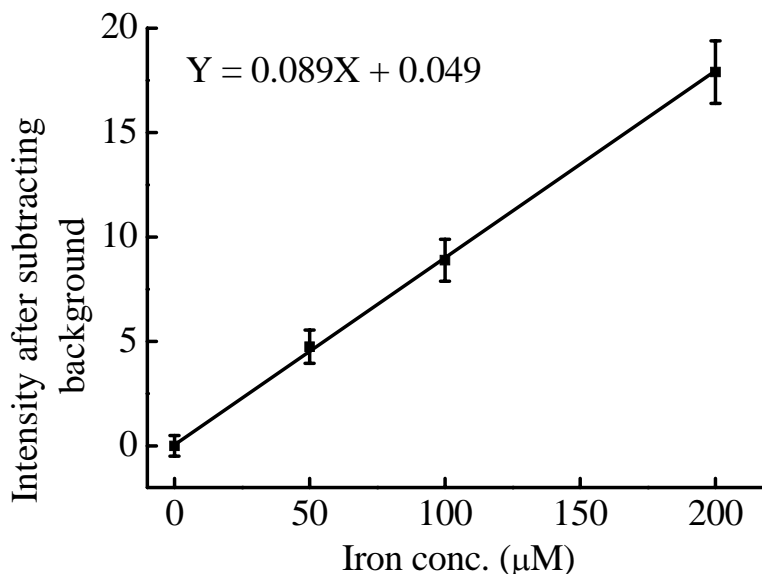


Figure 4.25 The calibration plot of total iron concentration and the red color intensity subtracting with background.

For glucose determination, Prussian Blue modified carbon working electrodes were used to detect hydrogen peroxide generated from the reaction between glucose and glucose oxidase. The devices were initially characterized using cyclic voltammetry. Figure 4.26 clearly shows a larger cathodic peak in the presence of hydrogen peroxide and glucose relative to the background electrolyte. The catalytic reaction occurs in a low potential region (-0.2 to 0 V versus on-paper Ag/AgCl). Next, a linear calibration curve was obtained using chronoamperometry at -0.2V 0 to 5 mM glucose ($Y = -1.0092X + 0.1515$, $R^2 = 0.9925$, %RSD of all glucose conc. $\leq 12\%$ ($n = 3$)) as shown in Figure 4.27.

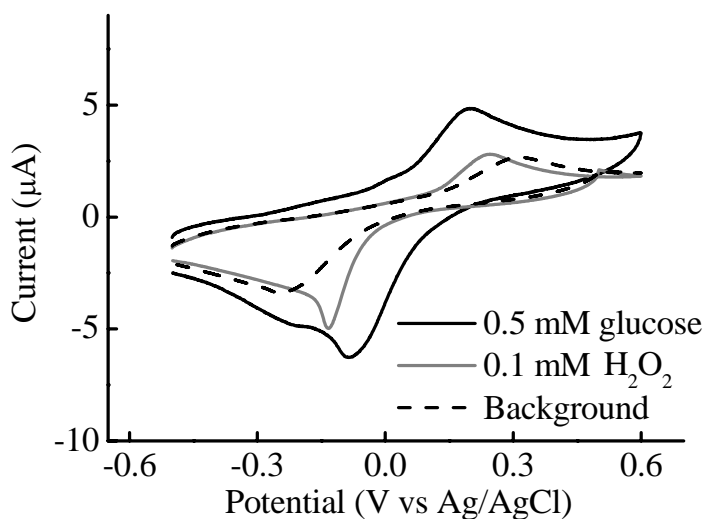


Figure 4.26 Cyclic voltammograms of the carbon mediator Prussian blue electrode in the absence and presence of 0.1 mM H_2O_2 , 0.5 and 5 mM of glucose at a 100 mV/s scan rate.

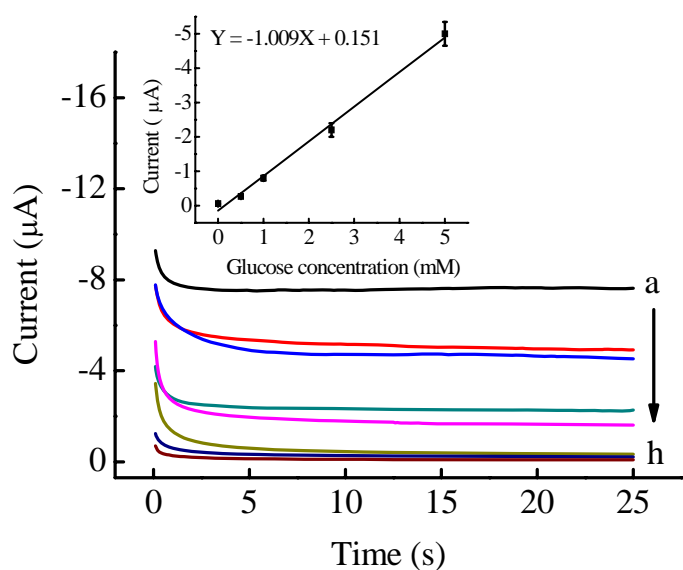


Figure 4.27 Chronoamperograms of glucose (a: 10 mM, b: 5 mM, c: Serum level 2, d: 2.5 mM, e: Serum level 1, f: 1 mM, g: 0.5 mM, h: background) determination at -0.2 V versus an on-chip Ag/AgCl. The calibration plot of anodic currents at 20 s of sampling time for determination of three analytes are shown in the insert, $n = 3$.

Finally, the glucose and total iron concentration in control human serum samples were determined simultaneously. Control serum samples are used to validate clinical assays. After sample preparation, the final sample solution was diluted by a factor of four giving final concentrations of total iron in human serum level 1, 2 and level 2 spiked with 200 μM of iron was 3.5, 12, and 62 μM , respectively. A correlation of the color intensity between the standard iron solution and iron in serum sample was observed visually and measured by Adobe PhotoshopTM. The color intensity of the iron reaction at serum sample level 1 did not show a significant difference visually. A linear calibration curve generated from gray scale measurements was used to interpret the iron in serum level 2 and spiked level 2 (Figure 4.25) samples. The serum level 2 and spiked level 2 samples were determined to contain 11 ± 2 and 58 ± 6 μM iron (Figure 4.27). The recovery of iron was determined to be 88-92% ($n = 3$). For the glucose test, the final concentration of level 1 and 2 samples after sample preparation was 1.4 ± 0.1 and 4.2 ± 0.4 mM, respectively. The results of both glucose and iron converted to their original concentrations are shown in Table 4.5. Using the paired t -test, no significant differences were found at the 95% confidence level between our measurements and the known values.

Table 4.5 Determination of glucose and total iron in control samples

Analyte	Human serum level 1		Human serum level 2	
	Certified Value	Proposed method	Certified Value	Proposed method
Glucose Concentration (mM \pm SD ^a)	5.6 ± 0.4	5.2 ± 0.5	16.8 ± 1.7	18.4 ± 2.2
Iron Concentration (μM \pm SD ^a)	14 ± 3	ND ^b	49 ± 9	44 ± 6

^a SD: standard deviation ($n = 3$)

^b ND: not detectable

4.12 Summary

Here, we demonstrate a wax screen-printing method for fabricating μPADs . The wax screen-printing method is rapid, inexpensive, simple, and suitable for developing countries. A

linear equation between the width of a hydrophobic barrier and the width of the printed line was used to predict the width of a hydrophobic barrier and a hydrophilic channel from the initial printed mask. Moreover, the screen-printing method does not suffer from problems of interference from residues remaining in the hydrophilic channel after fabrication. Finally, the fabrication method was shown to be useful for both colorimetric and electrochemical detection methods, and was applied to the simultaneous determination of glucose and total iron in biologically relevant samples.

4.13 References

- [1] Altinier, S.; Zaninotto, M.; Mion, M.; Carraro, P.; Rocco, S.; Tosato, F.; Plebani, M. Point-of-care testing of cardiac markers: results from an experience in an Emergency Department. Clin. Chim. Acta. 311 (2001): 67-72.
- [2] Sia, S. K.; Kricka, L. J. Microfluidics and point-of-care testing. Lab Chip 8 (2008): 1982-1983.
- [3] Burns, M. A.; Johnson, B. N.; Brahmasandra, S. N.; Handique, K.; Webster, J. R.; Krishnan, M.; Sammarco, T. S.; Man, P. M.; Jones, D.; Heldsinger, D.; Mastrangelo, C. H.; Burke, D. T. An Integrated Nanoliter DNA Analysis Device. Science. 282 (1998): 484-487.
- [4] Lin, R.; Burke, D. T.; Burns, M. A., Selective extraction of size-fractionated DNA samples in microfabricated electrophoresis devices. J. Chromatogr., A 1010 (2003): 255-268.
- [5] Shrinivasan, S.; Norris, P. M.; Landers, J. P.; Ferrance, J. P. A Low-Cost, Low-Power, Consumption Miniature Laser-Induced Fluorescence System for DNA Detection on a Microfluidic Device. J. Assoc. Lab Automation 11 (2006): 254-259.
- [6] Wen, J.; Guillo, C.; Ferrance, J. P.; Landers, J. P. Microfluidic-Based DNA Purification in a Two-Stage, Dual-Phase Microchip Containing a Reversed-Phase and a Photopolymerized Monolith. Anal. Chem. 79 (2007): 6135-6142.
- [7] Zheng, J.; Webster, J. R.; Mastrangelo, C. H.; Ugaz, V. M.; Burns, M. A.; Burke, D. T. Integrated plastic microfluidic device for ssDNA separation. Sens. Actuators, B 125 (2007): 343-351.

- [8] Martinez, Andres W.; Phillips, Scott T.; Butte, Manish J.; Whitesides, George M., Patterned Paper as a Platform for Inexpensive, Low-Volume, Portable Bioassays 13. Angew. Chem. Int. Ed. 46 (2007): 1318-1320.
- [9] Zhao, W.; Berg, A. v. d. Lab on paper. Lab Chip 8 (2008): 1988-1991.
- [10] Abe, K.; Suzuki, K.; Citterio, D. Inkjet-Printed Microfluidic Multianalyte Chemical Sensing Paper. Anal. Chem. 80 (2008): 6928-6934.
- [11] Li, X.; Tian, J.; Nguyen, T.; Shen, W. Paper-Based Microfluidic Devices by Plasma Treatment. Anal. Chem. 80 (2008): 9131-9134.
- [12] Martinez, A. W.; Phillips, S. T.; Wiley, B. J.; Gupta, M.; Whitesides, G. M. FLASH: A rapid method for prototyping paper-based microfluidic devices. Lab Chip 8 (2008): 2146-2150.
- [13] Martinez, A. W.; Phillips, S. T.; Carrilho, E.; Thomas, S. W.; Sindi, H.; Whitesides, G. M. Simple Telemedicine for Developing Regions: Camera Phones and Paper-Based Microfluidic Devices for Real-Time, Off-Site Diagnosis. Anal. Chem. 80 (2008): 3699-3707.
- [14] Wang, J. Electrochemical biosensors: Towards point-of-care cancer diagnostics. Biosens. Bioelectron. 21 (2006): 1887-1892.
- [15] Holcomb, R. E.; Kraly, J. R.; Henry, C. S. Electrode array detector for microchip capillary electrophoresis. Analyst. 134 (2009): 486-492.
- [16] Matson, W. R.; Langlais, P.; Volicer, L.; Gamache, P. H.; Bird, E.; Mark, K. A. n-Electrode three-dimensional liquid chromatography with electrochemical detection for determination of neurotransmitters. Clin. Chem. 30 (1984): 1477-1488.
- [17] Alvarez-Icaza, M.; Bilitewski, U. Mass production of biosensors. Anal. Chem. 65 (1993): 525A-533A.
- [18] Martin, R. S.; Gawron, A. J.; Lunte, S. M.; Henry, C. S. Dual-Electrode Electrochemical Detection for Poly(dimethylsiloxane)-Fabricated Capillary Electrophoresis Microchips. Anal. Chem. 72 (2000): 3196-3202.
- [19] Jiang, L.; Lu, Y.; Dai, Z.; Xie, M.; Lin, B. Mini-electrochemical detector for microchip electrophoresis. Lab Chip 5 (2005): 930-934.

- [20] Tangkuaram, T.; Ponchio, C.; Kangkasomboon, T.; Katikawong, P.; Veerasai, W. Design and development of a highly stable hydrogen peroxide biosensor on screen printed carbon electrode based on horseradish peroxidase bound with gold nanoparticles in the matrix of chitosan. *Biosens. Bioelectron.* 22 (2007): 2071-2078.
- [21] Chiu, M. H.; Wu, H.; Chen, J. C.; Muthuraman, G.; Zen, J. M. Disposable Screen-Printed Carbon Electrodes for Dual Electrochemiluminescence/Amperometric Detection: Sequential Injection Analysis of Oxalate. *Electroanalysis.* 19 (2007): 2301-2306.
- [22] Song, Y. S.; Muthuraman, G.; Chen, Y.-Z.; Lin, C. C.; Zen, J. M. Screen Printed Carbon Electrode Modified with Poly(L-Lactide) Stabilized Gold Nanoparticles for Sensitive As(III) Detection. *Electroanalysis.* 18 (2006): 1763-1770.
- [23] O'Halloran, M. P.; Pravda, M.; Guilbault, G. G. Prussian Blue bulk modified screen-printed electrodes for H₂O₂ detection and for biosensors. *Talanta.* 55 (2001): 605-611.
- [24] Hong, C.; Yuan, R.; Chai, Y.; Zhuo, Y. Amperometric Immunosensor for the Determination of alpha-1-Fetoprotein Based on Core-Shell-Shell Prussian Blue-BSA-Nanogold Functionalized Interface. *Electroanalysis.* 20 (2008): 2185-2191.
- [25] He, X.; Yuan, R.; Chai, Y.; Zhang, Y.; Shi, Y. A new antibody immobilization strategy based on electro-deposition of gold nanoparticles and Prussian Blue for label-free amperometric immunosensor. *Biotechnol. Lett.* 29 (2007): 149-155.
- [26] Moscone, D.; D'Ottavi, D.; Compagnone, D.; Palleschi, G.; Amine, A. Construction and Analytical Characterization of Prussian Blue-Based Carbon Paste Electrodes and Their Assembly as Oxidase Enzyme Sensors. *Anal. Chem.* 73 (2001): 2529-2535.
- [27] Zakharchuk, N. F.; Meyer, B.; Henning, H.; Scholz, F.; Jaworksi, A.; Stojek, Z. A comparative study of Prussian-Blue-modified graphite paste electrodes and solid graphite electrodes with mechanically immobilized Prussian Blue. *J. Electroanal. Chem.* 398 (1995): 23-35.
- [28] Kawakami, M.; Koya, H.; Gondo, S. Immobilization of enzyme to platinum electrode and its use as enzyme electrode. *Appl. Biochem. Biotechnol.* 28-29 (1991): 211-219.
- [29] Santoni, T.; Santianni, D.; Manzoni, A.; Zanardi, S.; Mascini, M. Enzyme electrode for glucose determination in whole blood. *Talanta.* 44 (1997): 1573-1580.

- [30] Miyashita, M.; Ito, N.; Ikeda, S.; Murayama, T.; Oguma, K.; Kimura, J. Development of urine glucose meter based on micro-planer amperometric biosensor and its clinical application for self-monitoring of urine glucose. Biosens. Bioelectron. 24 (2009): 1336-1340.
- [31] Tao, H.; Xian-En, Z.; Zhi-Ping, Z.; Li-Qun, C. A Screen-Printed Disposable Enzyme Electrode System for Simultaneous Determination of Sucrose and Glucose. Electroanalysis. 12 (2000): 868-870.
- [32] Pauliukaite, R.; Florescu, M.; Brett, C. M. A. Characterization of cobalt- and copper hexacyanoferrate-modified carbon film electrodes for redox-mediated biosensors. J. Solid State Electrochem. 9 (2005): 354-362.
- [33] Chen, X.; Li, C.; Liu, Y.; Du, Z.; Xu, S.; Li, L.; Zhang, M.; Wang, T. Electrocatalytic activity of horseradish peroxidase/chitosan/carbon microsphere microbicomposites to hydrogen peroxide. Talanta. 77 (2008): 37-41.
- [34] Zhang, J.; Oyama, M. A hydrogen peroxide sensor based on the peroxidase activity of hemoglobin immobilized on gold nanoparticles-modified ITO electrode. Electrochim. Acta. 50 (2004): 85-90.
- [35] Lindgren, A.; Ruzgas, T.; Gorton, L.; Csoregi, E.; Bautista Ardila, G.; Sakharov, I. Y.; Gazaryan, I. G. Biosensors based on novel peroxidases with improved properties in direct and mediated electron transfer. Biosens. Bioelectron. 15 (2000): 491-497.
- [36] Arkady, A. K. Prussian Blue and Its Analogues: Electrochemistry and Analytical Applications. Electroanalysis. 13 (2001): 813-819.
- [37] Ricci, F.; Amine, A.; Tuta, C. S.; Ciucu, A. A.; Lucarelli, F.; Palleschi, G.; Moscone, D. Prussian Blue and enzyme bulk-modified screen-printed electrodes for hydrogen peroxide and glucose determination with improved storage and operational stability. Anal. Chim. Acta. 485 (2003): 111-120.
- [38] Tietz, N. W. Clinical guide to laboratory tests. PA USA: W.B. Saunders Company, 1995.
- [39] Magner, E. Trends in electrochemical biosensors. Analyst. 123 (1998): 1967-1970.
- [40] Biovision. (Research products). www.biovision.com, 2008.
- [41] BioassaySystems. www.bioassaysys.com, 2007.

- [42] Price, C. P. Point-of-care testing in diabetes mellitus. Clin. Chem. Lab. Med. 41 (2003): 1213–1219.
- [43] Yager, P.; Edwards, T.; Fu, E.; Helton, K.; Nelson, K.; Tam, M. R.; Weigl, B. H. Microfluidic diagnostic technologies for global public health. Nature. 442 (2006): 412-418.
- [44] Chin, C. D.; Linder, V.; Sia, S. K. Lab-on-a-chip devices for global health: Past studies and future opportunities. Lab Chip. 7 (2007): 41-57.
- [45] Myers, F. B.; Lee, L. P. Innovations in optical microfluidic technologies for point-of-care diagnostics. Lab Chip. 8 (2008): 2015-2031.
- [46] Sia, S. K.; Kricka, L. J. Microfluidics and point-of-care testing. Lab Chip. 8 (2008): 1982–1983.
- [47] Zhao, W.; Berg, A. V. D. Lab on paper. Lab on a Chip. 8 (2008): 1988–1991.
- [48] One Step HCG Urine Pregnancy Test (Strip), AI DE Diagnostica Co. Ltd., Shandong, China (2009).
- [49] Hones, J.; Muller, P.; Surridge, N. The technology behind glucose meters: Test strips. Diabetes Technol. Ther. 10 (2008): S10–S26.
- [50] Kristensen, G. B. B.; Monsen, G.; Skeie, S.; Sandberg, S. Standardized Evaluation of Nine Instruments for Self-Monitoring of Blood Glucose. Diabetes Technol. Ther. 10 (2008): 467–477.
- [51] Penttila, A.; Karhunen, P. J.; Pikkarainen, J. Alcohol screening with the Alcoscan test strip in forensic praxis. Forensic Sci. Int. 44 (1990): 43–48.
- [52] One Step Drugs of Abuse Test, Beijing China: Core Technology Co. Ltd., 2009.
- [53] Oberhofer, T. R.; Towle, D. W. Evaluation of the rapid penicillinase paper strip test for detection of beta-lactamase. J. Clin. Microbiol. 15 (1982): 196–199.
- [54] Mosley, L. M.; Sharp D. S. The hydrogen sulphide (H₂S) paper strip test. SOPAC Technical Report 373 (2005).
- [55] Lin, Y. Y.; Wang, J.; Liu, G.; Wu, H.; Wai, C. M.; Lin, Y. A nanoparticle label/immunochromatographic electrochemical biosensor for rapid and sensitive detection of prostate-specific antigen. Biosens. Bioelectron. 23 (2008): 1659–1665.

- [56] Mao, X.; Baloda, M.; Gurung, A. S.; Lin, Y.; Liu, G. Multiplex electrochemical immunoassay using gold nanoparticle probes and immunochromatographic strips. Electrochem. Commun. 10 (2008): 1636–1640.
- [57] Dungchai, W.; Chailapakul, O.; Henry, C. S. Electrochemical Detection for Paper-Based Microfluidics. Anal. Chem. 81 (2009): 5821-5826.
- [58] Fung, K.-K.; Chan, C. P.-Y.; Renneberg, R. Development of enzyme-based bar code-style lateral-flow assay for hydrogen peroxide determination. Anal. Chim. Acta. 634 (2009): 89–95.
- [59] Fossati, P.; Prencipe, L.; Berti, G. Use of 3,5-dichloro-2-hydroxybenzenesulfonic acid/4-aminophenazone chromogenic system in direct enzymic assay of uric acid in serum and urine. Clin. Chem. 26 (1980): 227–231.
- [60] Domagk, G. F.; Schlicke, H. H. A colorimetric method using uricase and peroxidase for the determination of uric acid. Anal. Biochem. 22 (1968): 219–224.
- [61] Hamid, M.; Khalil ur, R. Potential applications of peroxidases. Food Chem. 115 (2009): 1177–1186.
- [62] Ugarova, N. N.; Lebedeva, O. V.; Berezin, I. V. Horseradish peroxidase catalysis I. Steady-state kinetics of peroxidase-catalyzed individual and co-oxidation of potassium ferrocyanide and *o*-dianisidine by hydrogen peroxide. J. Mol. Catal. 13 (1981): 215–225.
- [63] Carvalho, R. H.; Lemos, F.; Lemos, M. A. N. D. A.; Vojinovic, V.; Fonseca, L. P.; Cabral, J. M. Kinetic modelling of phenol co-oxidation using horseradish peroxidase. Bioprocess. Biosyst. Eng. 29 (2006): 99–108.
- [64] Björkstén, F. The horseradish peroxidase-catalyzed oxidation of iodide. Outline of the mechanism. Biochim. Biophys. Acta. 212 (1970): 396–406.
- [65] D Blake, D. A.; McLean, N. V. A colorimetric assay for the measurement of α -glucose consumption by cultured cells. Anal. Biochem. 177 (1989): 156–160.
- [66] Nixon, M.; Huggett, H. Citation classic-use of glucose-oxidase, peroxide, and *o*-dianisidine in determination of blood and urinary glucose. Curr. Contents Clin. Pract. 21 (1981): 18-18.
- [67] Guidotti, G.; Colombo, J.-P.; Foa, P. P. Enzymatic Determination of Glucose. Stabilization of Color Developed by Oxidation of *o*-Dianisidine. Anal. Chem. 33 (1961): 151–153.

- [68] Alexander, N. M. A spectrophotometric assay for iodide oxidation by thyroid peroxidase. Anal. Biochem. 4 (1962): 341–345.
- [69] Klassen, N.V.; Marchington, D.; McGowan, H.C.E. H₂O₂ determination by the I³⁻ method and by the KMnO₄ Titration. Anal. Chem. 66 (1994): 2921–2925.
- [70] Kreilgaard, L.; Frokjaer, S.; Flink, J. M.; Randolph, T. W.; Carpenter, J. F. Effects of additives on the stability of Humicola lanuginosa lipase during freeze-drying and storage in the dried solid. J. Pharm. Sci. 88 (1999): 281–290.
- [71] Arakawa, T.; Prestrelski, S. J.; Kenney, W. C.; Carpenter, J. F. Factors affecting short-term and long-term stabilities of proteins. Adv. Drug Deliv. Rev. 46 (2001): 307–326.
- [72] Izutsu, K.; Yoshioka, S.; Terao, T. Effect of mannitol crystallinity on the stabilization of enzymes during freeze-drying. Chem. Pharm. Bull. 42 (1994): 5–8.
- [73] Santagapita, P. R.; Buera, M. P. Trehalose-water-salt interactions related to the stability of beta-galactosidase in supercooled media. Food Biophys. 3 (2008): 87–93.
- [74] Martinez, A. W.; Phillips, S. T.; Whitesides, G. M.; Carrilho, E. Diagnostics for the Developing World: Microfluidic Paper-Based Analytical Devices. Anal. Chem. 82 (2009): 3-10.
- [75] Nie, Z.; Nijhuis, C. A.; Gong, J.; Chen, X.; Kumachev, A.; Martinez, A. W.; Narovlyansky, M.; Whitesides, G. M. Electrochemical sensing in paper-based microfluidic devices. Lab Chip. 10 (2010): 477-483.
- [76] Carvalhal, R. F.; Simão Kfourri, M.; de Oliveira Piazetta, M. H.; Gobbi, A. L.; Kubota, L. T. Electrochemical Detection in a Paper-Based Separation Device. Anal. Chem. 82 (2010): 1162-1165.
- [77] Apilux, A.; Dungchai, W.; Siangproh, W.; Praphairaksit, N.; Henry, C. S.; Chailapakul, O. Lab-on-Paper with Dual Electrochemical/Colorimetric Detection for Simultaneous Determination of Gold and Iron. Anal. Chem. 82 (2010): 1727-1732.
- [78] Bruzewicz, D. A.; Reches, M.; Whitesides, G. M. Low-Cost Printing of Poly(dimethylsiloxane) Barriers To Define Microchannels in Paper. Anal. Chem. 80 (2008): 3387-3392.

- [79] Fenton, E. M.; Mascarenas, M. R.; López, G. P.; Sibbett, S. S. Multiplex Lateral-Flow Test Strips Fabricated by Two-Dimensional Shaping. ACS Appl. Mater. Interfaces. 1 (2008): 124-129.
- [80] Carrilho, E.; Martinez, A. W.; Whitesides, G. M. Understanding Wax Printing: A Simple Micropatterning Process for Paper-Based Microfluidics. Anal. Chem. 81 (2009): 7091-7095.
- [81] Chiu, M.-H.; Wu, H.; Chen, J. C.; Muthuraman, G.; Zen, J. M. Disposable Screen-Printed Carbon Electrodes for Dual Electrochemiluminescence/Amperometric Detection: Sequential Injection Analysis of Oxalate. Electroanalysis. 19 (2007): 2301-2306.
- [82] Tao, H.; Xian-En, Z.; Zhi-Ping, Z.; Li-Qun, C. A Screen-Printed Disposable Enzyme Electrode System for Simultaneous Determination of Sucrose and Glucose. Electroanalysis. 12 (2000): 868-870.
- [83] Ricci, F.; Amine, A.; Tuta, C. S.; Ciucu, A. A.; Lucarelli, F.; Palleschi, G.; Moscone, D. Prussian Blue and enzyme bulk-modified screen-printed electrodes for hydrogen peroxide and glucose determination with improved storage and operational stability. Anal. Chim. Acta. 485 (2003): 111-120.
- [84] Kozak, J.; Gutowski, J.; Kozak, M.; Wieczorek, M.; Koscielniak, P. New method for simultaneous determination of Fe(II) and Fe(III) in water using flow injection technique. Anal. Chim. Acta. 668 (2010): 8-12.
- [85] Peterson, R. E. Improved Spectrophotometric Procedure for Determination of Serum Iron Using 4,7-Diphenyl-1,10-phenanthroline. Anal. Chem. 25 (1953): 1337-1339.
- [86] Zak, B. Simple procedure for the single sample determination of serum copper and iron. Clin. Chim. Acta. 3 (1958): 328-334.
- [87] Ryall, R.; Fielding, J. The co-precipitation of ferric iron and protein and the reducing capacity of serum as factors affecting the assay of serum iron. Clin. Chim. Acta. 28 (1970): 193-202.
- [88] Renedo, O. D.; Alonso-Lomillo, M. A.; Martínez, M. J. A. Recent developments in the field of screen-printed electrodes and their related applications. Talanta. 73 (2007): 202-219.

- [89] Tudorache, M.; Bala, C. Biosensors based on screen-printing technology, and their applications in environmental and food analysis. Anal. Bioanal. Chem. 388 (2007): 565-578.
- [90] Honeychurch, K. C.; Hart, J. P. Screen-printed electrochemical sensors for monitoring metal pollutants. TrAC, Trends in Anal. Chem. 22 (2003): 456-469.
- [91] Lu, Y.; Shi, W.; Jiang, L.; Qin, J.; Lin, B. Rapid prototyping of paper-based microfluidics with wax for low-cost, portable bioassay. Electrophoresis. 30 (2009): 1497-1500.

CHAPTER V

SENSITIVITY IMPROVEMENT OF IMMUNOASSAY

Development of a sensitive micro-magnetic chemiluminescence enzyme immunoassay for the determination of carcinoembryonic antigen

Wijitar Dungchai ^{a,b}, Weena Siangproh ^{a,b}, Jin-Ming Lin ^{b,*}, Orawon Chailapakul ^{a,*}, Si Lin ^c, Xitang Ying ^c

^aDepartment of Chemistry, Faculty of Science, Chulalongkorn University, Patumwan, Bangkok, 10330, Thailand

^bThe Key Laboratory of Bioorganic Phosphorus Chemistry & Chemical Biology, Ministry of Education, Department of Chemistry, Tsinghua University, Beijing 100084, China

^cBeijing Chemclin Biotech Co., Ltd. Beijing Academy of Science and Technology, Haidian, Beijing, 100094, China

*Corresponding author

Analytical and Bioanalytical Chemistry (2007) 387:1965–1971

Abstract

In this chapter, a micro-magnetic chemiluminescence (CL) enzyme immunoassay of high sensitivity, selectivity and reproducibility for the determination of tumor marker, carcinoembryonic antigen (CEA) in human serum was developed. The sandwich scheme assay has been utilized with fluorescein isothiocyanate antibody (FITC)-labeled anti-CEA antibody and alkaline phosphatase (ALP)-labeled anti-CEA antibody being used in the CL detection. The CL signal produced by the emission of photon from 4-methoxy-4-(3-phosphatophenyl)-spiro-(1,2-dioxetane-3,2'-adamantane) (AMPPD) was directly proportional to the amount of analyte present in a sample solution. The influences of the reaction time of antigen with antibody, the reaction time of substrate with label, the dilution ratio of ALP-labeled anti-CEA antibody, the concentration of FITC-labeled anti-CEA antibody and other relevant variables upon the CL signal, were examined and optimized. The CL responses depended linearly on the CEA concentration over the range of 2 ng/mL to 162 ng/mL in a logarithmic plot. The assay sensitivity as low as 0.69 ng/mL, was achieved. The intra- and inter- assay provided a good coefficient variance of less than 13 %. This method has been successfully applied to analysis of CEA in human serum. According to the procedure based on the spiked standards, the recoveries obtained were 80-110 %. Comparison experiments were carried out with the commercially available CEA chemiluminescence immunoassay. The satisfactory results were obtained from using paired t-test method (t value $< t_{critical}$ at 95% confidence).

5.1 Introduction

The determination of tumor marker plays an important role in clinical research and diagnosis. Currently, tumor markers are widely used to provide both an indication of response of therapy and disease progression or recurrence in patients with cancers [1-2]. Carcinoembryonic antigen (CEA) is a cell-surface glycoprotein with a molecular weight of 180-200 kD, that occurs in high levels in colon epithelial cells during embryonic development. Levels of CEA are significantly lower in colon tissue of adults, but can become elevated when inflammation or tumors arise in any endodermal tissue, including in the gastrointestinal tract, respiratory tract, pancreas and breast [3-5]. An overexpression of CEA protein has been detected in a variety of adenocarcinomas, including gastric, pancreatic, small intestine, colon, rectal, ovarian, breast, cervical and non-small-cell lung cancers. Carcinoembryonic antigen is also expressed by epithelial cells in several non-malignant disorders, including diverticulitis, pancreatitis, inflammatory bowel disease, cirrhosis, hepatitis, bronchitis and renal failure and also in heavy smokers [6-9]. Therefore CEA should not be regarded as a tumor-specific marker for the screening of general population for undetected cancers. However, the determination of carcinoembryonic antigen levels provides important information about patient prognosis, recurrence of tumors after surgical removal and effectiveness of therapy.

The analytical technique usually used for quantitative determination of CEA are immunological methods, which have been known as one of the most important methods in field of clinical diagnoses and biochemical studies because of its extremely high selectivity and sensitivity. The radioimmunoassay was the first developed method for circulating CEA in 1969 [10]. Even though, radioimmunoassay was the most commonly used method for antigen detection [11], however, radioactive labels are harmful to the operators. Hence, enzyme-linked immunosorbent assays (ELISAs) [12], piezoelectric immunoassay [13], RT-PCR[14], chemiluminescence (CL) assay [15-17], colorimetric immunoassay [18], fluoroimmunoassay [19,20], and liposome immunoassay [21] have been adapted to clinical analysis. Most of methods, unfortunately, require multiple

washing, separation steps, highly qualified personal, tedious assay time or sophisticated instrumentation. Electrochemical immunosensors [22-25] have become the predominant analytical technique for CEA detection. Nevertheless, these methods are so far from the commercial assay kits.

As small increases or decreases in tumor marker levels can be indicative of disease progression or early recurrence of disease, fluctuations in tumor marker levels can result in false-positive or false-negative assay values in a given patient. Although these traditional methods have low detection limit and are suitable enough for the determination of CEA in serum, a sensitive and rapid method for the analysis is still needed.

Our ultimate goal in this research is to provide a screening device for fast analysis, low limit of detection, and high accuracy to prevent false-negatives and positives and maintain confidence in the monitoring system. To reach our goal, a small volume microbead-based immunoassay with CL detection is being developed for the detection of CEA in human serum. The main advantages of bead-based immunoassay include increasing the surface area for immobilization of antigen or antibody and reducing the incubation time [26,27]. Focus was placed on CL because we need to get and develop a bead-based assay for making a commercial CEA test kits. Herein, we report the preliminary results for using bead-based chemiluminescence immunoassay (CLIA) for the determination of CEA in standard chemical form and human serum. The performance characteristics of bead-based (CLIA) are reported in the following sections.

5.2 Experimental Methods

5.2.1 Instrumentation

A universal luminometer (Chain-based flash glow device from Berthold Technologies GmbH & Co. KG, Germany) which used the sample tubes (with the dimensions of 12 mm × 60 mm length) and a CL micro-plate reader (BHP9504 from Hamamatsu Co., China) were used in this work. The incubation procedures were carried out using constant temperature at 37 °C (HHW 21.CR 600, China). The shaker (ZXWL-

100, China) was used for shaking the solution after adding the micro-magnetic beads. After the enzymatic reaction, the tubes can be directly placed into the luminometer for the measurement. Data acquisition and treatment were performed with an integrated 16-bit microprocessor system.

5.2.2 Materials and Methods

The immunomagnetic microbeads (3-micron) coated with anti-fluorescein isothiocyanate antibody (FITC) was purchased from Adaltis (Shanghai, China). The solution of FITC-labeled anti-CEA antibody (500 $\mu\text{g}/\text{mL}$), the standard solutions of carcinoembryonic (CEA) and alkaline phosphate-labeled carcinoembryonic antibody (ALP-labeled anti-CEA antibody) were obtained from Beijing Chemclin Biotech Co., Ltd. (Beijing, China). 4-Methoxy-4-(3-phosphatephenyl)-spiro-(1,2-dioxetane-3,2'-adamantane) (AMPPD) was purchased from Diagnostic Products Corporation (California, USA). Bovine serum albumin (BSA) and sodium azide were from Merck (Darmstadt).

The coating buffer for microbeads consisted of 0.1 mol/L Tris-HCl buffer, 0.1% (w/v) BSA and 0.1% sodium azide. The washing solution was 0.1 mol/L Tris-HCl buffer, (pH 7.4) and 0.1 mol/L NaCl. The solution of 0.1 mol L⁻¹ Tris-HCl buffer (pH 7.4) containing appropriate of BSA was used as dilution buffer for FITC-labeled anti-CEA antibody and ALP-labeled anti-CEA antibody. The CL substrate buffer contained with 0.1 mol L⁻¹ Tris-HCl (pH 9.5), 1 mmol/L MgCl₂ and 0.02% (w/v) NaN₃.

5.2.3 Immunoassay procedure

Schematic diagram was shown in Figure 5.1. Immunoassay procedures consisted of, First, 25 μL of carcinoembryonic antibody or serum samples was into the test tube. Then, 50 μL diluted ALP-labeled anti-CEA antibody and 50 μL diluted FITC-labeled anti-CEA antibody were added into the test tubes step by step and incubated for 1h at 37 °C. After the sandwich reaction, 50 μL coated anti-FITC-labeled magnetic beads were added and incubated with shaking for another 5 min. Then, the magnetic plate separation was inserted under the test tubes for bead separation (2 min). Antibody-coated bead and

any specific captured material were attracted by the magnets to the bottom of the test tubes and unwanted materials are removed from the test tubes. After that, the test tubes were gently tapped against tissue paper to remove all fluid. During the washing steps, the washing solution was added in the test tubes by placing outside the magnetic plate so the particles were suspended in the washing solution. Three times of washing were performed with 1.0 mL of the washing solution. Finally, 300 μ L CL substrate solution was added and incubated for 20 min at room temperature (keep in dark), and the emitted photons were measured.

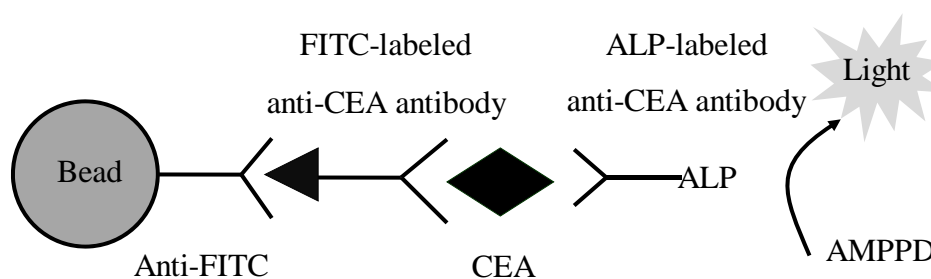


Figure 5.1 Schematic representation of bead-based chemiluminescence enzyme immunoassay for CEA detection.

5.2.4 Micro-plate chemiluminescence immunoassay (micro-plate CLEIA)

The immunoassay procedure was shown in the label of packet. Briefly, 50 μ L of antigen was added into the microwell. After that 50 μ L of anti-CEA antibody was added to react with the antigen thoroughly mixes for 30 s. Then, the microplates were allowed to stand sealed at 37°C for 1 h. The next step, five times washing were performed, 50 μ L of CL substrate were added and incubated (keep in dark) at room temperature for 30 min, the emitted photons were measured.

5.2.5 Data analysis

Standard and samples were measured, and CL intensity values were integrated. Standard curves were obtained by plotting the logarithm of CL intensity against the

logarithm of analyte concentration and fitted to linear equation of $\log(\text{RLU}) - \log(\text{concentration of analyte})$.

5.2.6 Human serum sample

Normal human serums obtained from the hospital in Beijing, China were spiked with CEA in different concentrations. All samples were analyzed using the micro-plate and micro-magnetic CLEIA without any pretreatment.

5.2.7 Statistical analysis

For comparing two measurement systems that are supposed to be equivalent, results were tested by paired t -Test and Bland-Altman model. The methods have been described in detail elsewhere [28,29].

5.3 Results and discussion

5.3.1 Optimization of immunoassay reagents

The immunoreaction reagent is a key parameter that effect on the sensitivity of immunoassay. Generally, the amounts of reagents were used as low as possible to accept the sensitivity for reducing the assay cost. Therefore, this experiment, the dilution ratios of ALP-labeled anti-CEA antibody and the concentrations of FITC-labeled anti-CEA antibody were studied. As shown in Figure 5.2, when the dilution ratios of ALP-labeled anti-CEA antibody were increased from 1:5000 to 1:500, the RLU responses were also increased at all examined concentrations of FITC-labeled anti-CEA antibody (use the standard CEA concentration of 162 ng/mL). From the results, the dilution ratio of ALP-labeled anti-CEA antibody at 1:500 was selected because this ratio provided the highest RLU intensity. Moreover, comparison results with 1:1000, the significant difference was observed from both of them. For the concentration of FITC-labeled anti-CEA antibody, it was found that the signals increase rapidly upon increasing the concentration between 0.1 and 0.5 $\mu\text{g/mL}$ and levels off thereafter (found in all dilution ratios of ALP-labeled anti-CEA antibody). So, the concentration of 0.5 $\mu\text{g/mL}$ FITC-labeled anti-CEA antibody was chosen.

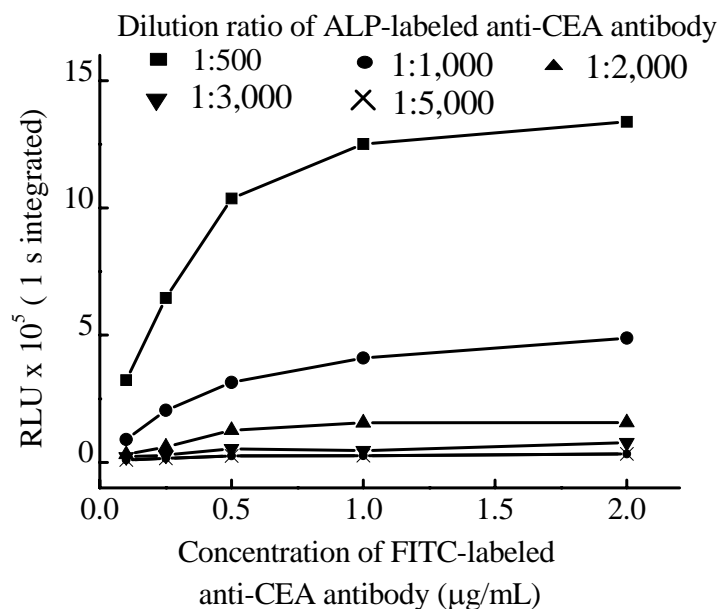


Figure 5.2 The relationships between concentration of FITC-labeled anti-CEA antibody and the dilution ratios of ALP-labeled anti-CEA antibody on the RLU values, using the standard CEA concentration of 162 ng/mL. The five curves were represented the different dilution ratio of ALP-labeled anti-CEA antibody at 1:500, 1:1,000, 1:2,000, 1:3,000 and 1:5,000, respectively.

From this immunoassay procedure, normally, the diluted ALP-labeled anti-CEA antibody and diluted FITC-labeled anti-CEA antibody were added into the test tubes step by step. Mixing two antibodies before adding into the test tubes may reduce the analysis time and the assay error from pipetting. Hence, the calibration curve was used to study the optimization of immunoassay procedure. The results showed that the obtained calibration curves were the same with two procedures (data not shown). Thus, the mixing procedure was employed for the next experiment.

5.3.2 Physicochemical parameter optimization

The experimental parameters including incubation time and incubation volume were studied with two goals: (1) to improve immunoassay sensitivity and (2) to study

immunoassay performance under the optimal conditions. These experiments were done using the proposed method described above.

5.3.2.1 Effect of immunoassay incubation time

From our knowledge, the time given to the immunoreagents to interact together may have a direct effect on the sensitivity of the immunoassay. For this reason, we have varied the length of immunoreaction time from 30 to 120 min for assessing the influence of the incubation time. Figure 5.3A shows the results from the assay performance as a function of the incubation time. The intensity increased with the longer incubation time. Under these conditions, we encountered at the 60 min incubation time. Because of the signal seems to stable and no significance differences were observed for higher time. In addition, the sensitivity of using 60 min for incubation time is much higher than at 30 min.

5.3.2.2 Influence of the reaction time between AMPPD CL substrate and ALP-anti CEA antibody

The results were shown in Figure 5.3B. It can be seen that the RLU increased with the incubation time in the range of 5-20 min at all studied volume (200, 300 and 400 μ L). After 20 min, the RLU signal did not change. This phenomenon can be explained using the fact that the half-life of luminescence product (AMPD) is between 2-30 min depending on the environment. After that it will be decomposed, giving the steady state of CL signal. Hence, at 20 min was selected for the reaction time of substrate and ALP-labeled anti-CEA antibody.

5.2.2.3 Effect of the shaking time to capture efficiency

In this system, the immunomagnetic beads coated with anti-FITC antibody is added into solution containing antigen to provide the binding. The shaking time of solution would be effected to the capture efficiency. The time of shaking was investigated within the range of 5-30 min. The experiment showed (Figure 5.3C) that the CL intensity increased with the longer shaking time. Under the studies, no significant differences were observed for RLU value between 5-15 min. This means 5 min was

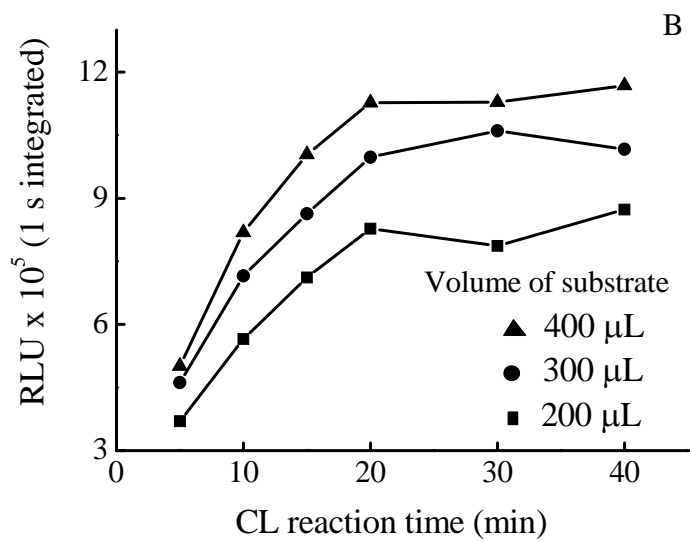
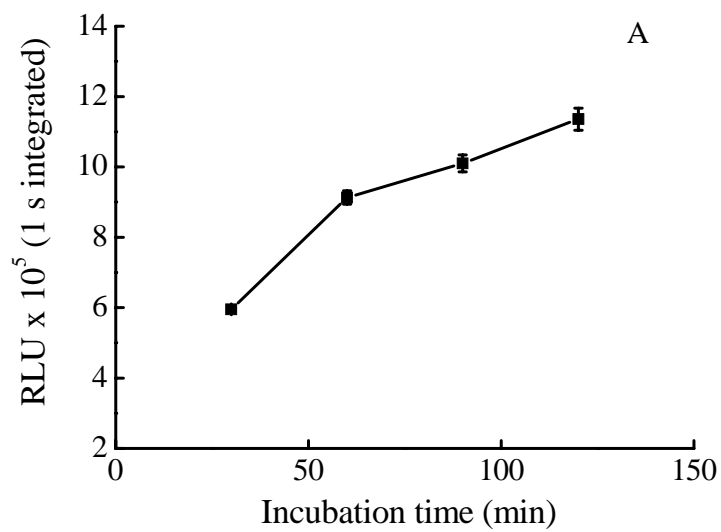
suitable enough time for the capture and analysis time was also reduced. Thus, a shaking time of 5 min is set for the experiment.

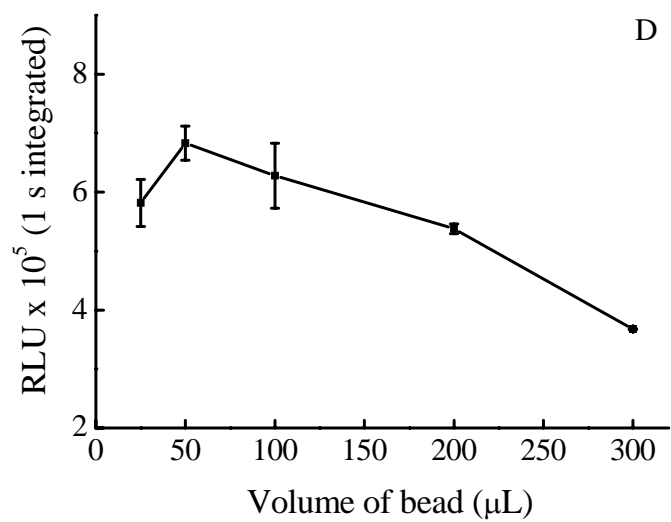
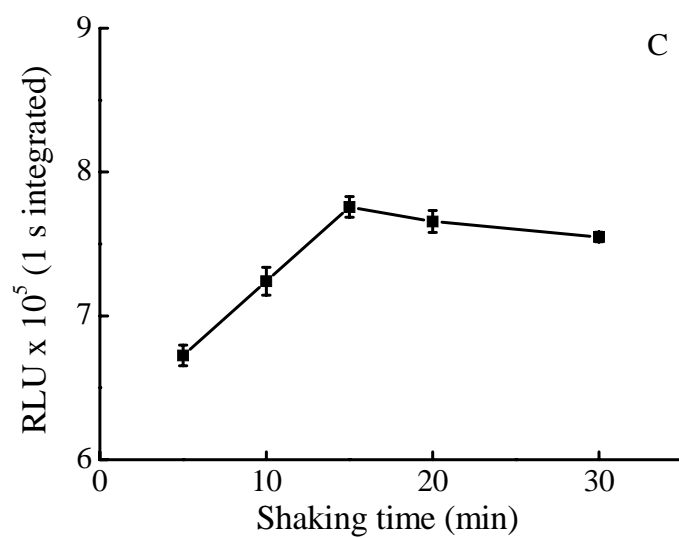
5.3.2.4 Effect of magnetic beads volume

The quantity of magnetic beads was critical for the CL intensity. In the condition of monolayer dispersion in the bottom of the tube would be needed. Hence, we studied the effect of volume of magnetic beads solutions on CL intensity. The results showed that the CL intensity increased with the volume of the solution containing magnetic beads up to 50 μL , while the intensity decreased after the volume of 50 μL as shown in Figure 5.3D. Finally, the 50 μL of magnetic beads was selected as optimal conditions.

5.3.2.5 Effect of the substrate volume to bead-based CLEIA

Substrate sensitivity refers to the signal intensity produced by a unit of enzyme activity. Thus, in this experiment, the volumes of substrate were studied from 100-500 μL . It was found that the CL intensity increased with larger volume of the solution over the examined range. The expected sigmoidal with a defined plateau did not receive. Therefore, the ratios (S/S_0) of the mean RLU signals with (S) and without (S_0) substrate were calculated as a function of volume. The S/S_0 ratio reaches a maximum value at 300 μL (Figure 5.3E). Hence, this volume was selected for all subsequent experiments.





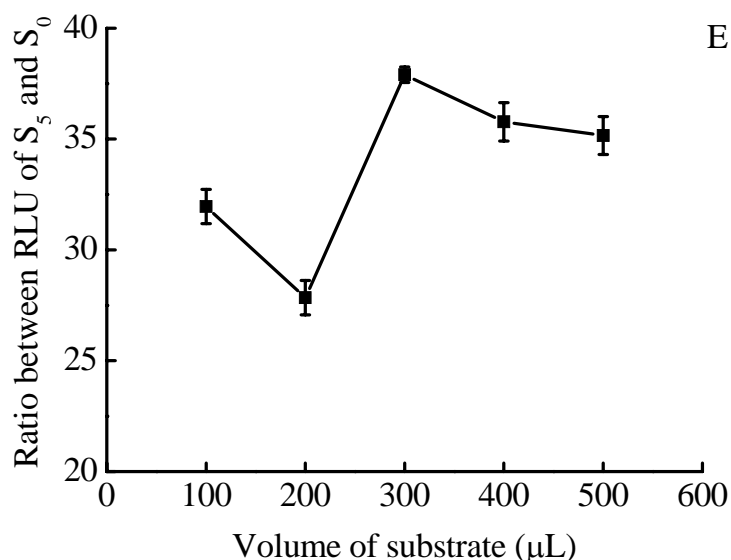


Figure 5.3 Physicochemical parameter optimization. (A) Influence of immunoassay incubation time on CL intensity. The antigen and antibody were incubated at different time (between 30 and 120 min) (B) Effect of the length reaction time between CL substrate and ALP-labeled anti-CEA antibody (C) Effect of the shaking time to capture efficiency between coated micro-magnetic beads and sandwich reaction (D) Influence of the volume of magnetic beads for the CL reponse and (E) Effect of substrate volume on the bead-based chemiluminescence enzyme immunoassay response.

5.3.3 Non-specific adsorption

The polystyrene tubes were used as a container for the immunoassay reaction. This kind of tubes showed high adsorption affinity feature, so the effect of non-specific adsorption on the surface of the tube was also investigated. The different concentrations of CEA were used to study the effect of non-specific adsorption on the proposed method. The experiment showed (Table 5.1) that the CL intensity in the absence of the solution containing magnetic beads did not change while the CEA concentrations were increased. In the other hand, the RLU intensity of the solution containing magnetic beads increased with the increasing of CEA concentrations.

Table 5.1 Studied of non-specific adsorption

CEA Conc. (ng /mL)	CL Intensity without magnetic beads	CL Intensity with magnetic beads added
0	7915	13201
2	7430	31652
6	7580	56693
18	6137	137346
54	10937	325130
162	10807	918547

5.3.4 Linearity-dilution effect

Linearity-dilution effect was studied to check the dilution effect of sample with the other solutions to provide an accurate quantitation. Human serum samples may be diluted with different solution such as cow serum in order to get the concentration within the examined range. The calibration curve was used to evaluate this effect. In this experiment, we selected to use the cow serum as a diluent solution. It was found that the relationships between the concentration of diluted CEA and the dilution factors gave the high linearity with correlation coefficient, $r = 0.9997$, as shown in Figure 5.4A. It means no effect between the human serum and cow serum so in the case of high level of CEA; we can use cow serum to dilute it before analysis.

5.3.5 Calibration and sensitivity

Under the optimal conditions, dose-response curve obtained with the CL detection of antigen-antibody reaction was displayed in Figure 5.4B. The linearity was in the range from 2 to 162 ng/mL. The detection limit or minimum detectable limit was defined as the mean RLU signals (S_0) at zero concentration plus two times of standard deviation (SD) ($LOD = S_0 + 2SD$). The detection limit of CEA was calculated by obtaining the average RLU signals for 10 replicates of zero standard and then pulsing 2SDs of the average. The RLU signals plus two SD was then extrapolated from log-log standard

curve and represents the sensitivity of the assay. The value of detection limit for CEA was 0.69 ng/mL.

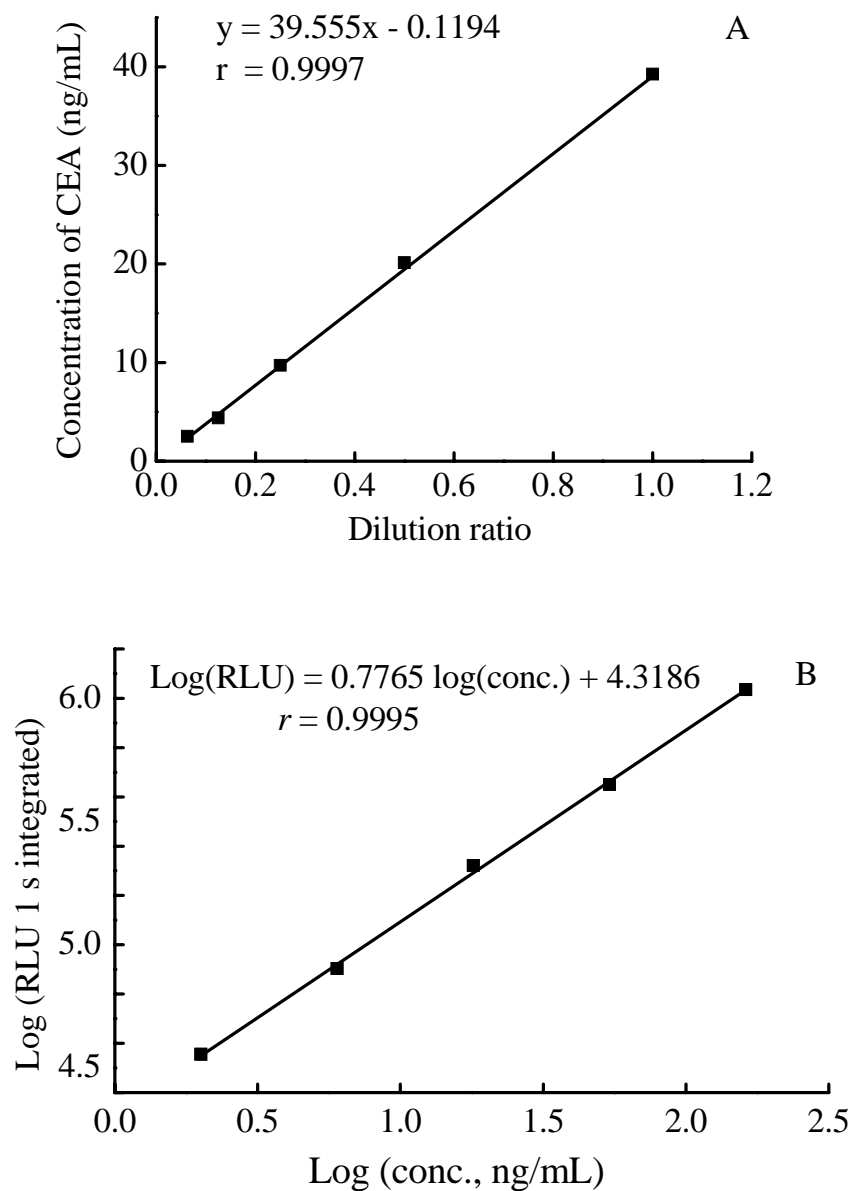


Figure 5.4 Relationship between the dilution factor, diluted concentration and the CL intensity. (A) Linearity-dilution test curve was plotted between diluted concentration and

dilution factors (B) Calibration graph of bead-based chemiluminescence enzyme immunoassay for the determination of CEA.

5.3.6 Precision

The important of the precision has often been stressed using bead-based CL-EIA for the quantitative analysis. The intra-precision of the analytical method was calculated by analyzing each concentration ten times per run in 1 day. Three different concentration levels were used for this study. Similarly, these methods were analyzed on ten times in the different times that each time used two test tubes for inter-precision. It can be observed that intra- and inter-coefficient of variation were in all cases below than 13%. The results of testing were listed in Table 5.2. These results referred that the proposed method exhibited the high reproducibility.

Table 5.2 Precisions of the micro-magnetic CL-EIA

Kind of assay	Conc. of CEA (ng/mL)	CV (%)
Intra-assay (n = 10)	6	8.7
	18	5.9
	54	4.9
Inter-assay (n = 20, detection of ten times)	6	12.1
	18	12.2
	54	7.1

5.3.7 Quantitative determination of CEA in human serums: comparison with commercially available CEA CL-EIA kit

The proposed method was applied to determine CEA in human serums. We examined the accuracy of the method for the determination of CEA in human serums by the method of calibration. Linear least square calibration curve provides the slope of 0.7408 RLU unit per ng/mL and correlation coefficient of 0.9994. Before analyzing the

normal human serums were spiked with CEA. The recoveries of added CEA ranged between 80% and 110% were obtained as displayed in Table 5.3.

Table 5.3 Concentration of CEA in spiked human serum, measured by the commercial micro-plate and magnetic microbead CL-EIA

Samples	Spiked CEA (ng/mL)	Founded CEA (ng/mL)		Recovery (%)
		Commerical micro-plate CL-EIA	The present magnatic microbead CL-EIA	
1	17.70	18.21	17.81	100.6
2	19.03	15.88	16.90	88.8
3	19.91	17.65	18.49	92.9
4	19.91	19.67	20.51	103.0
5	20.29	15.8	21.79	107.4
6	24.34	17.68	23.76	97.6
7	26.55	19.39	24.61	92.7
8	28.76	24.98	27.50	95.6
9	28.76	22.61	24.88	86.5
10	30.44	23.07	32.64	107.2
11	30.98	24.16	26.39	85.2
12	30.98	24.58	25.33	81.8
13	37.21	26.95	41.11	110.0
14	38.05	27.14	34.23	89.9
15	43.13	30.48	42.59	98.7
16	44.25	37.2	46.00	103.9
17	44.25	32.89	39.16	88.5
18	48.20	35.44	46.14	95.7

Samples	Founded CEA (ng/mL)			Recovery (%)
	Spiked CEA (ng/mL)	Commerical micro-plate CL-EIA	The present magnatic microbead CL-EIA	
19	50.74	35.63	46.061	90.8
20	53.27	62.98	50.81	95.4

Furthermore, both normal human serum and the spiked CEA concentrations in normal human serum samples were simultaneously determined using the commercially available CEA CL-EIA kit. The results shown in Figure 5.5A are for normal serums, and Figure 5.5B are for spiked CEA in normal serums, respectively. It can be seen that the data will be tightly scattered about the line for both of them. It means the measurements are comparable and acceptable. Moreover, to make sure, the paired *t*-test was used to evaluate these two immunoassay methods. It was found no significant difference at 95% confidence (*t* value is less than *t*_{critical}). Thus, the analyzed values of CEA in human serums can be accepted.

The limitation of proposed method may come from the large size of magnetic beads. Normally, this size of beads was widely used to in separation purpose. For the immunoassay, the efficiency derives from the binding of the target substance to the bead surface. The higher the accessible surface is the higher is the possible load per volume unit of a magnetic bead to improve exposure of the functionalized bead surface to the surrounding liquid. This problem can be solved by using the magnetic nanoparticles for increasing the additional advantages such as sensitivity. The determination of CEA in human serum using nano-magnetic CL-EIA is under study.

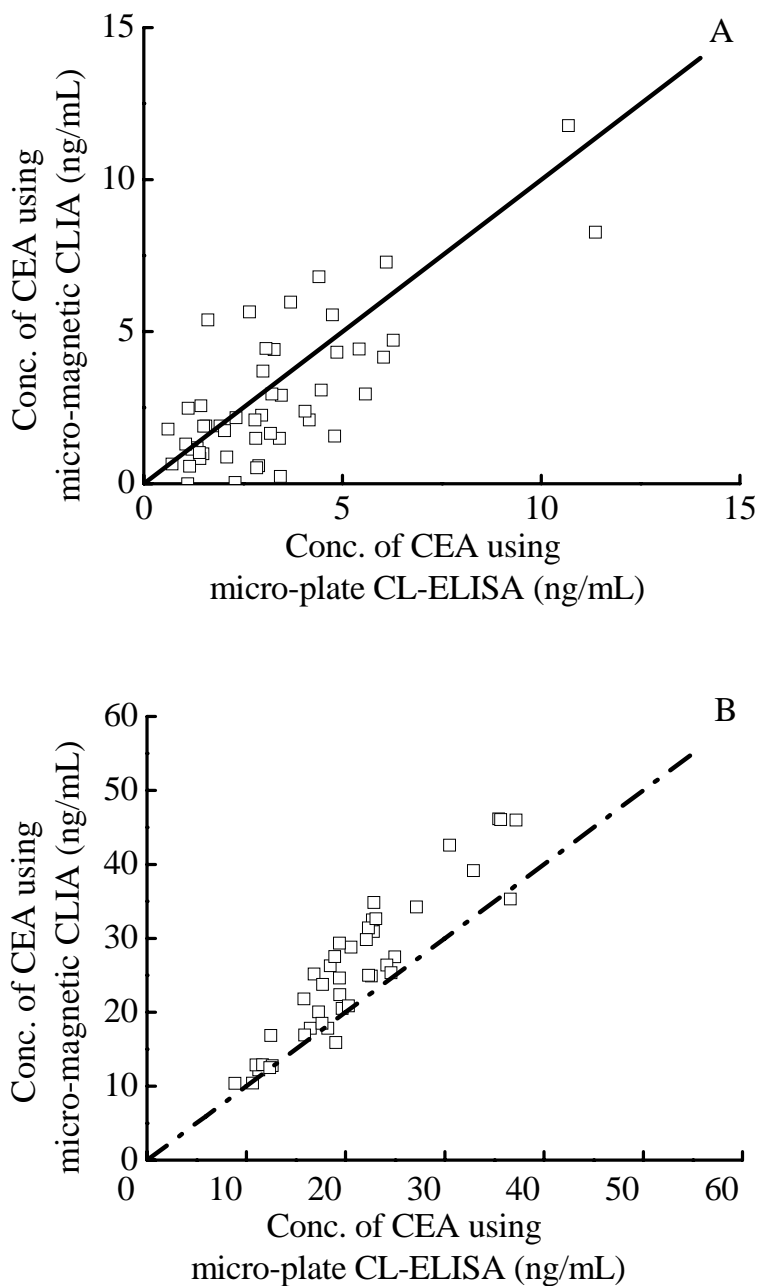


Figure 5.5 Comparing two measurement methods, bead-based chemiluminescence enzyme immunoassay and commercial test kit, for the determination of CEA in (A) normal human serums, and (B) disease serums by spiking CEA in normal human serums.

5.4 Summary

A highly sensitive, specific, and reproducible micro-magnetic CL-EIA has been developed and its feasibility has been demonstrated on analyte sample for the determination of CEA. The proposed assay consisted of anti-FITC antibody-coated magnetic beads, FITC-labeled anti-CEA antibody, ALP-labeled anti-CEA antibody and CL detection system. With the assay, CEA can be reproducibly detected in human serum at concentration as low as 0.69 ng/mL even though the incubation time was maintained. This concentration is lower than the commercial ELISA test kit about 50% (1 ng/mL for ELISA) [30,31]. In addition, this assay used magnetic bead particles and was performed in a total volume of 300 μ L making it is ideally suitable for high-throughput and robotics-based assay formats, for large volume detection. A stable calibration curve with a wide dynamic range was also established. The calibration curve was linear from 2 to 162 ng/mL. For our particular application, the dynamic range of the assay covers all CEA levels, used for evaluating human cancerous serum. If the RLU reading is higher or equal the highest point of the linear portion, the unknown samples can be diluted for a proportional measurement with diluent solution. Data from developed method showed the acceptable intra- (less than 10%) and inter-assay (less than 20%) precision and accuracy (80-110% recovery). In summary, this assay provides good advantages and could easily be accommodated into a variety of detection systems currently available on the market.

5.5 References

- [1] Michael, J. D. Serum Tumor Markers in Breast Cancer: Are They of Clinical Value. Clin. Chem. 52 (2006): 345-351.
- [2] Cheli, C. D.; Morris, D. L.; Neaman, I. E.; Dai, J.; Allard, W. J.; Yeung, K. K. Measurement of four tumor marker antigens in the sera of pregnant women. J. Clin. Lab Anal. 13 (1999): 35-39.
- [3] Mayer, R. J. Gastrointestinal cancer. Scientific American Medicine 12 (1996) New York: Scientific American.
- [4] Delwiche, R.; Zamcheck, N.; Marcon, N. Carcinoembryonic antigen in pancreatitis. Cancer. 31 (1973): 328-330.

- [5] Loewenstein, M. S.; Zamcheck, N. Carcinoembryonic antigen (CEA) levels in benign gastrointestinal disease states. Cancer. 42 (1978): 1412-1418.
- [6] Chu, T. M.; Lavin, P.; Day, J. Carcinoembryonic antigen: prognosis and monitoring of cancer. In: Lehmann FG, ed. Carcinoembryonic Proteins, 55-64. North-Holland: Amsterdam Elsevier, 1979.
- [7] Herbeth, B.; Bagrel, A. A study of factors influencing plasma CEA levels in an unselected population. Oncodev. Biol. Med. 1 (1980): 191-198.
- [8] Tabor, E.; Gerety, R. J.; Needy, C. F. Carcinoembryonic antigen levels in asymptomatic adolescents. Euro. J. Cancer 17 (1981): 257-258.
- [9] Stevens, D. P.; Mackay, I. R. Increased carcinoembryonic antigen in heavy cigarette smokers. Lancet. 2 (1973): 1238-1239.
- [10] Thomson, D. M.; Krupey, J.; Freedman, S. O.; Gold, P. Physicochemical studies of the carcinoembryonic antigens of the human digestive system. Proc. Natl. Acad. Sci. USA 64 (1969): 161-167.
- [11] Hernandez, L.; Espasa, A.; Fernandez, C.; Candela, A.; Martin, C.; Romero, S. CEA and CA 549 in serum and pleural fluid of patients with pleural effusion. Lung Cancer 36 (2002): 83-89.
- [12] Zhao, L.; Xu, S.; Fjaertoft, G.; Pauksen, K.; Hakansson, L.; Venge, P. An enzyme-linked immunosorbent assay for human carcinoembryonic antigen-related cell adhesion molecule 8, a biological marker of granulocyte activities in vivo. J. Immunol. Methods. 293 (2004): 207-214.
- [13] Shen, G. Y.; Wang, H.; Deng, T.; Shen, G. L.; Yu, R. Q. A novel piezoelectric immunosensor for detection of carcinoembryonic antigen. Talanta. 67 (2005): 217-220.
- [14] Wang, J. Y.; Lin, S. R.; Lu, C. Y.; Chen, C. C.; Wu, D. C.; Chai, C. Y.; Chen, F. M.; Hsieh, J. S.; Huang, T. J. Gastric cancer cell detection in peritoneal lavage: RT-PCR for carcinoembryonic antigen transcripts versus the combined cytology with peritoneal carcinoembryonic antigen levels. Cancer Letters. 223 (2005): 129-135.
- [15] Haggart, R.; Thorpe, G. H. G.; Moseley, S. B.; Kricka, L. J.; Whitehea, T. P. An enhanced chemiluminescent enzyme immunoassay for serum carcinoembryonic

- antigen based on a modification of a commercial. J. Biolumin. Chemilumin. 1 (1987): 29-34.
- [16] Findeisen, R.; Albrecht, S.; Richter, B.; Deutschmann, K.; Zimmermann, T.; Distler, W. Chemiluminometric determination of tissue polypeptide antigen (TPA), cancer antigen 15-3 (CA 15-3), carcinoembryonic antigen (CEA) in comparison with vascular endothelial growth factor (VEGF) in follow-up of breast cancer. Luminescence. 15 (2000): 283-289.
- [17] Zhuang, H. S.; Huang, J. L.; Chen, G. N. Development of a sensitive micro-magnetic chemiluminescence enzyme immunoassay for the determination of carcinoembryonic antigen. Anal. Chim. Acta 512 (2004): 347-352.
- [18] Eckert, K.; Fuhrmann-Selter, T.; Maurer, H. R.; Buttner, P. Simultaneous Determination of α -Fetoprotein and Carcinoembryonic Antigen in Human Serum by Time-Resolved Fluoroimmunoassay. Cancer Letters 105 (1996): 1-4.
- [19] Mastsumoto, K.; Yuan, J.; Wang, G.; Kimura, H. Simultaneous Determination of α -Fetoprotein and Carcinoembryonic Antigen in Human Serum by Time-Resolved Fluoroimmunoassay. Anal. Biochem. 276 (1999): 81-87.
- [20] Moura, R. M. A. M.; Matos, D.; Filho, M. M. G.; D'ippolito, G.; Sjzenfeld, J.; Giuliano, L. M. Value of CEA level determination in gallbladder bile in the diagnosis of liver metastases secondary to colorectal adenocarcinoma. Sao Paulo Med. J. 119 (2001): 110-113.
- [21] Haga, M.; Hoshino, S.; Okada, H.; Hazemoto, N.; Kato, Y.; Suzuki, Y. An improved chemiluminescence-based liposome immunoassay involving apoenzyme. Chem. Pharm. Bull 38 (1990): 252-254.
- [22] Zheng, G.; Patolsky, F.; Cui, Y.; Wang, W. U.; Lieber, C. M. Multiplexed Electrical Detection of Cancer Markers with Nanowire Sensor Arrays. Nature Biotech. 23 (2005): 1294-1301.
- [23] Limbut, W.; Kanatharana, P.; Mattiasson, B.; Asawatreratanaku, P.; Thavarungkul, P. A reusable capacitive immunosensor for carcinoembryonic antigen (CEA) detection using thiourea modified gold electrode. Anal. Chim. Acta 561 (2006): 55-61.

- [24] Liu, Y.; Jiang, H. Electroanalytical Determination of Carcinoembryonic Antigen at a Silica Nanoparticles/Titania Sol-Gel Composite Membrane-Modified Gold Electrode. Electroanalysis. 18 (2006): 1007-1013.
- [25] Li, X.; Yaun, R.; Chai, Y.; Zhang, L.; Zhuo, Y.; Zhang, Y. Amperometric immunosensor based on toluidine blue/nano-Au through electrostatic interaction for determination of carcinoembryonic antigen. J. Biotech. 123 (2006): 356-366.
- [26] Farrell, S.; Ronkainen-Matsuno, N. J.; Halsall, H. B.; Heineman, W. R. Bead-based immunoassays with microelectrode detection. Anal. Bioanal. Chem. 379 (2004): 358-367.
- [27] Biagini, R. E.; Smith, J. P.; Sammons, D. L.; MacKenzie, B. A.; Striley, C. A. F.; Robertson, S. K.; Snawder, J. E. Development of a sensitivity enhanced multiplexed fluorescence covalent microbead immunosorbent assay (FCMIA) for the measurement of glyphosate, atrazine and metolachlor mercapturate in water and urine. Anal. Bioanal. Chem. 379 (2004): 368-374.
- [28] Goulden, C. H. Methods of statistical analysis. 2nd ed. New York: Wiley, 1956.
- [29] Alman, D. G.; Bland, J. M. Measurement in medicine: The analysis of method comparison studies. The Statistician. 32 (1983): 307-317.
- [30] Carcinoembryonic Antigen (CEA) Enzyme Immunoassay Test Kit, Catalog Number: BC-1011, California, Biocheck Inc.
- [31] CEA ELISA Kit, Catalog Number: EK-38, Budapest Hungary, Institute of Isotopes Ltd.

CHAPTER VI

CONCLUSIONS AND FUTURE PERSPECTIVE

6.1 Conclusions

Electrochemical immunoassay was successfully developed for the determination of *S. typhi* in real samples with a low limit of detection (98.9 cfu/mL) and high accuracy (80-101% recoveries). Moreover, the developed method is fast analysis time (~4 h) compared with the typical method (7-10 days).

The multiple oxidative indicators and electrochemical detections for μ PADs were invented to improve the accuracy, sensitivity and selectivity for biomarker analysis. Both detection methods were successfully applied to simultaneously determine glucose, lactate and uric acid in human serum using oxidase enzyme (glucose oxidase, lactate oxidase, and uricase, respectively) reactions. Levels of three analytes in human serum samples measured using the paper devices were within error of the values measured using traditional tests. These results demonstrate the feasibility of using multiple oxidative indicators and electrochemical detection for paper-based microfluidic devices as an easy-to-use, inexpensive, and portable alternative device for point of care testing and self-monitoring diagnosis. In addition, a low-cost, simple, and rapid fabrication method for μ PADs using wax screen-printing was developed for implementation in developing countries. The minimum width of hydrophilic channel and hydrophobic barrier is 650 and 1300 μ m, respectively. The fabrication method was also shown to be useful for both colorimetric and electrochemical detection methods, and was applied to the simultaneous determination of glucose and total iron in biologically relevant samples.

Finally, the sensitivity of immunoassay was improved using a micro-magnetic bead. CEA can be reproducibly detected in human serum at concentration as low as 0.69 ng/mL. Limit of detection in this work is lower than the commercial ELISA test kit without using a micro-magnetic bead about 50% (1 ng/mL for ELISA).

6.2 Future perspective

In the future, μ PADs coupled with electrochemical immunoassay can be applied for the detection of other pathogenic bacteria. Furthermore, micro or/and nanomaterial applied in μ PADs could be improve the sensitivity of immunoassay.

VITA

- Name** : Miss Wijitar Dungchai
- Date of Birth** : January 29, 1983 (At Prachinburi, Thailand)
- | Education | Period | College/University | Qualification |
|------------------|---------------------|-----------------------------------|------------------------|
| | Jun 2001 - Apr 2005 | Chulalongkorn University, Bangkok | Bachelor of Science |
| | Jun 2005 – Oct 2010 | Chulalongkorn University, Bangkok | Doctoral of Philosophy |
- Research Grants:** The Royal Golden Jubilee Ph.D Program from Thailand Research Fund
- Home Address** : 205 Moo 4 Tambol Bupharm, Amphur Nadee, Prachinburi 25220, Thailand
- Publications** :
- Dungchai, W.;** Siangproh, W.; Lin, J. M.; Chailapakul, O.; Lin, S.; Ying, X. Development of a sensitive micro-magnetic chemiluminescence enzyme immunoassay for the determination of carcinoembryonic. *Anal. Bioanal. Chem.* 387 (2007): 1965-1971.
 - Dungchai, W.;** Siangproh, W.; Chaicumpa, W.; Tongtawe, P.; Chailapakul O. *Salmonella typhi* determination using voltammetric amplification of nanoparticles: A highly sensitive strategy for metalloimmunoassay based on a copper-enhanced gold label. *Talanta.* 77 (2008): 727-732.
 - Dungchai, W.;** Chailapakul, O.; Henry, C. S. Electrochemical Detection for Paper-Based Microfluidics. *Anal. Chem.* 81 (2009): 5821-5826.
 - Dungchai, W.;** Chailapakul, O.; Henry, C. S. Use of multiple colorimetric indicators for paper-based microfluidic devices. *Anal. Chim. Acta* 674 (2010): 227-233.
 - Dungchai, W.;** Chailapakul, O.; Henry, C. S. A low-cost, simple, and rapid fabrication method for paperbased microfluidics using wax screen-printing. *Analyst* (2010) *in press*.
 - Chuanuwatanakul, S.; **Dungchai W.;** Chailapakul, O.; Motomizu, S. Determination of trace heavy metals by sequential injection-anodic stripping voltammetry using bismuth film screen-printed carbon electrode. *Anal. Sci.* 24 (2008): 589-594.
 - Sangjarusvichai, H.; **Dungchai, W.;** Siangproh, W.; Chailapakul, O. Rapid separation and highly sensitive detection methodology for sulfonamides in shrimp using a monolithic column coupled with BDD amperometric detection. *Talanta* 79 (2009) 1036-1041.
 - Siangproh, W.; Leesutthipornchai, W.; **Dungchai, W.;** Chailapakul, O. Electrochemical Detection for Flow-based System: A Review. *J. Flow Inject. Anal.* 26 (2009) 5–25.
 - Injang, U.; Noyrod, P.; Siangproh, W.; **Dungchai, W.;** Motomizud, S.; Chailapakul, O. Determination of trace heavy metals in herbs by sequential injection analysis-anodic stripping voltammetry using screen-printed carbon nanotubes electrodes. *Anal. Chim. Acta* 668 (2010) 668, 54-60.
 - Apilux, A.; **Dungchai, W.;** Siangproh, W.; Praphairaksit, N.; Henry, C. S.; Chailapakul, O. Lab-on-Paper with Dual Electrochemical/Colorimetric Detection for Simultaneous Determination of Gold and Iron. *Anal. Chem.* 82 (2010) 1727-1732.